Pontifícia Universidade Católica
do Rio de Janeiro

Ricardo Cavalcanti Linhares

Wax deposits formation in petroleum pipelines: investigation of the deposit-liquid interface characteristics

Dissertação de Mestrado

Dissertation presented to the Programa de Pós-Graduação em Engenharia Mecânica da PUC-Rio in partial fulfillment of the requirements for the degree of Mestre em Engenharia Mecânica.

Advisor: Prof. Luis Fernando Alzuguir Azevedo

Rio de Janeiro
December 2020

Pontifícia Universidade Católica
do Rio de Janeiro

Ricardo Cavalcanti Linhares

Wax deposits formation in petroleum pipelines: investigation of the deposit-liquid interface characteristics

Dissertation presented to the Programa de Pós-Graduação em Engenharia Mecânica da PUC-Rio in partial fulfillment of the requirements for the degree of Mestre em Engenharia Mecânica. Approved by the Examination Committee:

Prof. Luis Fernando Alzuguir Azevedo
Advisor
Departamento de Engenharia Mecânica – PUC-Rio

Dra. Helena Maria Borja Veiga
Total E&P

Dr. Felipe Pereira Fleming
CENPES - Petrobras Research and Development Center

Rio de Janeiro, December 22th, 2020

Ricardo Cavalcanti Linhares

Graduated in Mechanical Engineering at PUC-Rio in 2018.

Bibliographic data

Linhares, Ricardo Cavalcanti

Wax deposits formation in petroleum pipelines : investigation of the deposit-liquid interface characteristics / Ricardo Cavalcanti Linhares ; advisor: Luis Fernando Alzuguir Azevedo. – 2020.
139 f. : il. color. ; 30 cm

Dissertação (mestrado) – Pontifícia Universidade Católica do Rio de Janeiro, Departamento de Engenharia Mecânica, 2020.

Inclui bibliografia

1. Engenharia Mecânica - Teses. 2. Wax deposition. 3. Flow assurance. 4. Interface temperature. 5. Flowing crystals. I. Azevedo, Luis Fernando Alzuguir. II. Pontifícia Universidade Católica do Rio de Janeiro. Departamento de Engenharia Mecânica. III. Título.

CDD: 621

To my parents, Jorge and Marcia, and
my sister Mariana.

Acknowledgments

First and foremost, I would like to thank my parents for their love and support throughout my life. This dissertation is a product of all their efforts to provide me with the best education possible. My sister also deserves my wholehearted thanks, she has always been by my side in the worst and best moments of my life.

I would like to thank my advisor Luis Fernando not only for his guidance and teachings but also for his friendship. His enthusiasm, dedication and kindness are an example for me. I feel very lucky to have had the opportunity to work with such a knowledgeable and pleasant person throughout these years.

I would like to thank my girlfriend, Thainá Ferraz, for being such a wonderful and comprehensive company along these years. I truly believe that she is one of the best persons to disseminate the wonders of positive psychology worldwide and I am thankful to have her by my side.

I would like to thank Diogo, my childhood friend, for believing in me and giving me confidence when I needed.

I would like to thank all of my friends in the Fluids Engineering Laboratory, for making the laboratory such a great place to work. The environment we are inserted is an important part of our life and it is amazing to be surrounded by ingenious and hardworking people. Among them, I would like to express a special thanks to Ivan, for his partnership and for the productive discussions about this project; Igor, for his attention and advises when I needed; Leonardo Fernandes for his companionship and valuable advises; also to Rodrigo, Paula, Omar, Leo Pinhal, Marcio and Alexandre.

Among all the excellent professors that I had during my master's degree I would like to give a special thanks to Rafael Menezes, Angela Nickele, Marcio Carvalho and Luis Azevedo. Their knowledge, patience and great mastery of the areas they teach were extremely important for my learning.

I would like to thank Dr. Felipe Fleming, for his invaluable insights and his enthusiasm on this project.

I would like to thank Petróleo Brasileiro S.A. (Petrobras) for sponsoring this research project.

This study was financed in part by the Coordenação de Aperfeiçoamento de Pessoal de Nível Superior - Brasil (CAPES) - Finance Code 001.

Abstract

Linhares, Ricardo Cavalcanti; Azevedo, Luis Fernando Alzuguir. **Wax deposits formation in petroleum pipelines: investigation of the deposit-liquid interface characteristics**. Rio de Janeiro, 2020. 139p. Dissertação de Mestrado – Departamento de Engenharia Mecânica, Pontifícia Universidade Católica do Rio de Janeiro.

Wax deposition in petroleum production and transportation lines is one of the most relevant problems faced by the industry in order to assure the flow of oil and gas at the designed economical rates. Significant losses occur due to decreased production, line replacements and maintenance costs associated with cleaning operations. Wax deposit formation on the inner wall of the pipes might occur when the warm oil from the well loses heat to the cold environment, typical of deep water production operations, and its temperature reaches a critical value at which wax crystal formation occurs. This critical temperature is the WAT, wax appearance temperature. The prediction of wax deposit formation by simulation models is of fundamental importance for the proper design and operation of petroleum lines. Several wax deposition models have been developed and employed over the years, incorporating different wax deposition mechanisms. In the present work, the wax deposition phenomenon was studied employing a model fluid flowing through an annular test section, built to offer simple and well-defined boundary and initial conditions for the deposition process. Optical access to the interior of the test section allowed for the registration of images of the wax deposit formation. A miniature temperature probe was designed and employed to obtain original information on the temperature profiles within the deposit as it was formed. Also, the probe registered the transient evolution of the deposit interface temperature for different flow rates and cooling rates. The transient formation of a cloud of wax crystals over the deposit interface and carried by the flow was registered by a high frame rate camera. The temperature within this cloud was measured by the temperature probe. The results have shown that the deposit interface temperature evolves from a value equal to the WAT of the fluid measured by microscopy, rapidly reaching a constant value which is intermediate between the WAT and the solution thermodynamic phase change temperature. This information contradicts one of the key assumptions included in the molecular diffusion deposition mechanism, and widely employed in academic and industrial simulation models.

The presence of wax crystals in the solution at temperatures above the WAT indicates that, locally, the WAT might differ from that obtained by microscopy, and that the local prevailing cooling rates could be lower than those imposed at the cold wall, allowing crystal formation above the deposit interface. The data obtained in the present work are of good quality and can be used as a reference to test wax deposition simulation models.

Keywords

Wax deposit; petroleum pipelines; flow assurance; flowing crystals; interface temperature.

Resumo

Linhares, Ricardo Cavalcanti; Azevedo, Luis Fernando Alzuguir. **Formação de depósitos de parafina em linhas de petróleo: investigação sobre as características da interface depósito-líquido**. Rio de Janeiro, 2020. 139p. Dissertação de Mestrado – Departamento de Engenharia Mecânica, Pontifícia Universidade Católica do Rio de Janeiro.

Deposição de parafina em linhas de produção e transporte de petróleo é um problema relevante para a indústria. Perdas significativas de produção e com operações de limpeza, desobstrução ou substituição de linhas ocorrem devido à formação de depósitos das frações mais pesadas do petróleo sobre a superfície interna dos dutos operando nas águas frias típicas da produção em águas profundas. A formação de depósitos de parafina nas superfícies dos dutos pode ocorrer quando o petróleo quente proveniente dos poços é resfriado abaixo de uma temperatura crítica onde há o início da formação de cristais de parafina. Esta temperatura é denominada TIAC – temperatura inicial de aparecimento de cristais. A previsão da deposição de parafina através de modelos de simulação é uma ferramenta fundamental para o projeto e operação das linhas de forma economia e segura. Diversos modelos de deposição de parafina vêm sendo desenvolvidos ao longo dos anos, incorporando diferente propostas para o fenômeno de deposição de parafina. No presente trabalho o fenômeno da deposição de parafina foi estudado utilizando um fluido modelo escoado em uma seção de testes anular construída de modo a oferecer condições de contorno e iniciais bem definidas. Acesso óptico ao interior da seção de testes permitiu a obtenção de imagens de qualidade da formação de cristais de parafina. Uma sonda de temperatura de pequenas dimensões foi utilizada para obter informações originais sobre perfis de temperatura no depósito durante sua formação. Também foram obtidas informações sobre a evolução temporal da temperatura da interface do depósito para diferentes vazões e taxas de resfriamento. A formação transitória de nuvens de cristais sobre a interface do depósito e carregados pelo escoamento foi registrada em imagens de alta frequência. A temperatura no interior dessas nuvens foi registrada pela sonda de temperatura. Os resultados mostraram que a interface do depósito evolui a partir da TIAC da solução medida por microscopia, atingindo rapidamente uma temperatura constante de valor intermediário entre a TIAC e a temperatura termodinâmica de mudança de fase da solução. Esta informação contraria umas das hipóteses fundamentais do mecanismo de difusão molecular, base dos modelos acadêmicos e industriais mais utilizados. A presença de cristais de parafina em solução em temperaturas acima da TIAC indica que, localmente, o valor da TIAC difere daquele obtida por microscopia, e que as taxas locais de resfriamento são inferiores às impostas junto à parede fria, permitindo a formação dos cristais acima dos depósitos. Os dados experimentais de qualidade obtidos no presente trabalho são uma importante referência para o teste de modelos de simulação do processo de deposição.

Palavras-chave

Deposição de parafina; garantia de escoamento; temperatura da interface; cristais em escoamento.

CONTENT

List of figures

List of tables

"Someone is sitting in the shade today because
someone planted a tree a long time ago"
Warren Buffet

1
Introduction

Petroleum is still the primary energy source in the world and, according to the national agency of petroleum (ANP), the oil production in Brazil is growing steadily in the last decades (Figure 1.1). Even though new sustainable energy sources are becoming increasingly important, fossil fuel usage presents the advantage of not being weather dependent and continue to be a competitive energy source. Even for a probable scenario of decreasing usage of fossil fuel energy, it is unlikely that its production and usage will end. Therefore, the investigation of methods to optimize the production and transportation of petroleum is still an important subject matter.

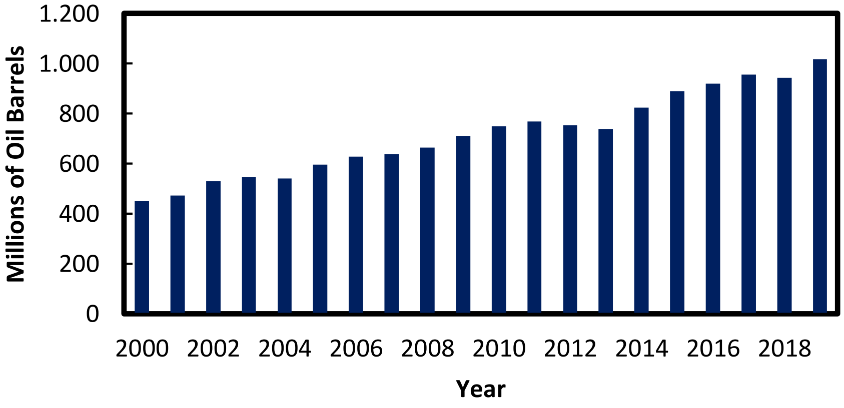

Figure 1.1: Oil barrels produced along the years in Brazil. Data obtained at the Brazilian national agency of petroleum, natural gas and biofuels.

The depletion of onshore reservoirs has caused production of new oil fields to move offshore and, in recent years, the depth of profitable production fields has increased significantly. With this increase, new challenges have also arise and among these, the formation of wax deposits in production and transportation pipelines remains a relevant problem to be addressed by the industry.

In large depths the ocean water temperatures is close to 4 °C. The heat transfer between the hot crude oil and the surrounding water leads to a decrease in the oil temperature. When this crude oil cools down, the solubility of heavier carbon components decrease and after reaching a certain temperature, wax crystals start to precipitate out of the solution possibly forming a deposit on the pipe wall. The critical temperature below which wax crystallization occurs is commonly known as the wax appearance temperature (WAT). The wax deposit formed leads to the reduction of the production rates and to the increase in the required pumping power, issues that result in significant capital losses.

Although every oil contains a certain percentage of paraffin wax, the severity of the wax deposit formation problem depends on the local production characteristics and on the wax content of the oil. A well-known case that exemplifies an extreme situation was the field operated by the Lasmo Company in the U.K in which wax deposition problems were so severe and recurrent that the oil field was entirely abandoned, resulting in estimated losses of 100 million dollars (Singh et al., 2000, Gluyas and Underhill, 2003).

Some known methods to mitigate wax deposition in pipelines are the usage of wax inhibitors, pipeline thermal insulation, internal pipeline coating and electrical heating of the lines, however none of them are ideal solutions. Although wax inhibitors present good results for certain cases, there still does not exist a universal inhibitor that is efficient for all types of crude oils, or even the efficiency of inhibitors has not been widely accepted by the industry.

In cases that a certain deposit has already been formed, the most widely used method for its removal is pigging. This procedure consists on the passage of a device with the diameter larger than the pipe diameter which is fitted with interference and driven by the flow, and expected to scrape and remove the deposited wax. The disadvantage of this method is that in order for the device to perform the cleaning, the oil production needs to be temporally stopped, causing high losses for the companies. Furthermore, for the pigging to be successful, the deposit must not be too thick or too hard, otherwise this could cause the device to be stuck within the lines, requiring costly operations to remove the stuck pig, or even the replacement of the line.

For this reason, the development of reliable wax deposition models is essential in order to assist in the design and operation of pipelines. With the knowledge of the deposit thickness and its hardness at a determined time and location, it is possible to optimize the pigs passage avoiding unnecessary interruption of the production and also avoiding the risk of getting the device stuck in the pipeline. Additionally, in the initial project stages, the knowledge whether the oil field is more susceptible for wax deposition will also aid to perform the correct calculation of the required level of insulation, avoiding unnecessary costs with overestimation in areas with small problems of depositions, and also the underestimation in severe locations which could cause catastrophic results. Therefore, solving this problem would result in a significant cost reduction which could be converted in investments as the implementation of a more sustainable process of exploration and usage of petroleum.

Wax deposition modelling consists basically of three interconnected steps (Zheng et al., 2017). The first is the calculations of the hydrodynamics, in which the velocity profiles and pressure drop are constantly being evaluated as the deposit changes. The second is the thermodynamic modelling by which phase equilibrium equations, components mass balances and constitutive equations are calculated (Huang et al., 2015). And lastly, the deposition mechanisms are important to indicate the amount of the precipitated crystals that will actually form a deposit. Therefore, the knowledge of the relevant wax deposition mechanisms is an essential step for the development of reliable wax deposition models. In the present work we intend to contribute to a better understanding of these deposit formation mechanisms.

With the purpose to facilitate the comprehension of this work, a brief overview of the most common wax deposition mechanisms mentioned in the literature will now be presented. Although many of them have already been discarded as relevant to the deposition process, its understanding is important to better comprehend the works and research strategies devised along the years.

Molecular diffusion

Molecular diffusion has been cited as a possible mechanism for wax deposition. Historically, it was one the first mechanisms proposed, and has been widely incorporated in both academic and industrial models. Although this mechanism is probably always present, its dominance has been questioned in recent studies. This transport mechanism occurs in the liquid form of the oil solution and is responsible for the transport of wax molecules towards the colder pipelines walls. As the pipe walls loose heat to the surrounding cold water, the crude oil in contact with the wall is the first region where a decrease in solubility occur. thus, the location where the first crystals precipitate. As the heavier wax components starts to precipitate out of the solution, a concentration gradient arises from the bulk region to the pipe walls, this concentration gradient is a requirement for the occurrence of this transport mechanism.

The molecular diffusion is commonly described by Fick's law of diffusion, presented in equation 1.1 (Burger et al., 1981),

$$\frac{dG}{dt} = D_m A \frac{dC}{dr} \qquad (1.1)$$

where G is the total mass of wax deposited by molecular diffusion, D_m is the molecular diffusion coefficient, A is the surface available for deposition and dC/dr is the concentration gradient. Even though originally proposed for isothermal binary mixtures, the equation is widely used on the complex wax solutions at non-isothermal conditions.

Shear dispersion

Differently from the molecular diffusion, this mechanism involves mass transport in the solid state. The migration of the precipitated crystals occurs due to shear forces imposed by the fluid flow. Studies of this motion applied to wax deposition have led to the conclusion that the motion is induced away from the wall and, therefore, should not contribute for wax deposition. The works that led to this conclusion will be later covered in the literature review section.

Brownian diffusion

As the shear dispersion, this mechanism could be, in theory, responsible for the lateral transport of solid suspensions. This motion is triggered by the existence of a concentration gradient of solid crystals, where due to the larger number of collisions in the region with higher concentration, the particles tend to move in the direction of the lower concentration region. As the precipitation of wax crystals normally initiates close to the cooled pipe walls, this particles motion would occur from the pipe walls to the centerline.

Gravity settling

This mechanism is related to the gravitational forces that could possibly induce the precipitated particles, denser than the oil, to sediment on the bottom of the pipes. Experiments comparing the total deposition in pipes positioned horizontally and vertically have shown that gravity settling is not a relevant deposition mechanism.

The objective of the present work is to perform well controlled experiments that can serve to help understand the basic mechanisms behind wax deposition and also to serve as a reliable base for validation of wax deposition models. In the present work, a flow loop experimental section was employed to allow for optical access to the interior of the pipe section, enabling original local measurements performed while the experiments were running.

The measurements included the time evolution of the deposit thickness, deposit-liquid interface temperature, deposit temperature profiles and the temperature of the region where suspended crystals were observed flowing over the deposit.

The present text was structured in eight chapters and three appendixes.

In Chapter 1 an introduction to the relevance of the study is presented.

Chapter 2 presents a brief literature review on wax deposition, commenting on what are considered the main works, and the newer contributions to the field.

Chapter 3 describes the experimental set-up, detailing the careful control of the boundary conditions employed.

In Chapter 4 the test fluid characteristics and properties are presented, as well as its WAT and WDT measured by cross polarized microscopy.

Chapter 5 presents the measurements of the deposit thickness for both high and the low cooling rates.

Chapter 6 describes the temperature profile inside the wax deposit, a valuable information to understand if the heat and mass transfer is driven by conductive or convective forces within it.

In Chapter 7 deposit-liquid interface temperatures are measured and the time evolution of this temperature is discussed.

Chapter 8 provides evidence of suspended wax crystals flowing in hot flow conditions above the deposit, and temperature measurements of this region are presented.

Finally, Chapter 9 presents the conclusion and the main findings of this work.

In the appendixes, the calibration of the temperature probe performed with calibrated thermometers and the uncertainties associated to the performed experiments are presented. Furthermore, high-resolution videos of the deposit formation and the wax crystal cloud are commented. Finally, the necessary information and data to validate new numerical models are also provided.

2
Literature Review

The main focus of this review is to discuss the wax deposition mechanisms proposed in the literature, and their relevance for the deposition process. In a first moment a brief historical overview is provided and some key works are mentioned. Afterwards, studies investigating the most common wax deposition mechanisms are presented, and subsequently a recent approach that has been receiving increasing attention is discussed. Finally, important themes for the development of the present work, as the deposit-liquid interface temperature, the influence of suspended wax crystals and the effect of the cooling rate on wax deposition are addressed.

2.1
Early studies on wax deposition

Problems with wax deposition in pipelines can already be found in the early 20th century, however at that time the researches were focused on themes such as the chemical and crystalline characteristics of the wax components, which were not useful in practice for the production of crude oils (Reistle and Blade, 1932). Since then, studies started to be directed to techniques for removing already formed deposits but there was not much attention given to the development of methods to prevent and inhibit wax deposit formation (Hunt, 1962).

Jessen and Howell (1958) seem to be the first to actually investigate the mechanisms behind wax deposition. In their work the authors propose two possible mechanisms, one is the growth of the deposit directly on the pipe surfaces and the other is the incorporation of precipitated crystals to the deposit. Hunt (1962) reached similar conclusions as those of Jessen and Howell. Also through the investigation of the effect of different pipe surface materials on wax deposition, the author finds that the deposition process is initiated on the pipe surface and its subsequent growth is attributed to molecular diffusion. At his work the author also indicates that the surface roughness plays an important role on the deposit formation.

Later, Burger et al. (1981) contributed with an extensive research presenting different possible wax deposition mechanisms. At their work mathematical and experimental investigations were conducted, leading to the conclusion that the deposition occurred by four different mechanisms: molecular diffusion, shear dispersion, Brownian diffusion and gravity settling, being this last one found to be negligible in flow conditions. The mechanisms presented in this work were vastly debated in literature and will be further discussed in next sections.

2.2
Thermodynamic modelling

As the research efforts started to shift towards the prediction of wax deposits formation along the pipelines, a growing body in the literature started to be dedicated to the development of numerical models of wax deposition. One of the first studies to be published presenting a thermodynamic model was Won (1985). In this work the author developed a model for solid-liquid equilibria with an ideal solution assumption, which would later be found to overestimate the deposit, demanding the need of taking into account the non-idealities of the solid-liquid equilibria. The non-ideality here stands for the differences between the molecular interaction of the many different components present in the mixture, which adds more complexity to the numerical modellings.

Throughout the years various approaches have been proposed for the thermodynamic models (Pedersen et al., 1984; Erickson et al., 1993; Lira Galeana et al., 1996; Coutinho et al., 2006), but even though great advancements have been accomplished, there still does not exist a model that satisfies all aspects of the wax deposition.

2.3
Molecular diffusion as a deposition mechanism

Although other mechanisms were studied and investigated, molecular diffusion was largely accepted as the main deposition mechanism (Bern et al., 1980;

Hamouda and Ravnϕi, 1992; Singh et al., 2000; Singh et al., 2001; Lindeloff and Krejbjerg, 2002; Erickson et al., 1993; Ribeiro et al., 1997; Creek et al., 1999).

Singh et al. (2000) presented a few important features of molecular diffusion on the wax deposition. In their experimental and numerical work, the wax deposition process was characterized primarily by the formation of a gel layer, followed by a process of diffusion of the wax molecules into the deposit, leading to the deposit growth and aging. Later, Singh et al. (2001) observed the existence of a critical carbon in which above it the molecules diffuse into the deposit and below it diffuse out.

Azevedo and Teixeira (2003) wrote a critical review pointing out some common adjusting procedures which led to the great acceptance of molecular diffusion as the main mechanism. In this paper the authors discuss the common procedure of tuning the diffusion coefficients in order to fit the total deposition found experimentally, making the molecular diffusion mechanism surely fit the response. It is also important to mention that the molecular diffusion in these models is commonly modelled by Fick’s law which is a model developed for binary mixtures which is not the case for the complex long chains of hydrocarbons contained in crude oils.

Since then, authors started to further investigate this issue and try to find the wax depositions mechanisms that could have been unnoticed or wrongly disregarded.

2.4
Acknowledgment of the contribution of other mechanisms

The evidence that the molecular diffusion mechanism is not appropriate to describe the wax deposition process have been corroborated over the years by different studies. Some of these studies compared the predicted deposit thickness from numerical simulations considering only the molecular diffusion with the measured deposit thickness from experiments. In these works, the deposit thickness were consistently underpredicted by the simulation models based solely on molecular diffusion (Leiroz and Azevedo, 2005); Edmonds et al., 2008). In the work of Leiroz and Azevedo (2005) the experiments were performed with simple geometries and controlled boundary conditions in stagnant fluid and channel flow, while Edmonds et al, used a series of flow loop experimental data for different flow rates.

Another method that provides further evidence of the molecular diffusion not being sufficient to predict and describe the wax deposition process is by verifying the effect of increasing the temperature difference between the hot solution below the WAT and the coolant. As the molecular diffusion is directly proportional to the temperature gradient, the higher the difference the bigger should be the wax deposit thickness. However, some authors in the literature have reported the exact opposite behavior (Janamatti et al., 2019; Hu et al., 2019). The authors observed that for higher temperature differences the rate of wax deposit formation decreases, contradicting the tendencies predicted by other models considering only molecular diffusion and calling attention for the need to investigate other deposition mechanisms. Moreover, an increase of the wax content in the deposit for higher temperature differences was also reported by the authors.

Yang et al. (2020) have conducted an investigation to find if wax deposition occurred under negative or zero temperature differences between the bulk oil temperature and the cooled wall. Under these conditions, according to the molecular diffusion theory, no deposition could occur over the pipe surfaces, as the direction of the temperature gradient is towards the center of the pipe or does not exists, respectively. The authors used a flow loop experiment with a condensate from an actual gas field in Azerbaijan. Differently from previous works in the literature (Cabanillas et al., 2016; Singh et al., 2000) the authors found a significant deposit under such circumstances. As one of the conditions for molecular diffusion to occur is a positive concentration gradient, for Yang et al. the need of another deposition mechanism to describe this process became clear.

Seodarmo et al. (2017) emphasized the need for a better understanding of wax deposition and in their work they investigated four widely used deposition models (Film mass transfer; Equilibrium; the model by Matzain, 1999; the model by Venkatesan et al.,2005) employing different experimental data sets from the literature. The authors concluded that none of these models is able to accurately predict all aspects of the wax deposition. The one they found to be the most accurate was the model of Matzain (1999), however this model was not capable of predicting the deposit aging, making it not adequate for long deposition times where the hardness of the deposit might be critical. These results indicate that some wax deposition mechanisms might be missing in the actual deposition models.

Huang et al. (2011) developed a molecular diffusion based model (MWP) which stays between two bounds, one where no bulk precipitation occurs and the other where all of it precipitates and forms a deposit. The authors use a kinetic coefficient found empirically in order to tune the amount of precipitated wax that contributes to the deposit formation. Even though good results of this model were found and its usage in field applications is large, this kinetic coefficient employed could be hiding other important deposition mechanisms.

Some authors also considered that the deposition process could be a combination of both molecular and thermal diffusion (Soret effect), each having its importance at different stages of the deposition process. Banki et al. (2008) developed a compositional model which the diffusion process is controlled by thermal and molecular diffusion, where both diffusion coefficients vary with time and position. Later, Hoteit et al. (2008) validated the model with experimental data reported in literature(Cordoba and Schall, 2001 and Singh et al., 2000;2001). The authors found that the temperature gradients close to the wall responsible for the thermal diffusion may quickly achieve a pseudo steady state, being more important at initial instants of wax deposition, while the concentration gradient that drives molecular diffusion still changes over time.

Mahir et al. (2019) investigated the mechanism involved in wax deposition for two different solutions, one with only one component, $C_{28,}$ and the other with a binary mixture of 10% C_{28} and 90% of C_{12}. As expected the authors reported that for the single component the experiments could be predicted with only heat transfer mechanisms. However, for the mixture of C_{12} and C_{28} heat transfer was also found to be present accompanied of the processes of mass transfer and solubility of wax. Moreover, the heat transfer was pointed out to have a greater importance in the beginning, for shorter times of wax deposition.

Zheng et al. (2017) attempted to tackle the wax deposit formation by considering the rheological aspects of the deposit, investigating its non-Newtonian behaviour. In their work the wax deposit was considered to form at the moment that the yield stress of the flowing mixture of liquid wax and solid wax was smaller than the shear rate induced by the flow, making the crystals to stop flowing. The method was employed in a field scale pipeline and excellent agreement was found for the deposit wax content as well as for the pressure drop and temperature, proving to be a promising method.

2.5
Wax deposition governed by heat transfer

Along the years several works from the Calgary University group have taken a different approach to the wax deposition process. The group have supported the claim that the deposition is primarily controlled by heat transfer (Bidmus and Mehrotra, 2004; Bhat and Mehrotra, 2004; Parthasarathi and Mehrotra, 2005; Mehrotra and Bhat, 2007; Fong and Mehrotra, 2007; Bidmus and Mehrotra, 2009; Tiwary and Mehrotra, 2009; Haj Shafiei et al., 2014; Haj-Shafiei et al., 2019; Ehsani and Mehrotra, 2019; Ehsani and Mehrotra, 2020).

In their modelling, the heat transfer calculation consists in a series of convective and conductive resistances corresponding to the hot and cold flow streams and the surface in which the deposit occurs respectively. Recently, Mehrotra et al. (2020) wrote a review compiling experimental and numerical studies that supports this approach. The biggest motivation for this theory is the evidence found by their experiments that the deposit-liquid interface temperature is the WAT for the entire deposition time. This theme will be further discussed on the following section.

2.6
The deposit-liquid interface temperature.

An important parameter to help understand the deposition problem which deserves further investigation is the deposit-liquid interface temperature. The divergent assumptions regarding this region end up leading to different conclusions about what are the mechanisms involved in the wax deposition process.

In order for the molecular diffusion to occur, there must be a difference in concentration, which in turn is only possible in the presence of a temperature gradient. The motivation for the authors who believe in heat transfer as the sole responsible for wax deposition, is that the deposit-liquid interface temperature presents a constant value for the WAT for the entire deposition time and therefore, the lack of a temperature gradient could not allow for molecular diffusion to occur.

The first work to be published supporting this idea was Bidmus and Mehrotra (2004) where the authors performed experiments using a draft tube which presented good agreement with their model that considered solely heat transfer at a thermal pseudo steady state. In their work they claim that the deposit-liquid interface temperature was measured to be the WAT. This assumption was proved by comparing the total deposit mass correspondent to different interface temperatures tested in their model with the deposit found experimentally. The value for the interface temperature that presented the smallest error was consistently very close to the WAT. However, no direct measurement of the interface temperature was indeed performed at that time and the associated uncertainties of their experiments were large enough to mask a possible increase in temperature. Later, Bidmus and Mehrotra (2008a; 2008b) performed direct measurements of the deposit-liquid interface temperature under static and sheared conditions with a 3,2 mm temperature probe, finding that for both cases the interface temperature was the same as the WAT under their experimental uncertainties. However, attention must be draw to the size of the thermocouple tip, that could be too big for precisely measuring this region with high temperature gradients, as also to the measuring procedure employed, where the pre-positioned thermocouples could be disturbing the deposition process. For these mentioned reasons, the measurements uncertainties could be too high and an increase in the interface temperature could have been unnoticed.

Recently, Mehrotra et al. (2020) wrote a review showing the evolution of their heat transfer model as well as the experiments that supports this approach. Moreover, in this review the authors emphasized that until now the increase in temperature of the deposit-liquid interface, required for the molecular diffusion mechanism, have not been detected by experimental measurements.

Ehsani et al. (2019a; 2019b) presented an interesting discussion regarding a new WAT that could be formed under different experimental conditions. The authors point out that for some cases, as in the cold flow regime, when precipitation starts to occur the heavier paraffins are the first to leave the solution, and thus the remaining mixture displays a higher concentration of lower alkanes resulting in a new WAT that it is lower than the original one. However, the recent work developed by our research group, numerically predicted an increase in the concentration of heavier wax components in the fluid above the deposit (Veiga et al., 2020), what could indicate the exactly opposite effect, where an increase in the WAT of this region could occur.

Veiga (2017) performed direct measurements of the interface temperature in an annular test section with a temperature probe of 0.2 mm. The test section was built with an external acrylic pipe that allowed the visualization of the wax deposit formation over the internal copper pipe. With their set-up, the interface temperature could be measured with an ongoing experiment where the probe was lowered the exact distance that the deposit thickness indicated. The deposit thickness was measured by a camera positioned in a location right before the measuring mechanism as this last one obstructed the view of the deposit. The author found an indication that the interface temperature increased throughout time but due to the high uncertainties of the measurement this could not be confirmed. Later, Lima (2018) improved the test section by allowing optical visualization at the location where the measurements were taken, thus allowing greater precision. However, the author found that the probe main body that was almost 8 times smaller than the pipe hydraulic diameter was causing a recirculation of the flow and the higher temperature of the bulk flow could be affecting his measurements.

2.7
The presence of suspended flowing wax crystals

The presence of suspended wax crystals flowing above de deposit interface has been reported, casting doubt if the temperature above the interface was lower than the WAT in order for these crystals to exist. Another question related to the suspended crystals is if they have any contribution to the deposit formation.

The most common procedure to investigate the suspended crystals is through cold flow experiments. Cold flow experiments have been performed by many authors (Todi et al. 2006; Merino-Garcia and Correra 2008; Jemmett et al. 2013;Cabanillas et al. 2016; Haj Shaffiei, 2019; Ehsani et al., 2019a) and the presence of flowing crystals over the deposit have been reported when the bulk temperature is below the WAT. However Lima (2018), equipped with a high speed camera, visually identified the presence of crystals flowing in hot flow regime above the deposit interface.

Cabanillas et al. (2016) investigated the influence of the suspended crystals on the wax deposit for a channel flow loop under laminar conditions where the inlet temperatures were below the WAT. Three different boundary conditions were employed by controlling the temperature of the channel wall, which were above, the same as and below the inlet bulk temperature. The last case, with a negative heat flux, was the only one which deposition occurred for both the cases with suspended crystals and without them, where the last one presented higher deposit thicknesses thus proving its influence on wax deposition.

Haj-Shafiei and Mehrotra (2019) also performed experiments to identify if the suspended crystals in cold flow regime contributes to the thickness of the wax deposit. In order to achieve that, the authors compared the final thickness of the deposit in experiments filtering the suspended crystals and others without filtering, and differently from Cabanillas et al., it was found that these ones did not contribute to the final thickness. It is important to mention that this comparison was made by weighting the test section and even though the mass was found to be the same that not necessarily means the deposit thickness was kept the same for the different types of experiments. Besides the continuing investigation in relation to the suspended crystals in Ehsani et al. (2019a), a comparison of the experimental results with a model only considering heat transfer was also presented, and as this one provided values similar to the total deposit, the authors reinforced their theory that the heat transfer is indeed the dominant deposition mechanism, if not the only, in the wax deposition process.

As can be seen from the works described above, the influence of suspended crystals on wax deposition is not a consensus in the literature and requires further investigation.

2.8
The importance of the cooling rate

Another important aspect to discuss is the effect of the cooling rate on the wax crystals formation. It has been reported in literature that depending on how fast the waxy oil is cooled down not only the crystals size is affected but also its appearance temperature.

The crystallization process is known to require a certain degree of supercooling to commence and, for that reason, the WAT tends to be lower than the solid-liquid equilibrium temperature (Andrade et al., 2017). However, Andrade et al. (2017) performed micro DSC and rheometer experiments finding that lower cooling rates provided higher WAT values, becoming closer to the solid-liquid equilibrium temperature, even though not the same. Nevertheless, in the case of the wax dissolution temperature the authors found that when the heating rates tends to zero the supersaturation necessary to dissolve the last wax crystal would no longer exist, thus leading to the exact value of the solid-liquid equilibrium temperature.

This temperature increase was also noticed by Ronningsen et al. (1991) where they investigated the wax precipitation temperature (WPT) of 17 different waxy oils using cross polarized microscopy, differential scanning calorimetry (DSC) and viscosimetry. The difference though was only observed for the polarized microscopy experiments which were claimed to be the most precise method and the most conservative as its WAT values were lower than those for the other techniques.

This trend of an increase in the WAT with a decrease on the cooling was also reported by other authors (Japper-Jaafar et al., 2016; Jiang et al., 2001; Paso et al., 2009; Kasumu et al., 2013) that proposed a linear equation to find the WAT depending on the cooling rate and the concentration of wax in the oil. Even though the equation presented good results for the experimental data presented at their work the authors alert that it may not be valid for others waxy crude oils. The cooling rates employed were between 0.05 to 0.4 °C per minute.

As the previous mentioned authors, others have also considered a linear correlation between the cooling rate and the wax appearance temperature, however, Ruwoldt et al. (2018) mentions that this assumption might be an over simplification. In order to investigate this subject, they performed experiments using differential scanning calorimetry, cross polarized microscopy and viscosimetry, finding a nonlinear behaviour for cooling rates between 2 °C/min and 20 °C/min, while the linear assumption was only valid for cooling rates between 0.5 °C/min and 2 °C/min.

Regarding the structure of the wax crystals, Cazaux et al. (1998) performed an investigation using different methods: rheometry, x-ray diffraction, small angle x-ray scattering and microscopy. In their findings, the authors pointed out that the most important parameters for the structure of the waxy oil gel, such as size, shape and number of paraffin crystals are dependent on the temperature and cooling rate history.

Haj-Shafiei et al. (2019) used confocal laser scanning microscopy to study the structure of the wax crystals and their growth kinetics. The authors identified that in a first moment for low cooling rates the crystals were bigger and the void fraction was higher, however after reaching a certain final temperature the fractal dimension of the crystals was the same for every different cooling rate employed, indicating that the final structure of the crystals are similar for low temperatures. Haj-Shafiei and Mehrotra (2019) further investigated this issue by verifying the influence of different cooling rates on the wax deposition process but at this time a cold finger apparatus and a flow loop were employed. In their experiments the authors reported that the wax deposits were smaller as the cooling rate decreased and also as the temperature difference between the solution and the cooled wall temperature was smaller.

2.9
Conclusions and contributions of the present work

As it is possible to see in this brief literature review, there is still considerable disagreement regarding the main mechanisms involved in the wax deposition process and the physics behind it is still an open subject in the literature, requiring further investigation of this subject.

In the present work, a laboratory-scale pipe section was used to perform experiments under well controlled conditions to serve as a reliable base for validating new wax deposition models. Experiments for high and low cooling rates were performed and the differences between the deposit thicknesses and characteristic temperatures were compared. Furthermore, reliable measurements of the deposit-liquid interface temperature were obtained in the present work in order to provide relevant information on its temporal evolution. Information regarding the suspended wax crystals flowing above the interface in the hot flow regime are also provided.

3
Experimental Setup

The experimental set up was built in the Fluids Engineering Laboratory (LEF) of the Pontifícia Universidade Católica do Rio de Janeiro. The set-up was previously described in details at Veiga (2017) as well as in our recently published paper (Veiga et al., 2020), thus further details of this configuration can be found there. In this work, an overview of the important features of the test section and a description of the modifications made will be detailed.

The schematic view of the test section employed in this work is presented in Figure 3.1. The main part of the set-up consisted of an annular assembly that will be later detailed in this section. This annular pipe section was placed inside a tank filled with water which was thermally controlled by a thermostatic unit. The waxy solution was stored in a stainless steel cylindrical tank which was heated and homogenized by a heating plate with a magnetic stirrer positioned under its bottom. A volumetric pump was responsible for pumping the waxy solution at a constant flow rate through the annular section after passing by a filter positioned at its entrance. Two thermostatic baths were used to alternate between pumping hot and cold water inside the internal pipe and a set of four ball valves were used to perform this transition. A temperature probe was located at 80% of the total length of the annular assembly. The arrows displayed in the figure indicate the flow direction of the fluids and, as it is shown, in the experiments performed the water pumped inside the annular section was always flowing concurrently with the waxy solution.

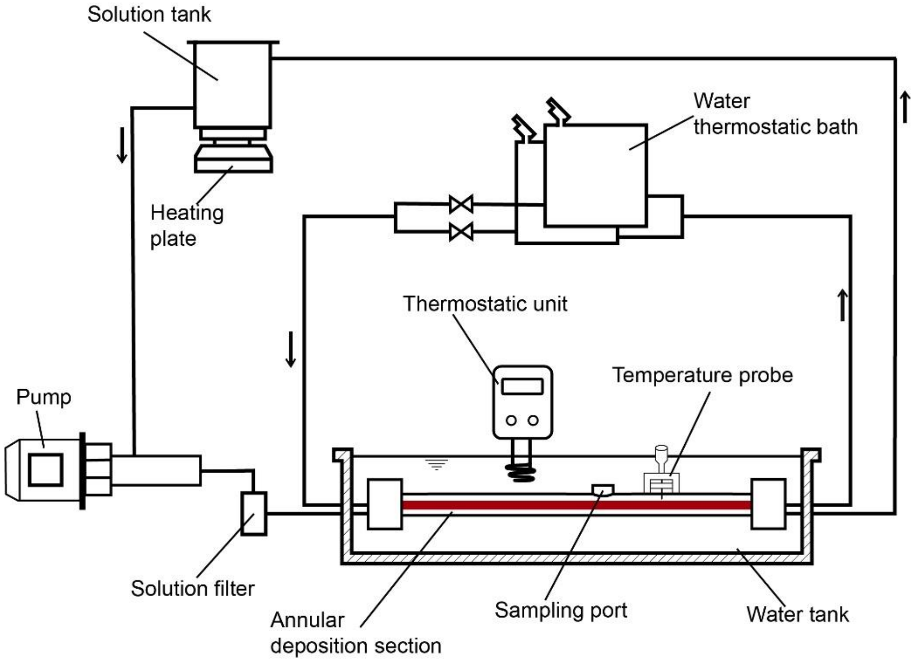

Figure 3.1: Schematic view of the test section employed in the wax deposition studies.

Each of the components presented in Figure 3.1 will be detailed in the following subsections.

3.1
The annular test section

The main objective of our experiment was to build a set-up that could provide real time data acquired while the experiments were running, which could be used to both contribute to the understanding of the deposition phenomena and to serve as benchmark for simulations models. The set up devised to achieve this goal was an annular assembly formed by a copper pipe with 19 mm of external diameter mounted concentrically in the interior of an acrylic pipe of 34 mm of internal diameter, thereby forming a gap of 7.5 mm (Figure 3.2a). Before the beginning of the test hot water would flow inside the copper pipe and hot wax solution was pumped through the annular region formed between the copper and the external Plexiglas wall. The experiment began when, through a valves maneuver, or by the imposition of a cooling ramp, cold water started to flow inside the copper pipe, then, the surface in contact with the flowing wax solution started to cool down and wax deposit starts to formed around the copper pipe as shown in Figure 3.2.

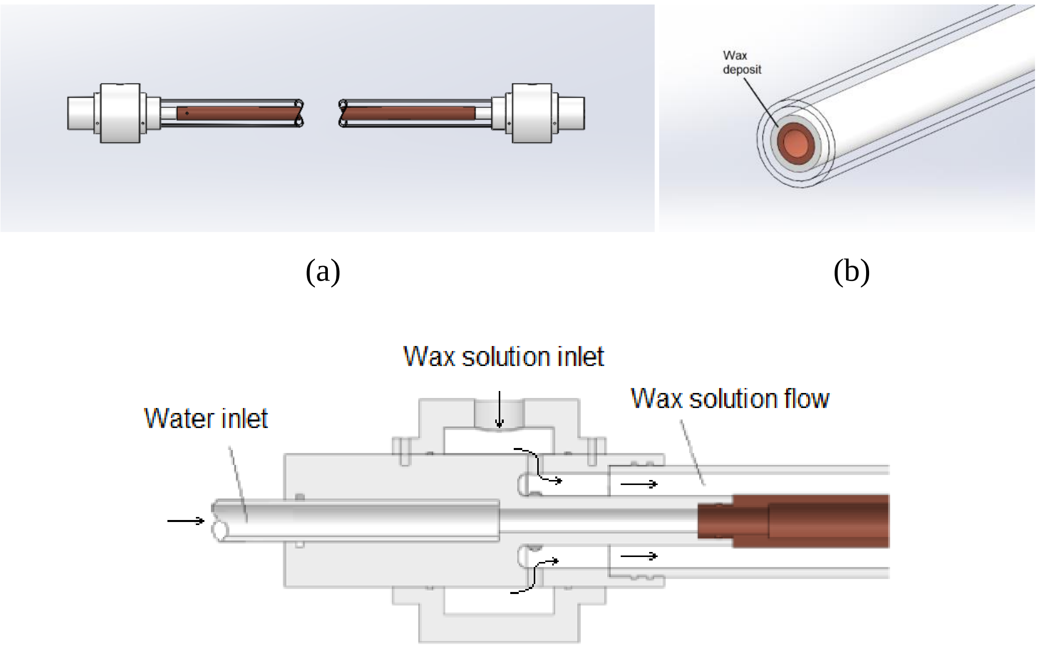

(a) (b)

(c)

Figure 3.2: Schematic view of the annular deposition assembly. (a) side view of the assembly. (b) representation of a wax deposit around the inner copper tube of the annular assembly. (c) detail of the cross section of the left supporting part and flow distributor

The assembly built at the entrance to direct the water and the wax solution to their spaces can be seen in Figure 3.2(c). This mechanism shows that water flowed directly inside the copper pipe and wax solution entered in a round chamber with 6 small orifices along its circumference. These evenly distributed holes enabled a uniform wax solution flow entrance at the annular region. The assembly was made of polypropylene, a non-conductive material that would allow deposition only over the copper pipe, not interfering in the experiment. The junction of the copper and the polypropylene was carefully machined so that there were no bumps or discontinuities.

This assembly previously described was placed inside a rectangular tank filled with hot water (Figure 3.3). The purpose of that was to provide well controlled boundary conditions for the experiments and also to avoid wax deposition on the external tube which could block the visualization of deposition over the copper pipe. The water inside the tank was heated and controlled with a Thermo Haake DC30 circulating unit. The tank sidewalls were made of transparent plexyglass in order to allow for visualization and image acquisition of the wax deposition process taking place.

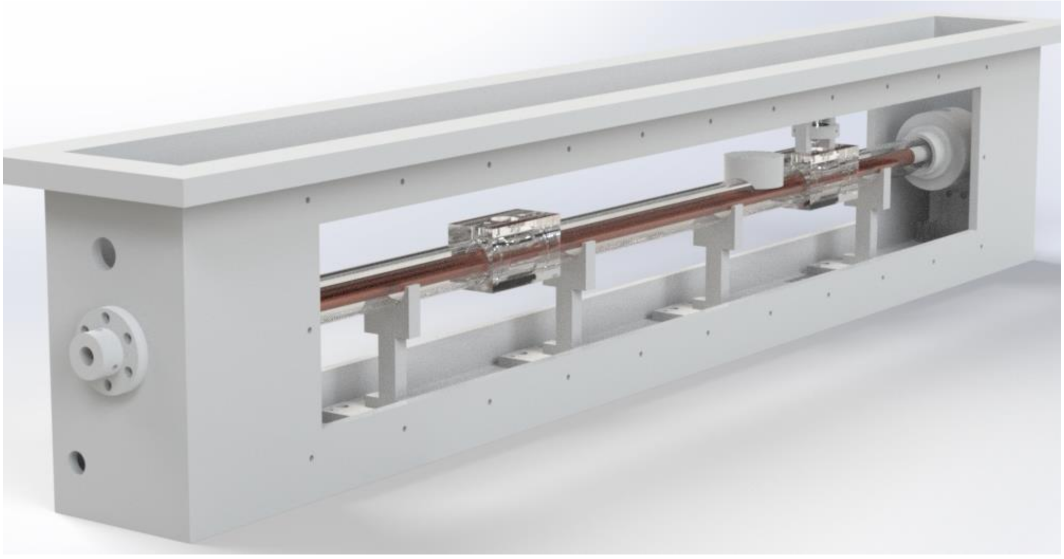

Figure 3.3: 3D image of the water tank with the concentric pipes inside.

A volumetric pump was used to pump the wax solution stored in the reservoir inside the annular section while the thermostatic baths pumped water inside the copper pipe. The circulating unit kept the water around the annular section at a controlled temperature and a sampling port and a temperature probe were used for measurements. Heating tapes were used surrounding the tubes in order to prevent wax deposition along the lines. Also, fiber glass insulating sleeves were used to avoid heat losses.

3.2
Wax solution reservoir

The reservoir was made of stainless steel with a total capacity of 36 liters but was only filled with 23.2 L of the oil solution. The reservoir volume was calculated considering the maximum deposit expected on the annular section. The total depletion of the experiments performed were calculated to be in the order of 8%, which corresponds to a final wax fraction in solution of 18.7%.

Below the reservoir a heating plate with a magnetic stirrer was placed to homogenize the wax solution composition and to control its temperature. Heating tapes were also used on its surroundings in order to stabilize the temperature and avoid heat losses. The tank was closed with an acrylic lid to ensure the solution did not change its composition over time.

3.3
The volumetric pump

The pump used to circulate the wax solution through the annular section was the progressing cavity pump Netzsch NEMO021. This is a type of positive displacement pump that allows to control the exact volume of wax solution injected in the test section, providing an important boundary condition to simulation models. A frequency inverter was used to control the flow rate. The model chosen was the cfw08 from WEG with a frequency range of 0 to 60 Hz. The maximum flow rate produced by the pump was 2.1 m^3/h however in this work the maximum flow rate used was 0.61 m^3/h.

The pump was calibrated by the gravimetric method employing kerosene at 40◦C. The calibration curve relating the pump frequency of revolution to flow rate is presented in Figure 3.4.

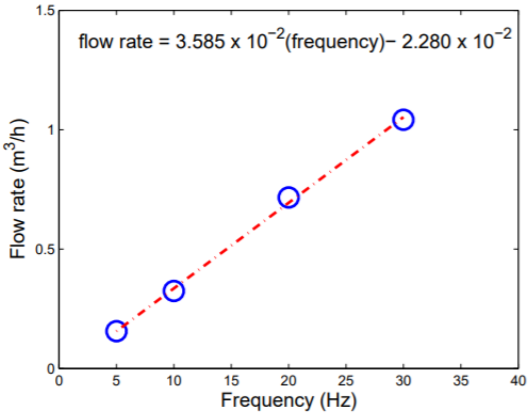

Figure 3.4: Volumetric pump calibration curve from Veiga (2017).

At the exit of the volumetric pump a 2 μm filter was installed to prevent the entry of solid wax inside the annular region. Furthermore, heating tapes and wool insulation were used surrounding both the pump and the filter, in order to avoid wax crystals formation.

3.4
Temperature control

As mentioned before, the test section was carefully instrumented to assure that the experiments provide well defined boundary conditions for the simulations.

In this subsection the system used for controlling the temperature of the experiments will be presented.

For the annular region where the hot oil solution flowed, two thermocouples were used, one positioned at the beginning and the other at the end of the pipe. For the water tank surrounding the annular section, a thermocouple was simply placed inside the water to assure that the circulating unit Haake DC30 was providing reliable values.

In order to control the spatial and temporal evolution of the cooling wall without disturbing the flow, eleven chromel-constantan thermocouples were placed inside the copper pipe. The pipe was machined to have 11 circular holes with 4 mm diameter, where copper plugs were inserted. These plugs were drilled with a 1 mm hole allowing the insertion of the thermocouples, which were fixed in position with a conductive epoxy resin. Details of the assembly are shown in Figure 3.5.

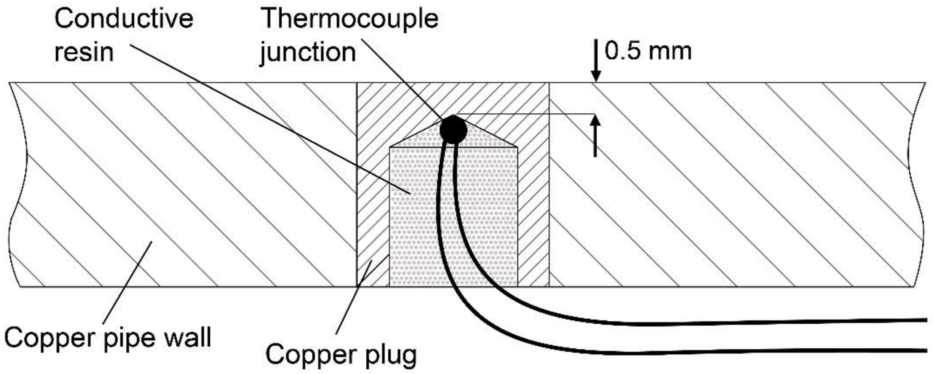

Figure 3.5: Detail of the thermocouple probe installation for measuring the copper pipe surface temperature.

Two different thermostatic baths were used for pumping the water inside the copper pipe. The first one was the Haake A25 from thermofisher scientific with the Pc200 circulating unit and the other was the Huber C-410 with the Pilot one controller.

Rubber hoses were used for directing the waxy solution inside the test section and heating tapes were used surrounding the tubes in order to prevent wax deposition along the lines. Moreover, fiber glass insulating sleeves were used to avoid heat losses. The heating tapes were connected to a variable autotransformer which a PID controller turned on when the temperature of the thermocouple positioned inside the lines was lower than the value set.

3.5
Temperature measurement mechanism

A mechanism was developed to precisely position the thermocouple tip inside the annular region while the wax deposition process was taking place. The mechanism can be seen in Figure 3.6 and consists mainly of a micrometer head attached to a bearing, which converts the translation and rotation movement in translation only, moving vertically the PVC platform fixed to it. The temperature probe was fixed below this platform and through this vertical movement it was inserted in the annular test section. The advantage of the micrometer head was not only the fine resolution of its motion, but also the possibility of making measurements of the deposit thickness inside the annular region while the experiment was running.

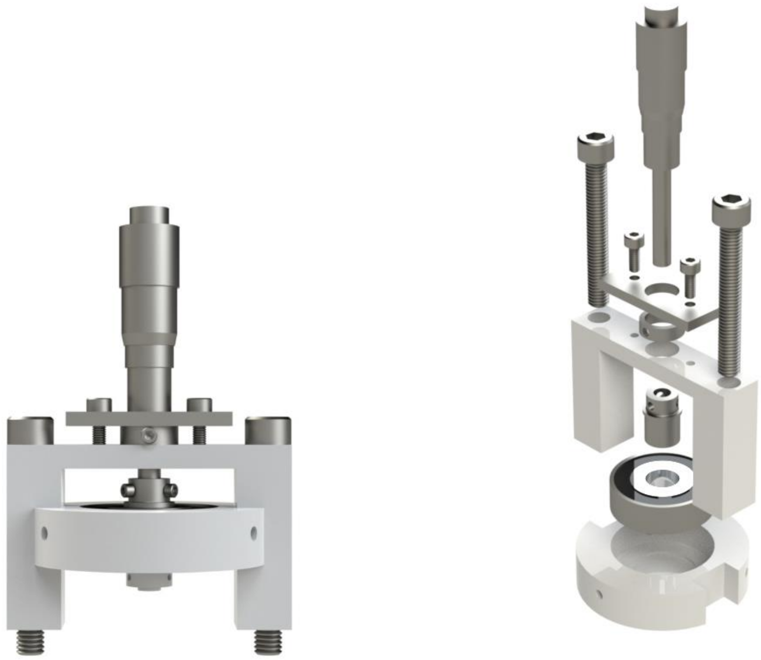
(a) (b)

Figure 3.6: Measuring apparatus (a) Front view (b) Exploded view.

The mechanism was located at 80% of the axial pipe length, where an acrylic block was machined as shown in Figure 3.7. This block was important not only for allowing a better visualization avoiding distortions of the circular pipe but served also as a base for the measuring mechanism.

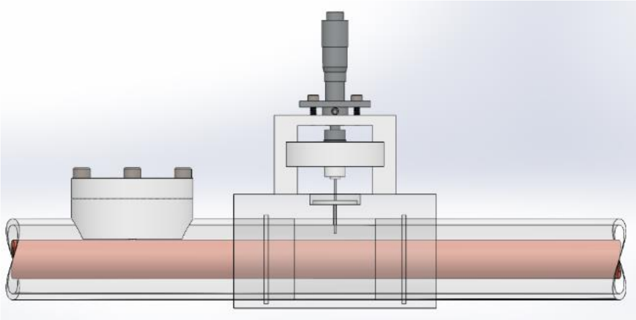

Figure 3.7: Measuring section located at x/L=0.8.

3.5.1
Temperature probe

During this work the temperature probe had a few modifications in order to fit different kind of experiments and to provide more accurate results. All of the probes were built with chromel-constantan thermocouples (type E) and their differences and peculiarities will now be described.

1. In the first probe built, each thermocouple wire had 0.076 mm diameter and after welded together they formed a 0.2 mm measuring tip. The thermocouple was positioned inside a glass tube of 1 mm external diameter and 0.8 mm internal diameter. As shown in Lima (2018), the 1 mm tube was causing fluid recirculation and the solution flowing from the bulk could be being redirected to the tip of the probe where all the measurements were being acquired. In order to avoid this issue, the tip of the probe was moved 1.5 mm away from the 1 mm tube, fixing the problem (Figure 3.8a).

2. The second probe was fabricated to increase the precision on the measurements of the interface temperature. Due to the high temperature gradient in this area a new bare wire thermocouple with a 0.1 mm welded junction from Omega engineering was used. To avoid the wires from touching each other, each of them was put into a 0.25 mm glass tube which in turn were fixed inside a 1 mm glass tube that was essential for sealing the orifice that this assembly would enter.

3. The third probe was similar to the second one but the 1 mm tube was moved further away from the tip of the probe as it was found that when the bigger glass tube of 1 mm diameter reached the wax deposit interface, this one could affect

the temperature profiles experiments (Figure 3.8b). The evidence of this disturbance will be later discussed on the results section of chapter 6.

In short, the first probe was found not to provide accurate results, the second probe was useful for the deposit-liquid interface temperature experiments and for measuring deposit thickness, but unable to make the deposit temperature profiles and, finally, the third probe was the optimal one that was able to perform all experiments presented in this work.

From now on in this work, the probes detailed above will be referred as probe 1, 2 and 3 respectively.

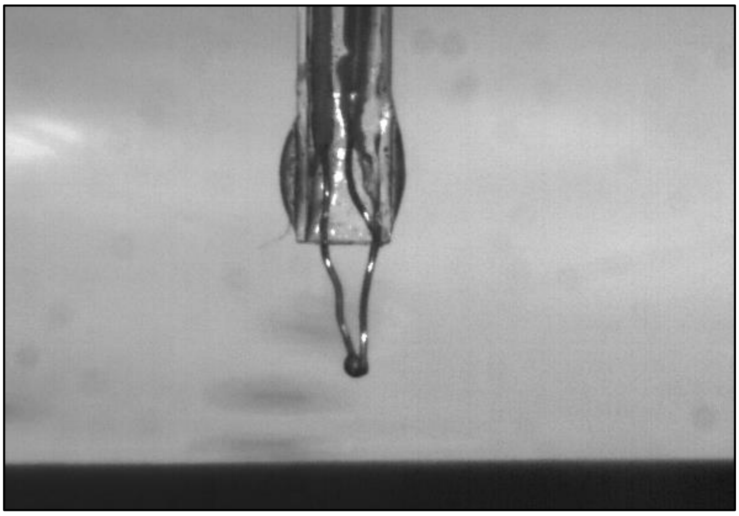

(a)

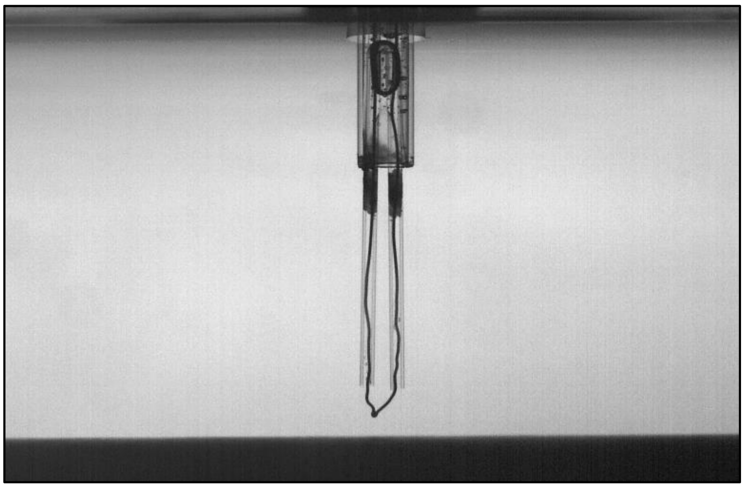

(b)

Figure 3.8: Different probes developed throughout the present work with the following thermocouple junction size: (a) 0.2 mm (b) 0.1 mm.

3.6
Camera

The camera used in the experiments was the Redlake Motion Pro X3 high speed camera. Its full resolution was 1280 x 1024 and it has a sensor array area of 12μm x 12μm. The camera had a 4 Gb onboard memory and was able to make videos of 1000fps.

The camera was mounted over a XY coordinates table and a horizontal motor-driven trail parallel to the test section that allowed the camera to move along the entire test section. This mounting was essential as the field of view was very narrow due to the apparatus used that will be further described and allowed fine adjustments on the image focus.

The lens used was the Nikon AF Micro Nikkor 105mm f/2.8. Extension rings were used in order to increase the image magnification. For the interface temperature experiments, 1 extension ring of 27.5 mm and a c-mount was used. For the wax crystals cloud tests another extension ring of 27.5 mm was added to increase magnification. With the addition of these extensions, the light exposure was naturally decreased and in experiments with a high frame rate this illumination was even lower.

The test section illumination was a critical aspect for the proper visualization of the wax crystals flowing above the wax deposit and also for proper identifying the probe entrance inside the deposit interface. It was employed two kinds of illuminations to acquire good images, a backlight and a frontal light. A built in house led panel provided the backlight and the frontal illumination was obtained from the microscopy halogen light source KL 1500 LCD from Zeiss. While the backlight was important to bring contrast between the pipe and the background, the frontal light was important to make a direct illumination over the deposit making it stands out on the images. For the images where the suspended wax crystals were the goal, the frontal illumination was critical as it had to be precisely positioned over them in order to make them reflect and not appear as a dark blur.

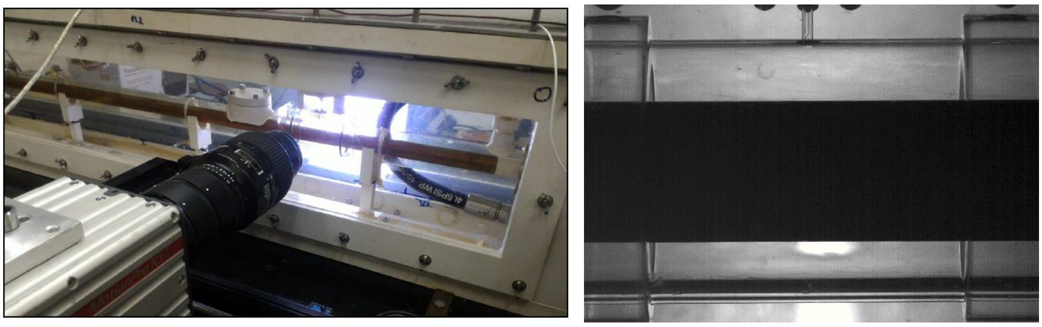

(a) (b)

Figure 3.9: (a) Picture of the camera imaging the wax deposit formed in the annular test section positioned inside the water tank. (b) Sample picture of the wax deposit interface (dark region).

3.7
Data acquisition

The instrument used for acquiring the thermocouples temperatures was the data logger unit from Agilent Technologies model 34970A with an USB port to communicate with the computer. A multiplexer board with 20 channels made possible obtaining simultaneous data along the annular section. For temperature measurements it was used the board internal reference for type E thermocouples. The data logger has its own software, Benchlink data logger pro 3, which was used for real time monitoring and data exporting. The data was exported as csv files and were later post-processed with Microsoft Excel.

4
Test Fluid

One of the distinct features of this work is the test fluid solution used. The test fluid consisted of a mixture of 20% solvent, C_{12}, and a wax with hydrocarbons ranging from C_{22} to C_{39}. The solvent was obtained from Shangai IS Chemical Technology and the paraffin wax was obtained from distillation of the crude oil at the Flow Assurance Laboratory at the Center of Research and Development (Cenpes), from Petrobras. In the literature what is commonly found is the usage of solvents such as querosene that has a long hydrocarbon array mixed with the chosen wax composition which have common chains. The fact that the solvent used at this present work was apart from the wax carbon range made it possible to identify the exact amount of solvent that was inside the wax deposit at a given time. Moreover, the usage of a simple fluid with known properties make it easier to precisely reproduce the thermodynamic calculations on simulations, thus providing better comparisons with the experiments. The chromatography technique was performed to obtain precisely the amount of each component present in our test fluid and furthermore the separation between the solvent and the wax paraffin can be better seen on the results presented in Figure 4.1.

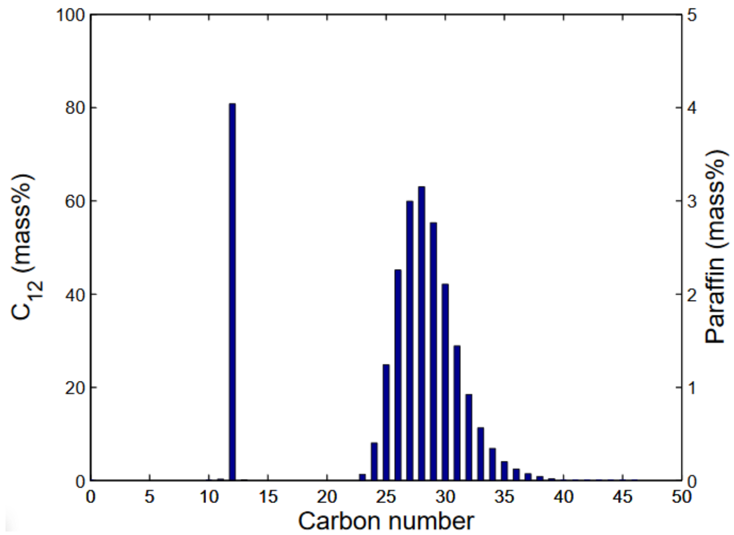

Figure 4.1: Mass based chromatography of the test fluid. Figure from Veiga et al. (2017).

The density of the test fluid was 747.8 kg/m^3 at 40 °C and Figure 4.2 shows its variation for different temperature values.

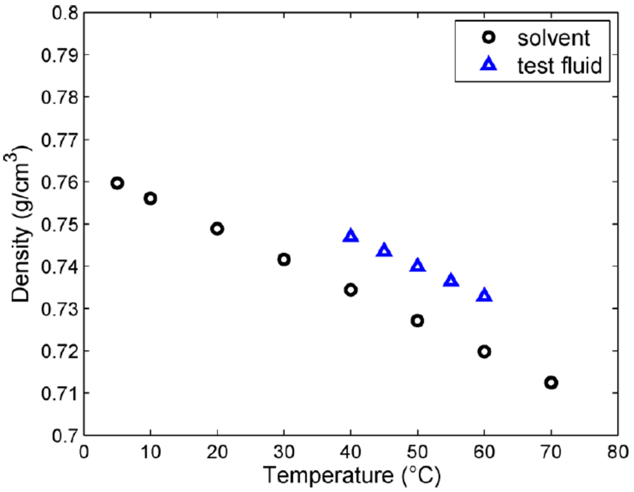

Figure 4.2: Density variation with the temperature of the test solution and C_{12} solvent. Figure from Veiga et al. (2017).

Viscosity measurements of the test fluid were also measured previously by Veiga et al. (2017). The Anton Paar Physica MCR-301 rheometer was used with a Couette geometry. Three different shear rates were employed at the tests and these measurements are presented in Figure 4.3. For temperatures above the WAT it is possible to see that there is no significant change of these values. The shear rate of the experiments performed at the annular test section were estimated to be between 80 s^{-1} and 120 s^{-1} and at 38.6 °C the viscosity is 1.463 mPa.s.

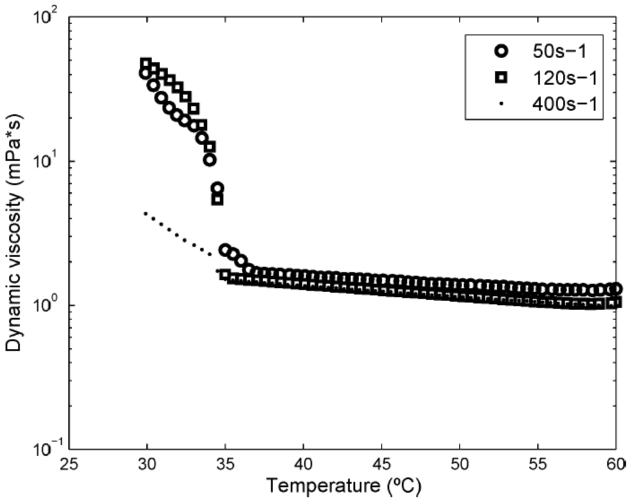

Figure 4.3: Temperature variation of the viscosity of the test fluid for three shear rates. Figure from Veiga et al. (2017).

4.1
WAT and WDT measured by microscopy

Simultaneously with the annular test section experiments, an apparatus was developed to obtain reliable measurements of the wax appearance temperature (WAT) and wax disappearance temperature (WDT). These are important temperatures for the understanding of the wax deposition phenomena. As many of the assumptions and interpretations of the results of the annular section regarding the interface temperature and deposit temperature profile depends on the WAT and WDT, it is imperative to obtain precise and reliable values for them.

In literature many methods can be found for the determination of the WAT and WDT. A few of the most commons are the differential scanning calorimetry, viscosimetry, and cross polarized microscopy. The last one is considered one of the most accurate and conservative because it is possible to see the first wax crystal to form (Ronningsen et al., 1991), thus this method was chosen for our measurements.

A common method to cool down or heat up the samples is through a Peltier plate, however in order to avoid external temperature influence over the samples a special apparatus was developed. This new cross polarized microscopy set-up was designed so as to keep the samples at a uniform and well controlled temperature also allowing an easy and reliable investigation of the effect of different cooling rates on the WAT and WDT values. For the present work, however, only a 0.3 °C/min was used for the cooling and heating of the samples.

The device presented in Figure: 4.4 consist of a main rectangular body covered on both sides by transparent acrylic plates to allow for a bottom to top illumination, essential for cross polarized microscopy experiments. The inferior acrylic plate was glued on the main body while the top one was fixed with screws pressing the plate against an o-ring, providing an easy way to access the interior of the apparatus. Figure: 4.4(b) illustrate an exploded view of the mechanism showing the modules which are easily removed and built from the outside. The tubes filled with waxy oil solution are placed over the “H” format support and pressed over by a complementary part to avoid the samples from moving. This assembly was built over trails that allowed for an adaptation to fit different sizes of samples.

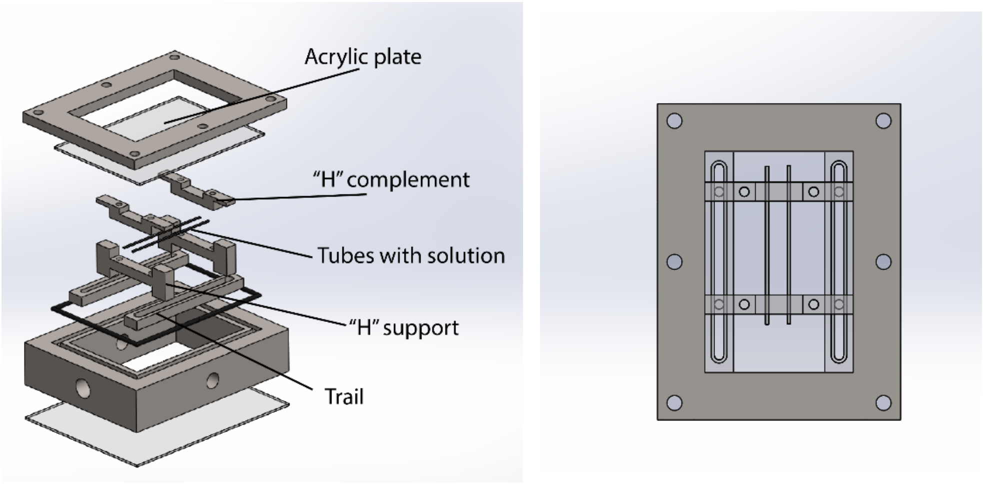

(a) (b)

Figure: 4.4 Apparatus developed for cross polarized microscopy measurements (a) exploded view (b) Top view

The thermostatic bath used for pumping the water inside the apparatus was the Haake A25 of Thermofisher scientific which allowed setting the cooling and heating ramps to the corresponding desired rates. A chromel-constantan thermocouple (type E) was positioned inside the apparatus close to the tubes filled with oil with the intent to have a higher precision of the exact temperature which the wax crystals appears or disappears. The thermocouple was connected to the data logger of Agilent Technologies, model 34970A. In order to obtain more precise results, the data logger was synchronized with the Axiocam MRC which was attached to the Stemi 2000-C microscope from Zeiss. This method allowed a careful analysis of the images at the end of the experiments to determine at which time the last crystal disappeared (WDT) or the first crystal appeared (WAT), avoiding subjectivity on its determination. The camera acquisition rate was 0.2 Hz. The lighting was also provided by the microscopy halogen light source KL 1500 LCD from Zeiss and as mentioned before, was made from bottom to top in order to reflect the first crystals that appeared.

The internal diameter of the glass tubing was of 0.8 mm and its filling was made by immersing the tube directly inside the annular test section solution reservoir. It was ensured that prior to the filling the reservoir was well mixed by the magnetic stirrer. The temperature that the samples were acquired was 50 °C. After removing the tube horizontally from the reservoir, the waxy oil inside the tube quickly became solid, avoiding any kind of leaking and facilitating the sealing process. With this method of filling it was common that the very ends of the tube kept a small empty part. For this reason, the tubes extremities were cut to be completely filled at the time they were sealed. The sealing of the extremities was attempted in three different ways: With 10 minutes epoxy mixture, caulk and acetic silicone. The last one was found to be the most effective and thus it was used for the experiments presented in this chapter. After waiting the silicone to dry, the tubes were positioned over the "H" support and the apparatus was properly closed.

A concern raised with this experiment was if the heating and cooling rate of the thermocouple positioned close to the tubes would faithfully represent the temperature inside them. For that reason, an experiment was performed to verify if the difference really existed. Two different tubes were prepared, one with the waxy oil and the other with dodecane, the solvent, and a thermocouple was placed inside each of them. The choice of filling one of the tubes with C_{12} was due to the possibility that during the process of crystals formation the crystals heat could be released in the tube with the waxy oil, and consequently affect the results.

As the intent of this experiment was to verify if the internal thermocouple temperature could follow the external temperature, the highest cooling and heating rates that our equipment could perform were employed as they would be the most critical cases. The cooling rate employed was 0.55°C/min and the heating rate was 0.9°C/min. After keeping the water flowing inside at 45 °C for 15 minutes the cooling ramp was started lowering the temperature to 30°C and the heating ramp was performed right after it. The results for the cooling and the heating ramp are presented in Figure 4.5Figure 4.6 respectively. It can be seen that there is no difference between the ramps of the external thermocouple and the ones placed inside the glass tubes, in other words, the external thermocouple represents exactly the cooling and heating ramp inside the tubes. For each figure an enlarged view is also presented to show the small differences between the thermocouples.

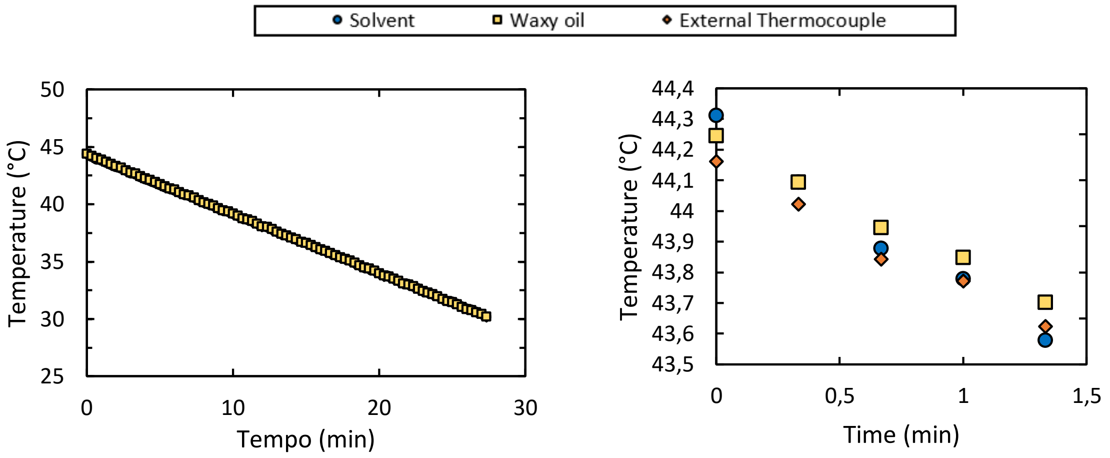

(a) (b)

Figure 4.5: Cooling ramp of 0.55°C/min measured by thermocouples in different locations.

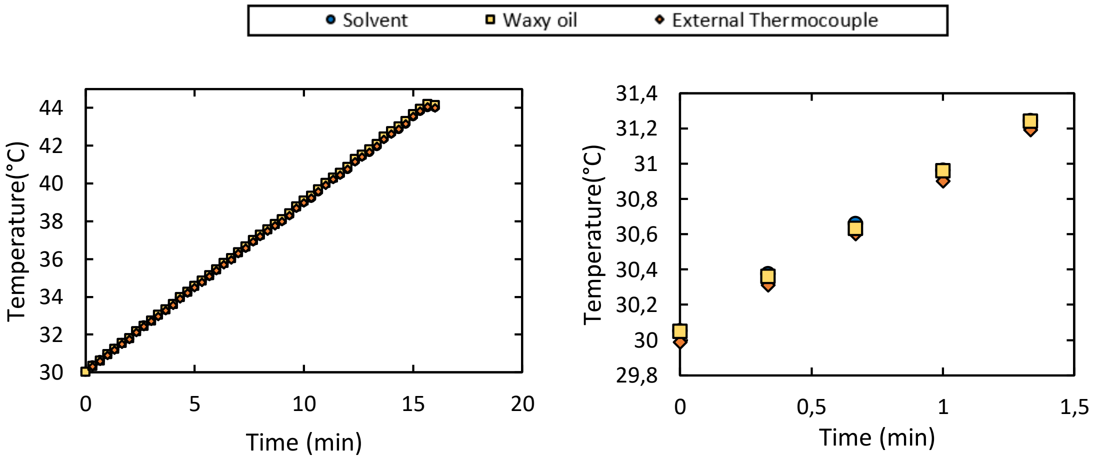

(a) (b)

Figure 4.6: Heating ramp of 0.9°C/min measured by thermocouples in different locations.

One could wonder why the experiments to find the WAT and WDT were not performed with the thermocouple inside the tubes in the first place, but the disturbance caused by the intrusion of a thermocouple close to the waxy oil tube could affect principally the WAT, acting as nucleation site. Moreover, for cross polarized microscopy to be successful there could be no barrier to avoid the light coming from the bottom, and thus if crystals appeared over the thermocouple it would not be possible to see them. In order to avoid such problems, this method was only used to verify the equality of cooling and heating rates.

The thermal history is known to influence the results of WAT and WDT (Ronningsen et al., 1991; Chang et al., 2000; Zhao et al., 2012) and for that reason, before every measurement a reset was performed flowing water at 60 °C inside the apparatus for 1 hour. Afterwards, the temperature was lowered for 40°C at a cooling rate of 0.5°C/min and kept at it for 15 minutes. Only then, the cooling ramp of 0.3°C/min was set lowering the temperature from 40°C to 30°C.

The results of the measured WAT and WDT are presented in Table 4.1. Three experiments were performed for each case and the uncertainty of the measurements was ±0.3°C. It is interesting to comment that the WAT value obtained by the cross polarized microscopy was very proximate to the temperature which there was a sudden increase on the dynamic viscosity values presented on Figure 4.3.

Table 4.1: WAT and WDT obtained by the Cross polarized microscopy method.

WAT	WDT
35.6°C	37.5 °C

As an additional information, it is worth mentioning that during the WAT and WDT experiments a few measurements were performed without resetting the thermal history of the samples and this was found to cause a gradual decrease on the WDT after each measurement varying the temperatures between 40 °C to 30 °C and 30 °C to 40 °C. However, since this was not the focus of the present work this behavior was not further investigated.

5
Deposit thickness measurements

The results obtained for the transient evolution of the wax deposit thickness will be presented in this chapter. These results describe the characteristics of the wax deposition formation for the three different values of the Reynolds numbers investigated. Due to the transparent test section design described in chapter 3, the experimental technique employed provided information on the deposit growth, captured while the experiments were running. This is a significant improvement over other experimental techniques reported in the literature that require the interruption of the flow and the disassembly of the test section to gain access to the deposit in order to conduct thickness or weight measurements. For this reason, the data obtained is considered of high quality and, besides providing valuable information on the deposition phenomena, can be used for validating deposition models.

The experiments were conducted for three values of the Reynolds number and for two different cooling rates of the inner copper wall. The measurements were performed at a fixed axial position, $x/L = 0.8$, the position of the probe. The experimental procedures employed are described next.

5.1
Experimental Procedure

In preparation for a data run, the solution kept in the stainless steel tank and filling the test section needed to be melt, since at the laboratory temperature it was in the solid state. This was achieved by activating the heating and stirring plate under the tank, setting it initially at an elevated temperature of approximately 130^{o}C. The heating tapes surrounding the rubber hoses were also activated in order to melt the wax solution and allow for the solution to flow freely. Heating tapes mounted around the stainless steel tank side wall were also activated to provide additional heat to the solution. The tank where the annular test section was installed was filled with water and the Haake DC30 temperature controller was turned on and set 38.6°C.

While the wax test solution was being heated in the test section, the temperatures of the two thermostatic baths were set, one at a hot temperature level of 38.6 °C, and the other at a cold temperature level of 12.6 °C. In order to help stabilize the temperature of the solution in the test section, the hot bath valve was kept open to allow for hot water flow through the inner copper pipe of the annular test section.

After approximately 1 hour, the wax was already completely melted and the heating plate temperature could be lowered to 40°C. Thermocouples inside the rubber hoses, water tank and solution reservoir were monitored to assure that the wax was completely in the liquid state presenting no risk of flow obstruction. After that, the volumetric pump could be safely turned on at a desired flow rate.

The flow rate set at the pump corresponding to the desired Reynolds number was determined by equations 5.1 and 5.2.

$$Re = \frac{\rho . v . D_h}{\mu} \qquad (5.1)$$

Where Dh is the hydraulic diameter calculated as the difference between the external and internal diameter, so the Reynolds is written as,

$$Re = \frac{4. Q}{\pi (D_e + D_i) . v} \qquad (5.2)$$

The desired flow rate in m^3/s was set in the pump controller with use of the calibration curve shown in Figure 3.4. It is important to mention that this Reynolds number corresponds to the initial experimental conditions, with all the properties evaluated at 38.6 °C and no deposit formed yet. The Reynolds numbers investigated in the present work were 736, 1440 and 2073, which converted to the value at the frequency inverter corresponded to 6.5 Hz, 12.1 Hz and 17.15 Hz, respectively.

Also, prior to the initiation of all experiments, the temperature probe was retracted inside the acrylic wall in order to avoid the promotion of any disturbances on the flow and on the wax deposit.

After the preparation procedure described, the camera was positioned imaging at the probe location, and the back light panel was turned on.

The deposit thickness was measured with the mechanism described in section 3.5. The first step in the measuring procedure was to determine the reference position by touching the copper pipe surface with the probe tip and registering the reading of the micrometer barrel. After that, the experiment was initiated by allowing cold water flow to the interior of the copper pipe. The cooling rate for the experiment was set by selecting the cooling procedure, as will be described in the next section. After the wax deposition started, the deposit thickness at a desired time was measured by lowering the probe until it touched the deposit. The camera was set in the live image mode to allow for a precise determination of the position of the probe tip entering the deposit interface. At this position, the reading of the micrometer barrel was registered and the deposit thickness calculated by subtracting the reference position value. As only two cooling rates were employed in the present work, they will be referred to as the high and low cooling rates. The procedures employed to impose these cooling rates are described below.

5.1.1
High cooling rate experiments

The first set of experiments was performed imposing the highest cooling rate that the experimental set up could deliver. As mentioned before, for this high cooling rate, two thermostatic baths were used. In the beginning of the experiment, the valve connected to the hot bath (38.6°C) was opened allowing the circulation of the hot water inside the copper pipe and returning to the bath in a closed loop. Meanwhile, the valves connected to the cold bath (12.6°C) were closed, forcing the water to recirculate inside the bath reservoir. The experiment started by a quick manual valve maneuver in which the hot bath valves were closed and the cold bath valves were opened, allowing cold water into the copper pipe what triggered the initiation of the wax deposition on the copper wall. The total time for the valve maneuver was approximately three seconds. The data acquisition system was activated 15 seconds prior to the valve maneuver, in order to initiate the temperature measurements. An 1 Hz acquisition rate was used.

This cooling system did not impose a constant cooling rate to the copper wall, as could be verified by monitoring the transient readings of the thermocouples installed in the wall. It was verified that the cooling consisted of two different ramps, one at 32 °C/min and the other at 0.25 °C/min, and then a final constant value was achieved, as shown in Figure 5.1. The reason for this was due to the heat transfer from the hot wax solution to the cold water, causing the 12.6°C temperature inside the cold bath to raise. Besides that, the remaining hot water that was already inside the copper pipe would enter in the cold bath as soon as the valves were switched, contributing for the increase in temperature. Only after approximately 30 minutes the temperature of the wall stabilized at 12.6°C. Figure 5.1 also indicate that the cooling ramps were virtually the same for the three values of Reynolds employed, which is a good feature of the test section.

It should be mentioned that the readings of the 11 thermocouples installed in the copper pipe wall were spatially uniform, within the uncertainty levels associated with the measurements. This behavior is a consequence of the combined effect of the high thermal conductivity of copper, and of the thickness of the pipe wall. For this reason, Figure 5.1 presents the time variation of the spatially-averaged copper wall temperature.

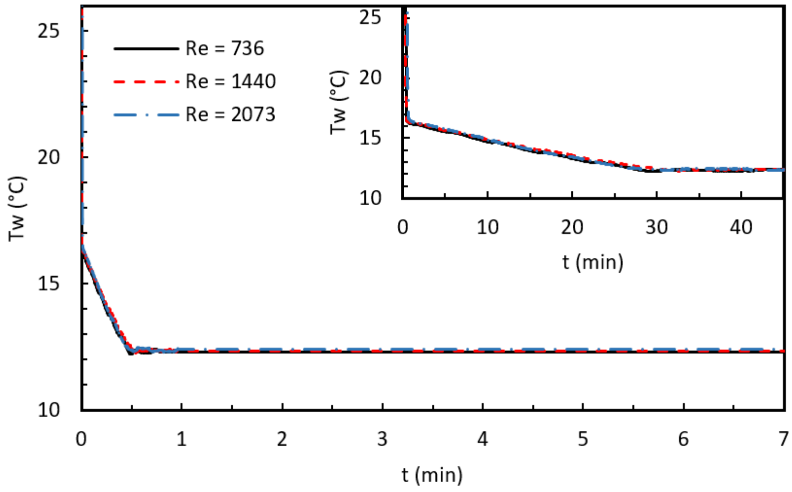

Figure 5.1: Temporal variation of the spatially-averaged copper pipe wall temperature, for Reynolds numbers 743, 1440 and 2073.

For the high cooling rate experiments, the deposit thickness measurements were carried out after the first 5 minutes of experiment and after that, for every 30 minutes. The total time of one typical experiment was 7 hours, and, altogether, 15 thickness measurements were performed.

The heating plate temperature needed to be controlled throughout the whole experiment to make sure that the entrance solution temperature would always be at 38.6°C. An interesting observation was that along the experiment, the heating plate sometimes needed to be increased and other times needed to be decreased and this effect could be explained due to the changing characteristics of the deposit over time. For example, at the beginning of the experiment when the valve maneuver was performed the reservoir temperature quickly started to lower, however, after a while the deposit started to behave as an isolation of the cold wall and the cooling of the oil inside the reservoir was not that intense.

5.1.2

Low cooling rate experiments

For the low cooling rate experiments, only one thermostatic bath was used, CC-410 from Huber, with the cooling ramp imposed by the bath own controller at 0.25 °C/min. As in the previous case, the data logger was started 15 seconds before the start of the cooling ramp at an acquisition rate of 1 Hz. The time needed for the water at 38.6°C to reach 12.6 °C was 104 minutes. This cooling ramp was measured by the thermocouples installed inside the copper pipe wall.

As the temperature of the copper pipe dropped, the power to the heating plate and tapes were adjusted in order to maintain a constant temperature for the solution inflow of 38.6 °C. The deposit thickness measurements began after the first 25 minutes of experiment when a significant deposit had already formed, allowing the thermocouple tip to be completely inserted in it. The measurements were taken with intervals of 10 minutes until reaching 185 minutes of experiment where two more measurements were taken with 30 minutes interval. The total experiment time was 4 hours and 5 minutes.

As described for the high cooling rate experiments, the temperature probe of 0.1 mm was retracted until reaching the measurement times, when it was lowered and positioned inside the deposit.

5.2
Deposit thickness results

The results of the high cooling rate are presented in Table 5.1. These values were measured at the location of the probe and correspond to a dimensionless axial position of X/L = 0.8. The uncertainty calculated for the deposit thickness measurements was ± 0.17 mm, which is considered a small value, and is an indication of the quality of the results obtained.

The table presents the transient evolution of the deposit thickness from 5 to 420 minute, and for the three values of the Reynolds number investigated. The deposit thicknesses are presented both in dimensional and dimensionless formats. The dimensionless deposit thickness is obtained with the internal and external values of the annular space, as indicated in the following equation,

$$\boldsymbol{\delta}^* = \frac{(\mathrm{r} - \mathrm{r_{int}})}{(\mathrm{r_{ext}} - \mathrm{r_{int}})}$$

Each data point presented in the table represents the average of three replications of the experiments.

Table 5.1: Transient evolution of the deposit thickness for the high cooling rate case.

Deposit thickness						
Time (min)	Re = 736		Re = 1440		Re = 2073	
	δ*	(mm)	δ*	(mm)	δ*	(mm)
0	0.54	4.07	0.52	3.91	0.49	3.65
30	0.69	5.20	0.66	4.95	0.62	4.67
60	0.71	5.32	0.68	5.06	0.64	4.77
90	0.71	5.34	0.67	5.04	0.64	4.79
120	0.71	5.34	0.68	5.07	0.64	4.80
150	0.72	5.37	0.68	5.07	0.64	4.80
180	0.71	5.36	0.68	5.08	0.64	4.81
210	0.72	5.37	0.68	5.08	0.64	4.82
240	0.72	5.37	0.68	5.09	0.64	4.81
270	0.72	5.39	0.68	5.09	0.64	4.83
300	0.72	5.40	0.68	5.10	0.64	4.83
330	0.72	5.40	0.68	5.10	0.65	4.84
360	0.72	5.43	0.68	5.10	0.65	4.85
390	0.72	5.44	0.68	5.09	0.65	4.85
420	0.73	5.45	0.68	5.10	0.65	4.86

A graphical representation was also prepared in order to better visualize the time variation of the deposit thickness. As can be observed in Figure 5.2, for the three values of the Reynolds numbers, the growth rate of the deposit thickness is rather fast, and attains a constant value after approximately 50 minutes after the deposition is initiated by the cooling of the wall. The results also show that the steady state deposit thickness decreases as the Reynold number increases. Two possible explanations can be proposed for this behavior. For higher Reynolds numbers the thermal boundary layer is comparatively thinner, and the position of the isotherm corresponding to the thermodynamic equilibrium temperature is closer to the wall. This is the temperature above which no solid can exist. Also, one can think of a proposed wax deposit formation mechanism in which the yield stress associated with the crystal gel layer formed at the wall overcomes the shear stress imposed by the flow on the deposit. The higher the Reynolds number the higher the imposed shear stress, what would lead to a thinner deposit.

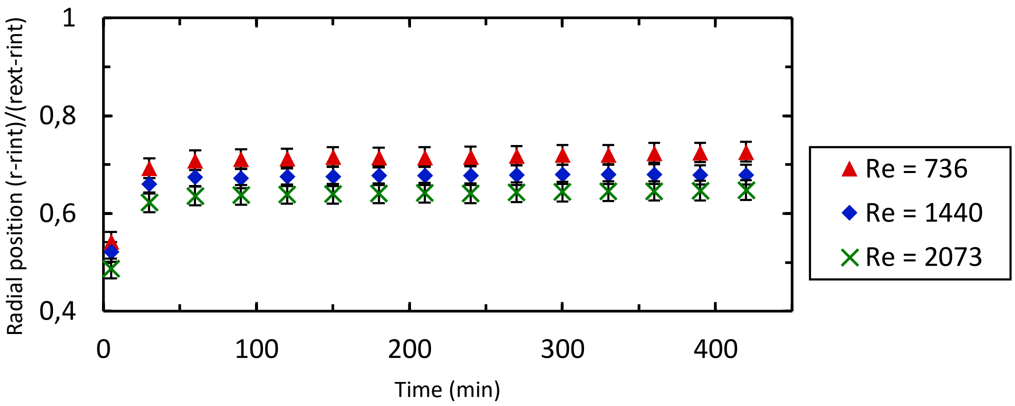

Figure 5.2: Transient variation of the dimensionless deposit thickness for the three values of the Reynolds numbers tested. Results for the high cooling rate experiments.

The deposit thickness results for the low cooling rate experiments are presented in Table 5.2 and in Figure 5.3. The results in Figure 5.3 show, as expected for the lower cooling rate, that a much smaller grow rate is observed. The deposit thicknesses slowly grow until reaching the steady state value close to 115 minutes, a little bit after the thermostatic bath reaches the final temperature of 12.6 °C, in other words, not long after the copper wall reaches a constant temperature, the deposit stopped growing. It is interesting to note that up to 60 minutes the deposit thickness is the same for the three Reynolds numbers and only then the differences start to arise.

Table 5.2: Transient evolution of the deposit thickness for the low cooling rate.

Deposit thickness						
Time (min)	Re = 736		Re = 1440		Re = 2073	
	δ*	(mm)	δ*	(mm)	δ*	(mm)
25	0.09	0.65	0.10	0.72	0.09	0.66
35	0.18	1.33	0.19	1.45	0.18	1.33
45	0.28	2.07	0.27	2.00	0.26	1.95
55	0.37	2.77	0.34	2.58	0.33	2.50
65	0.44	3.33	0.41	3.06	0.41	3.06
75	0.52	3.88	0.46	3.46	0.47	3.49
85	0.57	4.31	0.53	3.97	0.52	3.91
95	0.62	4.64	0.57	4.28	0.58	4.31
105	0.66	4.97	0.61	4.57	0.61	4.57
115	0.70	5.28	0.63	4.75	0.63	4.76
125	0.71	5.32	0.65	4.85	0.64	4.80
135	0.71	5.34	0.65	4.88	0.64	4.83
145	0.72	5.36	0.66	4.92	0.65	4.87
155	0.72	5.37	0.66	4.94	0.65	4.87
165	0.72	5.38	0.66	4.94	0.65	4.87
175	0.72	5.38	0.66	4.95	0.65	4.87
185	0.72	5.37	0.66	4.97	0.65	4.87
215	0.72	5.38	0.67	5.00	0.65	4.91
245	0.72	5.39	0.67	5.01	0.65	4.88

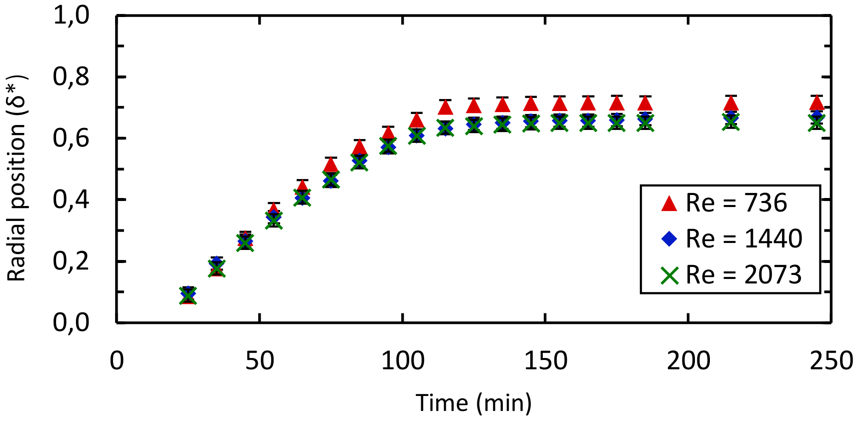

Figure 5.3: Transient variation of the dimensionless deposit thickness for the three values of the Reynolds numbers tested. Results for the low cooling rate experiments.

Figure 5.4 was prepared to show a comparison of the results from the two cooling rates presented in the previous figure for each Reynolds number tested. The results show that for every Reynolds number the deposit thicknesses converge to exactly the same value after the innitial transient period. This finding indicates that whatever deposition mechanism is favored or inhibited by the magnitude of the cooling rate, its effect on the deposit thickness is confined to the transient growth period. In order to proper generalize this observation, a wider range of cooling rate should be tested.

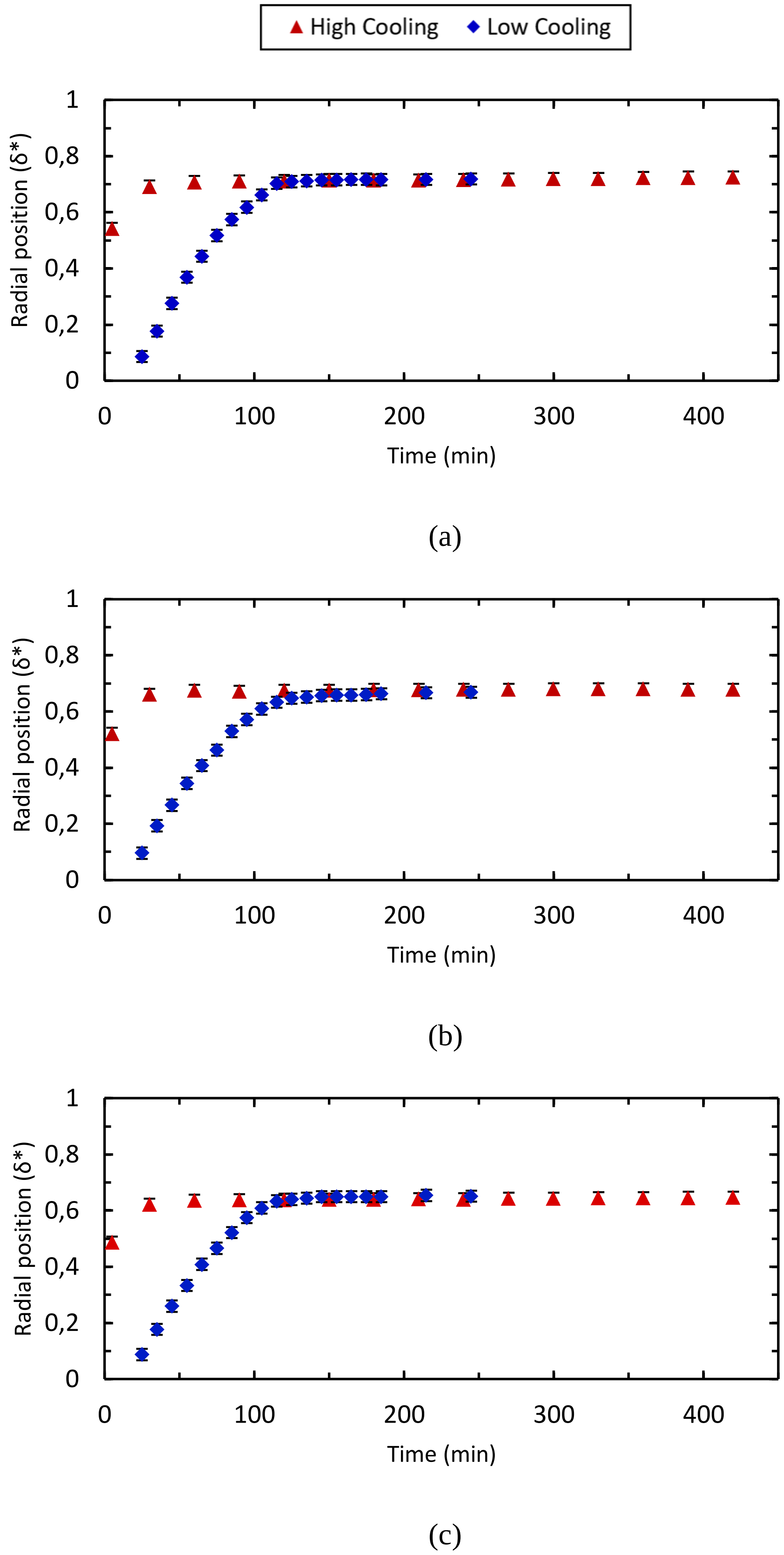

Figure 5.4: Comparison of the deposit thickness throughout time for different cooling rates for Reynolds: (a)736 (b)1440 (c)2073.

6
Deposit temperature profile

Deposit temperature profiles within the wax deposit were measured employing the small temperature probe available in the test section. Information of the temperature profiles in the deposited wax layer can be used to access the relative importance of the transport mechanisms in the deposit. Since the deposit is a porous matrix formed by solid wax filled with liquid wax, it is conceivable that convective and diffusive heat transfer mechanisms act simultaneously. A study of the temperature profiles within the deposits formed under the different flow conditions represented by the three Reynolds numbers investigated could, in principle, offer some information on the relative importance of these two transport mechanisms.

The knowledge of temperature profiles within the deposits formed under different flow conditions can also be valuable information to validate numerical simulation models of the wax deposit formation process.

The presentation of the temperature profile results is preceded by a description of the different experimental procedures employed to obtain reliable measurements. Information on bad results obtained with a previously designed probe were also included. The reasons for the unrealistic results obtained were found and corrected after extensive investigation, and that information is shared here to serve as a guide for future studies employing similar temperature probes.

6.1
Experimental procedure for temperature profile measurements

Temperature profiles in the deposit were measured for experiments with duration of 5 minutes, 1 and 4 hours. Each experiment was conducted for the three values of the Reynolds number investigated, namely, 736, 1440 and 2073. Temperature profiles were also measured for the case where the flow was switched off, what was termed as the zero Reynolds number experiment. Due to time limitations, temperature profiles measurements were only conducted for high cooling rate configuration.

Prior to the temperature profile measurements, the test section was set to steady state conditions for the desired flow rate to be tested, employing the same procedures already described in chapter 5 for the deposit thickness measurements. After steady sate, the cooling of the inner pipe was initiated and, after the desired elapsed time for the particular data run of interest, profile measurements began by manually rotating the micrometer barrel holding the temperature probe, that was previously retracted within the Plexiglas pipe wall.

At first, the spacing between measurements was chosen to be the same as the probe size, 0.1 mm. At each probe radial position, the probe was left for 10 seconds acquiring temperature data at the frequency of 1 Hz set at the data acquisition system. This size of the temperature record was chosen as a compromise between the uncertainty level of the mean and the necessary acquisition time before the probe could be moved to another position. For shorter duration experiments, however, the total time necessary to measure the complete temperature profile was considered excessive when compared to the time for the formation of the deposit. Indeed, the total descending time at this fine spatial resolution was 12 minutes and 30 seconds, what corresponds to approximately 20% of one-hour deposition experiment. In view of that, spatial resolution of 0.2 mm was selected for the experiments, what reduced in half the total time for the acquisition of a temperature profile and still offered a good spatial resolution for the profile. Since the main interest was to measure temperature profiles within the deposit, and not in the flowing liquid solution, the descending of the probe was started before the time required for the deposit to reach a certain desired position. The deposit position associated with a particular deposition time was known from previous experience obtained with the deposit thickness measurements experiments reported in chapter 5. With this information in hand, probe descending could be started in advance and reach the deposit interface precisely at the required time, thereby, decreasing the total time to perform a profile measurement operation.

Even employing the larger probe displacement and starting earlier the probe descending operation, the total probe measuring time was larger than the deposition time for experiments of short duration, such as 5 minutes. In these cases, a different procedure was devised and its importance in certain experimental conditions is presented. In this procedure only two temperature measurements were performed at two different radial positions in the deposit. After that, the experiment was stopped and the deposit removed by flowing warm water through the copper pipe. After steady state was obtained at the warm temperature level, the deposition experiment was initiated again and two more temperature measurements were performed at radial locations different from the previous ones. This procedure of forming the deposit, measuring temperatures at two radial positions and removing the deposit was repeated until a complete temperature profile within the deposit was obtained.

6.2
Unrealistic profile measurements

Veiga (2017) performed temperature profile measurements using the same test section as that utilized in the present work. Although considered a small probe compared to those reported in the literature, unrealistic results were obtained for some operating conditions. In the present work this issue was investigated in detail. The thermocouple probe used by Veiga (2017) had a junction diameter of 0.2 mm and it was supported by a 1-mm-diameter glass pipe. For the 2073 Reynold number case and after 1 hour of deposition, Veiga (2017) obtained the unrealistic, S-shaped temperature profile shown in Fig. 6.1. Several tests were conducted to try to identify the problem without success. Issues related to probe support thermal conduction and probe vibration due to vortex shedding were addressed.

Our studies with a smaller probe, 01.mm, revealed the same problems as those reported by Veiga (2017). We found however, that the S-shaped profile occurred at the position where the 1-mm glass support penetrated the deposit. The flow recirculation triggered by the support induced hot fluid to the deposit, thereby distorting the profile. Based on these observations a new probe was designed and fabricated. In this design the 1-mm glass tubing supports were kept at a large distance from the thermocouple junction. This probe, named probe 3, produced excellent results, as can be verified in Figure 6.2. The repeatability of the three measurements with this new probe is remarkable and the s-shape profile completely vanished.

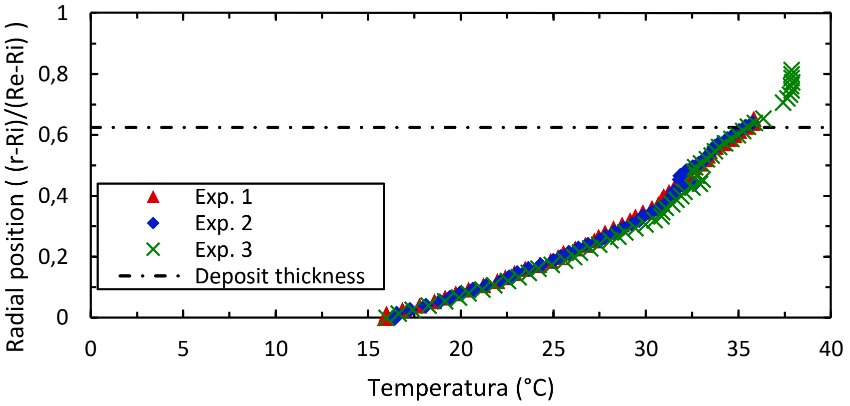

Figure 6.1: Temperature profile inside the deposit for Reynolds number of 2073 for 1 hour of experiment.

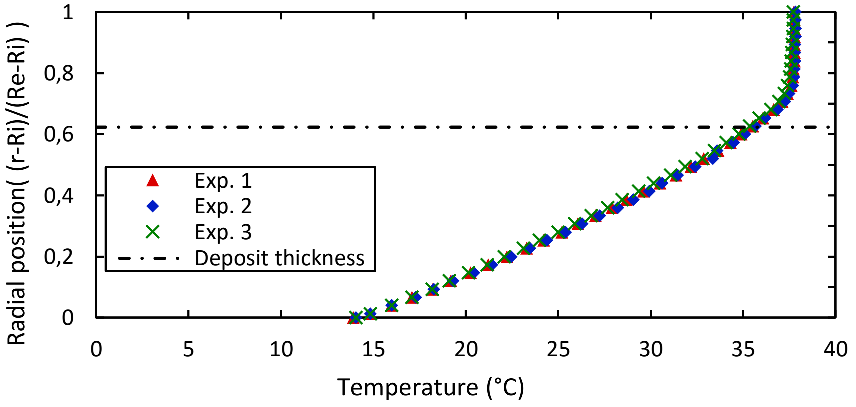

Figure 6.2: Comparison of three different experiments employing probe 3 design, for Reynolds number of 2073 after 1 hour of experiment.

Since the results with this new probe were very different and more precise than those from Veiga (2017), it was decided to conduct these experiment for all ranges of Reynolds number and deposition times, as will be presented in the next section.

6.3
Temperature profile results

The deposit temperature profile measurements were performed for three different Reynolds number, 736, 1440 and 2073 and for three different times, 5 minutes, 1 hour and 4 hours. All of these cases presented the same excellent repeatability as that shown in Figure 6.2.

A comparison between the average temperature profiles for different Reynolds numbers is shown in Figure 6.3 (a) to (c). The horizontal dashed lines represent the deposit position for each Reynolds number, at the given time. Above these lines the solution is flowing in the liquid state and a thermal boundary layer over the deposit surface can be identified, linking the deposit interface temperature, close to the WAT of the solution, to the bulk liquid temperature at 38.6ºC up to the external plexiglas wall. Inside the deposit, the temperature decreases monotonically until reaching the copper wall temperature. It can be observed that the temperature of the position corresponding to the copper pipe surface for long deposition times is not exactly 12.6°C, the temperature measured by the thermocouples imbedded in the wall. This was attributed to the fact that the probe tip is a sphere and the temperature measured at the copper surface was influenced by the surroundings. Furthermore, it is possible to observe that due to the cooling ramp employed, shown in chapter 5, in the first five minutes of experiment the thermostatic bath has not yet reached its final equilibrium temperature and, for that reason, the profiles corresponding to five minutes of deposition present higher temperature levels at the wall.

A comparison of the profiles for different Reynolds number values and for the same deposition time, shows that profiles corresponding to higher Reynolds numbers present steeper gradients within the deposit, and thinner thermal boundary layers over the deposit surface. As already shown in chapter 5, the higher the Reynolds number the thinner the deposit, since the position of the isotherm corresponding to the phase change temperature is closer to the wall. Also, higher Reynolds number flows are associated to higher shear stress levels imposed on the deposit what could lead to thinner deposits.

The same temperature profile data presented in Figure 6.3 can be cast in a different format to show the changes of the profiles with deposition time, for a fixed value of the Reynolds number. This information is presented in Figure 6.4 where it can be seen that the deposit temperature increases with time as the deposit thickness increases. Also, the temperature profiles for one and four hours of deposition time are coincident. The difference from the five-minutes profiles in relation to the longer time deposition profiles decreases for higher Reynolds number due to higher convective heat transfer at the interface for higher values of the Reynolds number.

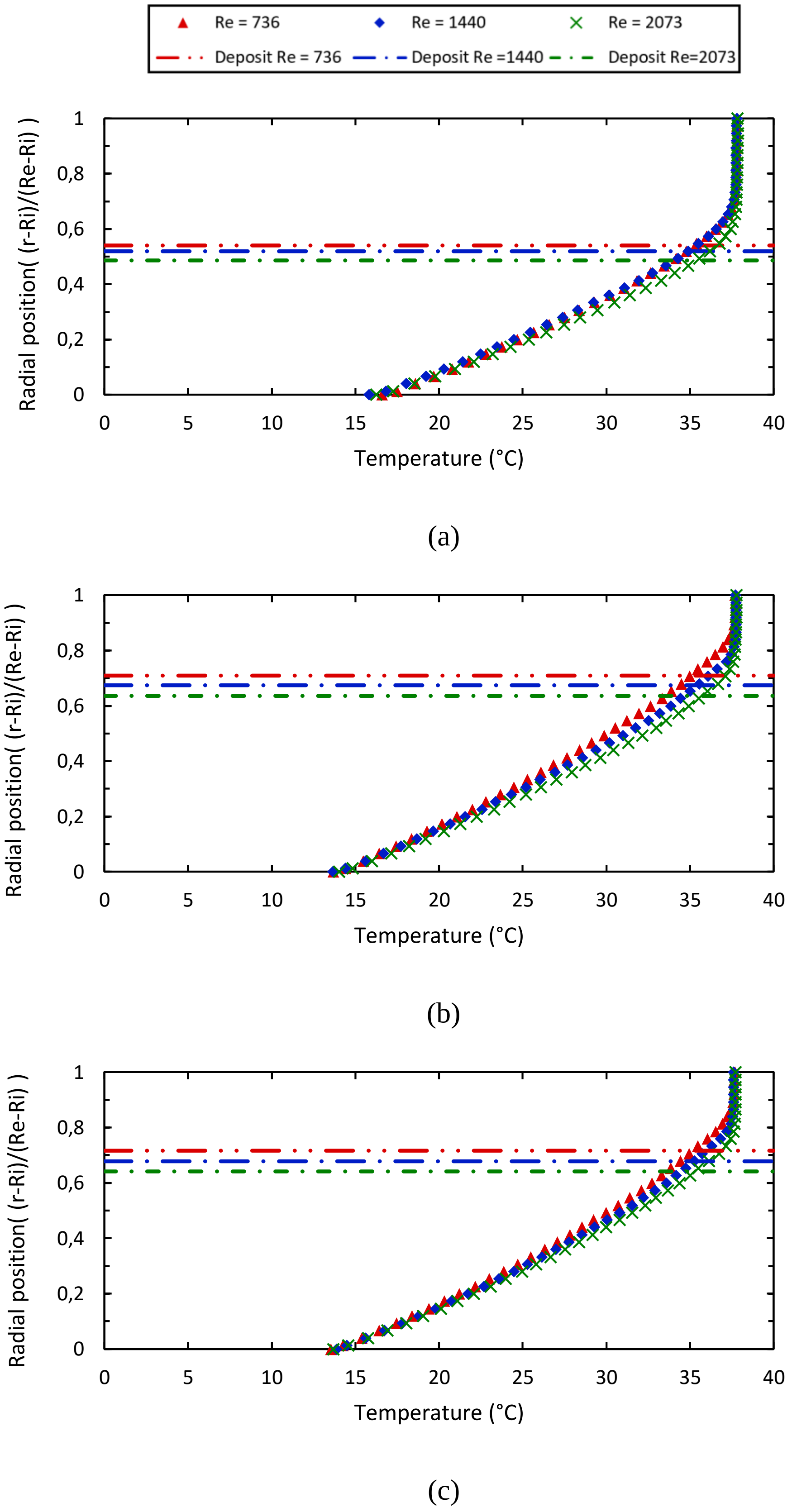

Figure 6.3: Comparison between three different Reynolds number experiments for (a)5 minutes (b)1 hour (c) 4 hours wax deposition time.

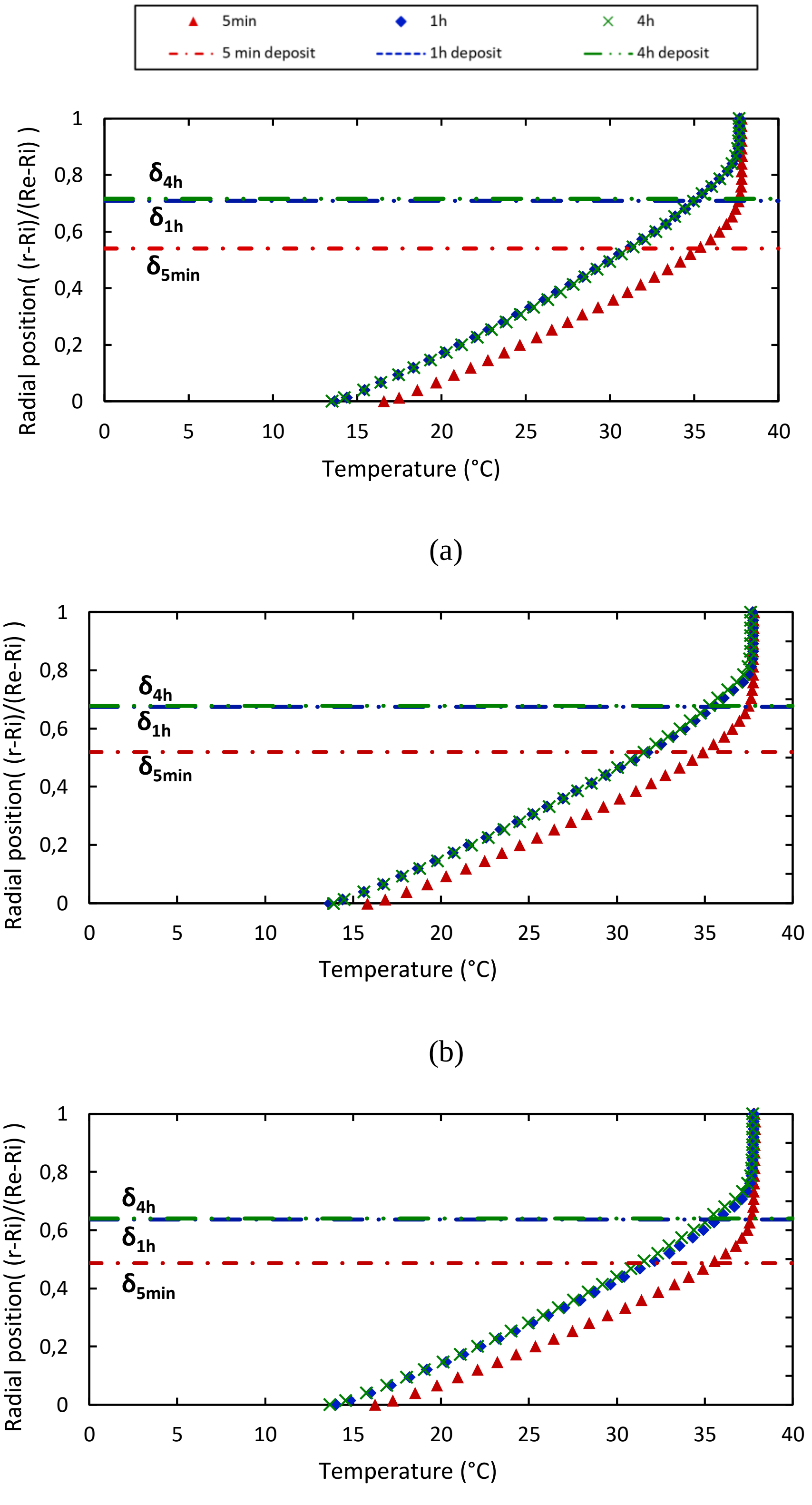

(a)

(b)

(c)

Figure 6.4: Temperature profile at x/L=0.8 for different time intervals for Reynolds number: (a) 736 (b)1440 (c)2073.

As mentioned in the experimental procedure, the time to perform the five minute experiments measurements was too big, being even longer than the deposition time desired to measure, and for that reason, an alternative measuring method was used to verify the accuracy of those results.

The Reynolds number 736 was chosen for the validation of the five minutes' results. This lowest Reynolds was chosen because this condition provides the higher growth rate, which consequently means a faster change of the deposit temperatures. If in this most critical case the temperature profiles do not present any difference it can be assumed that the other Reynolds number cases also will not.

Figure 6.4 presents the comparison between the two different methods. As it is possible to see, the results are in excellent agreement, indicating that the 5 minutes' measurements obtained previously with the first method provide reliable results for the Reynolds cases presented despite the measuring time being apparently too long.

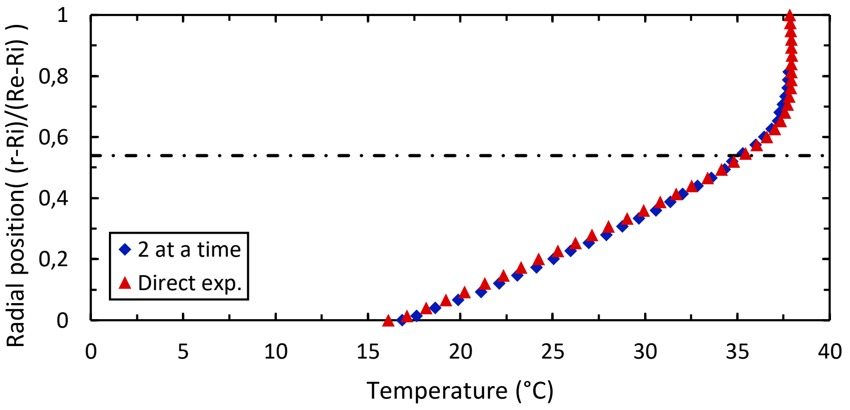

Figure 6.4: Comparison between two different measuring methods of the deposit temperature profile with Reynolds 736 for a 5 minutes experiment.

6.4
Comparison with pure thermal conduction profiles

The measured profiles just presented can be used to assess the dominant heat transfer mechanism within the deposit. Banki et al. (2008) have proposed that the shear stresses imposed by the liquid flowing at the deposit interface could possible induce liquid motion within the porous deposit matrix. In this case, convective mechanism could play a role in the heat transfer process in the deposit. In order to verify this hypothesis, the measured temperature profiles were compared with temperature profiles obtained by the solution of the steady sate conduction heat transfer equation in the deposit

The theoretical conduction profile was calculated using the measured interface temperature and the wall temperature as boundary conditions for the steady state heat conduction equation in cylindrical coordinates with constant thermal conductivity, as indicated in equation 6.1.

$$T(r) = \left[\frac{(T_{wall} - T_{interface})}{\ln\left(\frac{r_{wall}}{r_{interface}}\right)}\right].\ln(r/r_{wall}) + T_{wall} \qquad (6.1)$$

T_{wall} – Temperature of the cold wall, the copper pipe.

$T_{interface}$ – Deposit- liquid interface temperature – values found in chapter 7.

r_{wall} – Radius of the copper pipe.

$r_{interface}$ – Radius correspondent to the deposit thickness.

The comparisons between the averaged measured profiles and the conductive temperature profiles are presented in Figure 6.5 to Figure Figure 6.7.

An overall observation of the comparisons between measured and conductive profiles shows very good agreement for all times and Reynolds number values investigated. This agreement is an indication that, for the range of parameters investigated, convection mechanisms are not present within the deposit, and conductive heat transfer prevails.

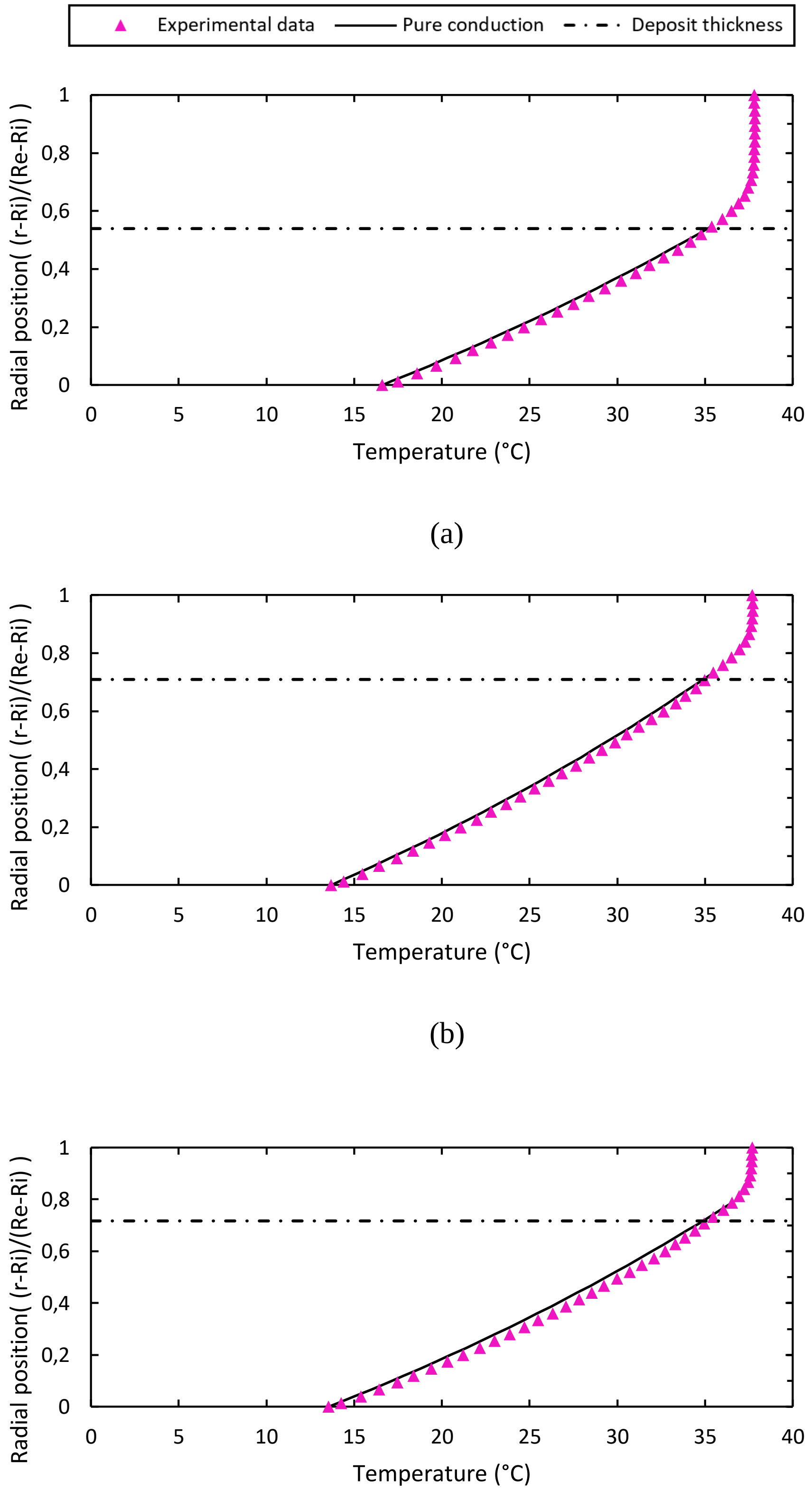

(a)

(b)

(c)

Figure 6.5: Comparison between the experiments and the conductive theoretical profile for Reynolds number 736 at the given times: (a) 5 minutes (b) 1 hour (c) 4 hours.

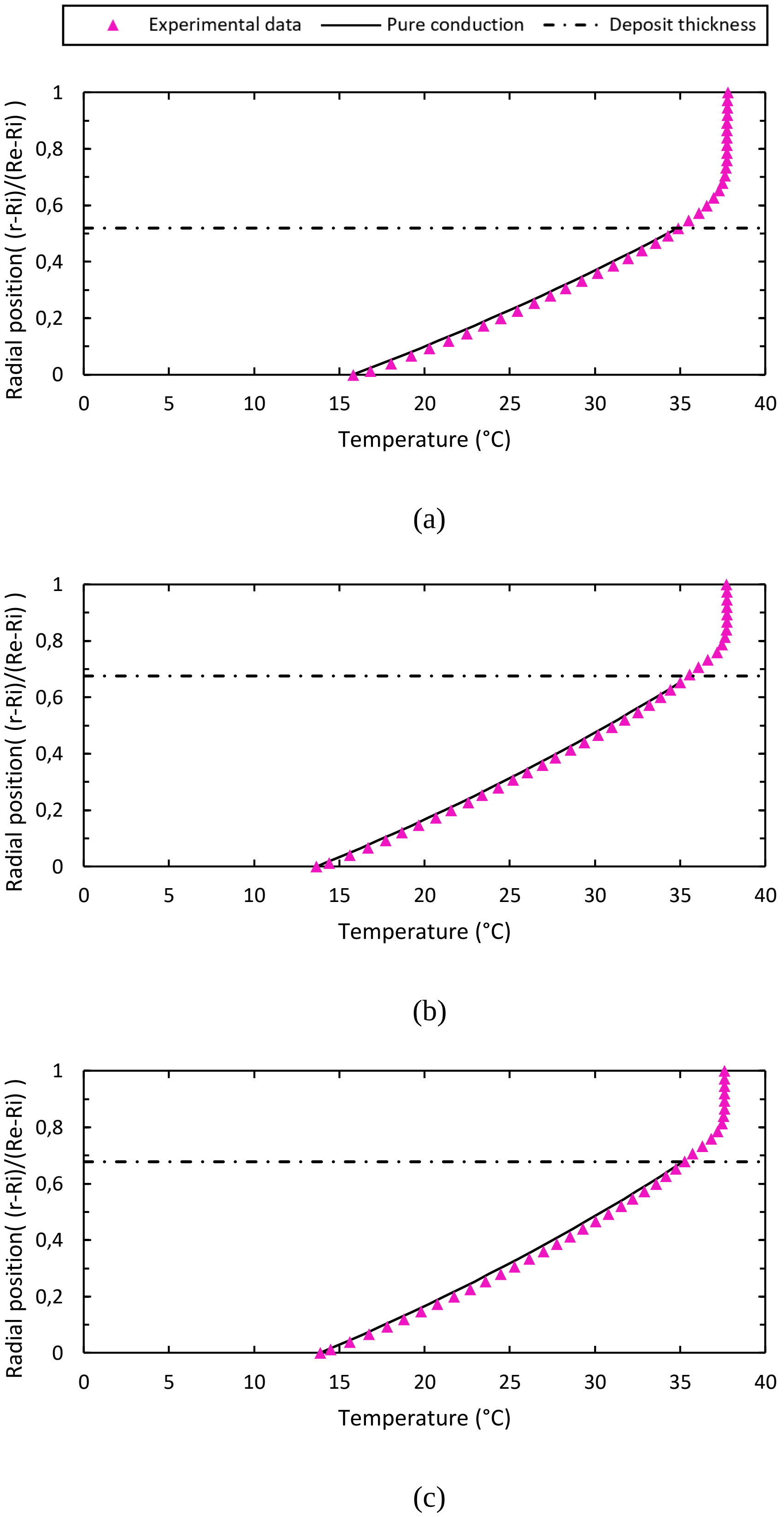

(a)

(b)

(c)

Figure 6.6: Comparison between the experimental results and the conductive theoretical profile for Reynolds number 1440 at the given times: (a) 5 minutes (b) 1 hour (c) 4 hours

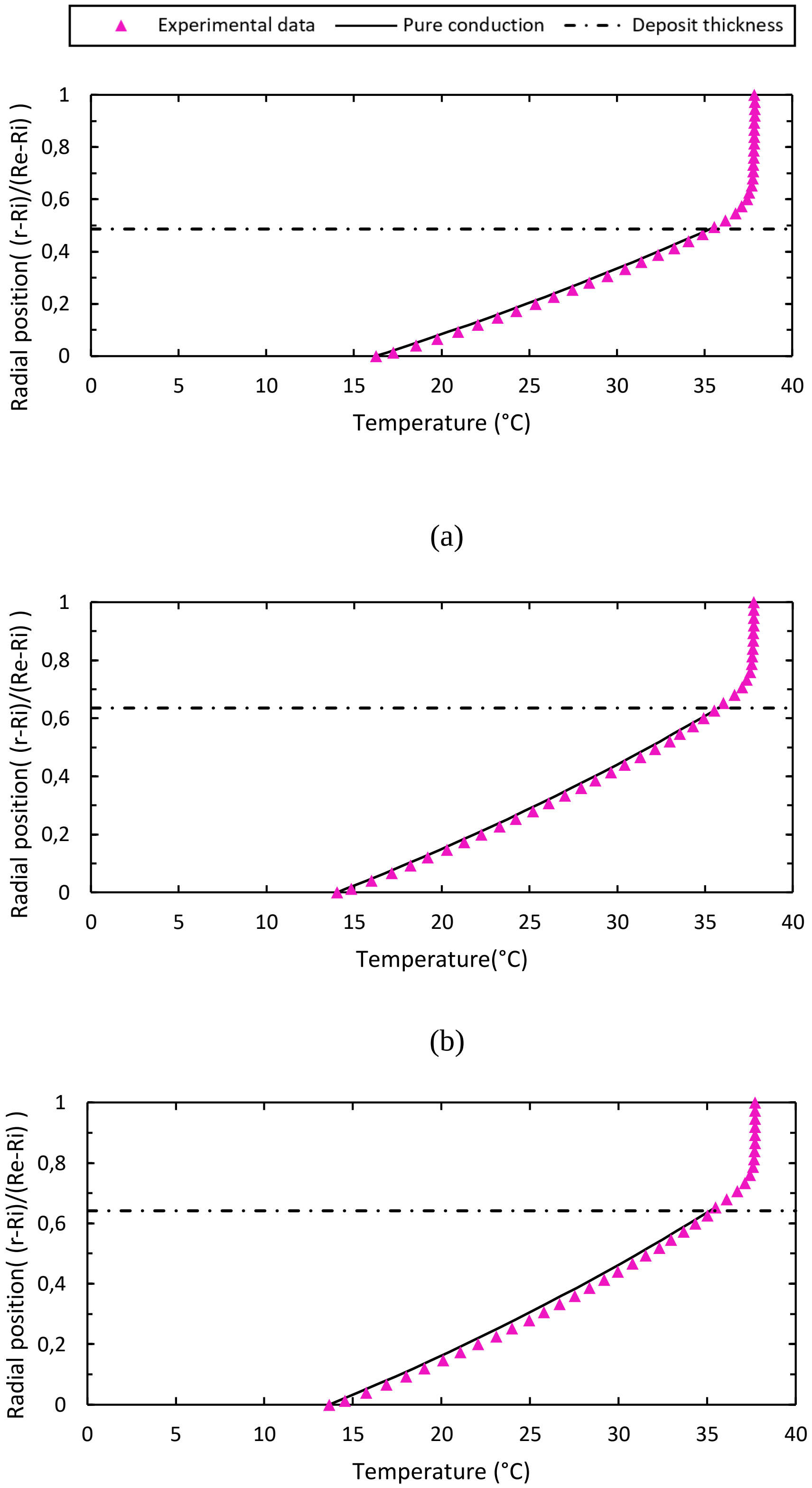

(a)

(b)

(c)

Figure 6.7: Comparison between the experimental results and the conductive theoretical profile for Reynolds number 2073 at the given times: (a) 5 minutes (b) 1 hour (c) 4 hours.

6.5
Temperature profiles for no flow condition

Temperature profiles were also measured for experiments with no solution flow. These experiments, called the zero Reynolds number cases, offer information on the deposit formation under pure conduction and mass diffusion conditions. They also provide a data base for validating numerical simulations.

Differently from the cases with flowing oil previously shown, due to the higher deposit growth rate, the deposit temperature profiles for 5 minutes were not accurately predicted by measuring the complete temperature profile at once in just one experiment. Figure 6.8 shows a comparison between the two different measuring methods described in the section 6.1 and a great difference can be observed. The results indicate that as the time passes, the deposit gets colder, what agrees with the fact that the cooling wall is still reaching the steady state of 12.6°C. For that reason, it is possible to observe that as we get closer to the cold wall, the temperature values get more distant from each other, what is reasonable as the direct measurements represent a longer deposition time by the time the probe reaches the cold wall. It is interesting to note that both profiles match the exact same temperature value at the deposit interface what is expected as the liquid region commences to be measured before the actual experiment time.

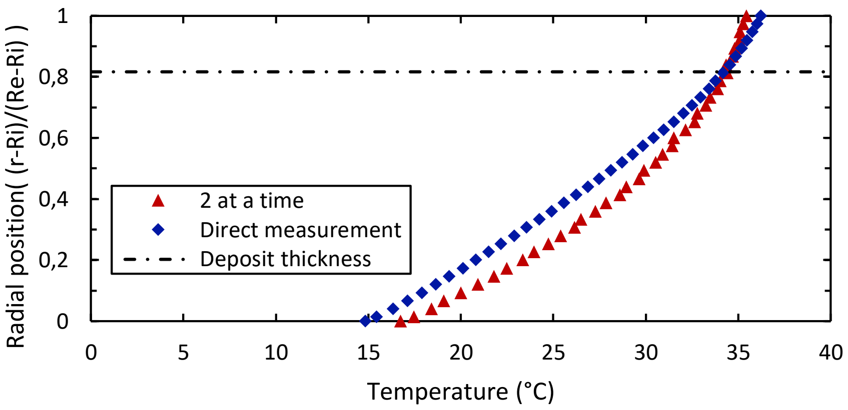

Figure 6.8: Comparison between two different methods of measuring the deposit temperature profile of 5 minutes for Reynolds zero.

As for the other Reynolds number cases, Figure 6.9 shows the comparison between the pure conductive profiles and the experiment performed for 5 minutes, 1 and 4 hours. The horizontal dashed line in the 5 minutes' experiment corresponds to the deposit thickness at that time. For the longer deposition times, as the deposit covered the entire annular region, no lines dashed lines can be seen.

The 1 and 4 hours' experiments matches exactly the theoretical conductive temperature profile, as expected. However, the 5 minutes' theoretical profiles, interestingly, poorly represents the experimental results. This outcome could be explained by the fact that the solution used to plot the theoretical solution has a transient parcel that has been disregarded, a hypothesis that is flawed for small deposition times. One might question, though, why for the Reynolds numbers different from zero the theory represented so well the measured profiles. The explanation for this could be that for Reynolds zero, the deposition growth rate was much higher and last longer than the other cases. This way, when at 5 minutes of deposition time the deposit is still rapidly growing, and the assumption of permanent regime is far away from the truth.

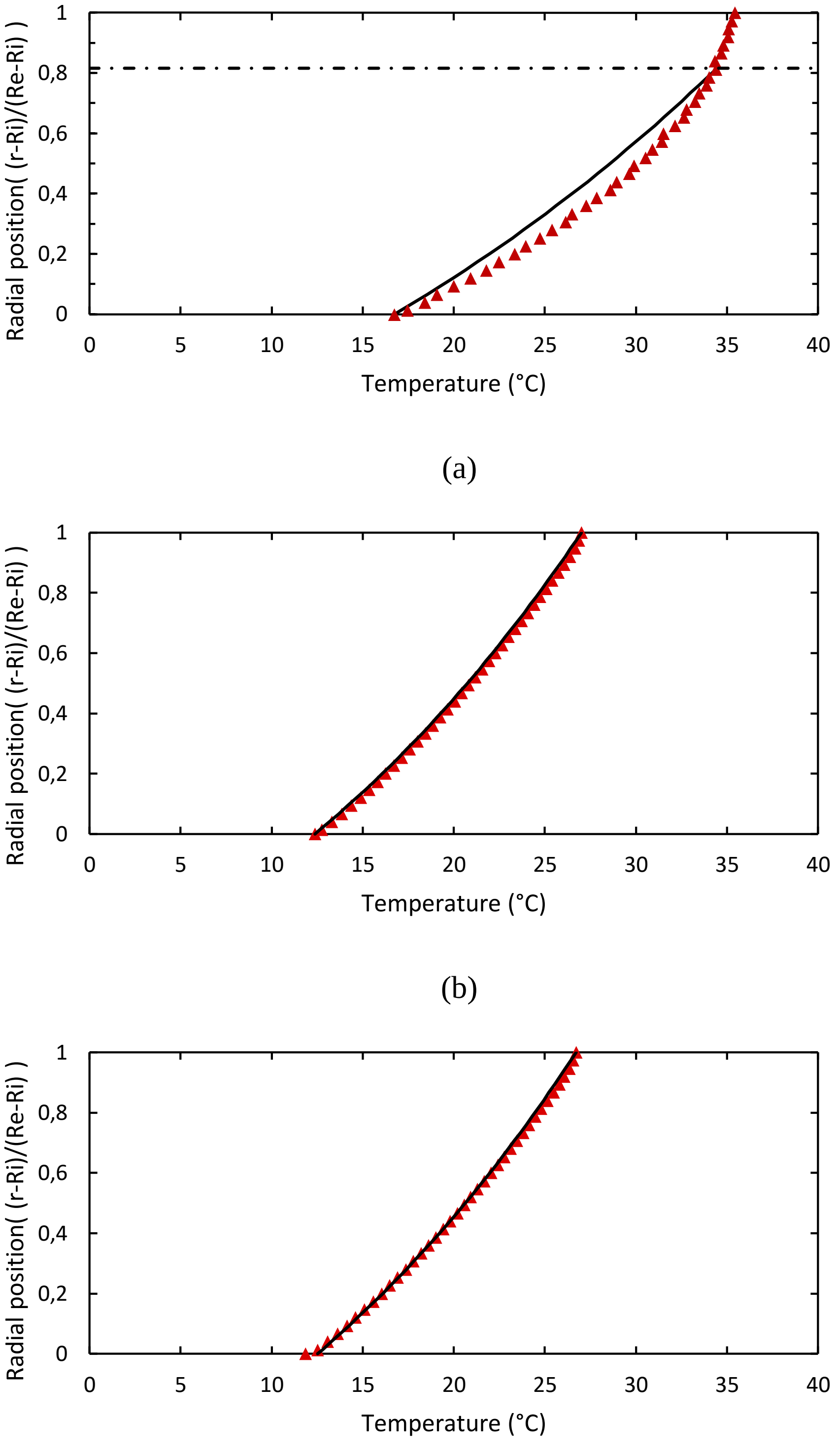

(a)

(b)

(c)

Figure 6.9: Comparison between experimental measurements and pure conduction theoretical result for (a) 5 minutes (b)1 hour (c) 4 hours.

A comparison between the deposit temperature profile for different times for the zero Reynolds case is presented in Figure 6.10. Only one horizontal line indicating the deposit thickness is presented in the figure, as for the longer deposition times the annular gap was completely obstructed. It is possible to observe that temperature profiles for the 1 and 4 hours' case is the same.

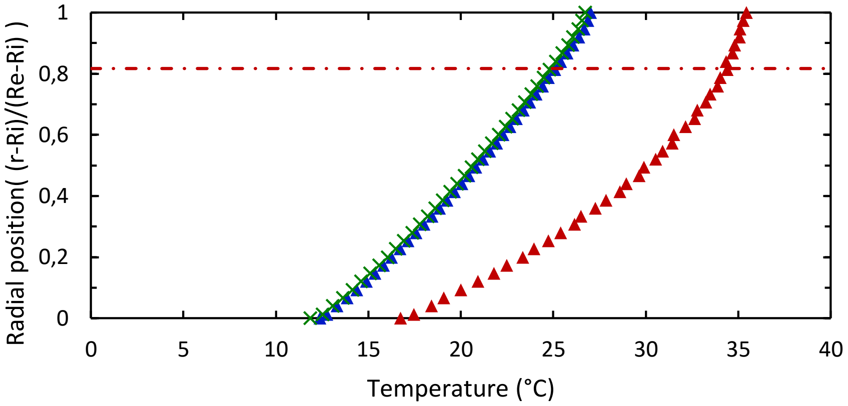

Figure 6.10: Temperature profile at x/L=0.8 for different time intervals for zero-Reynolds case.

7
Deposit-liquid interface temperature

Information on the evolution of the wax deposit-liquid interface temperature can offer some insight into the heat and mass processes governing the deposit formation. In the case of a pure substance being cooled by a wall, such as water, a certain degree of sub-cooling is necessary to trigger the nucleation of ice crystals at the wall. After that, the solid front evolves at the constant phase change temperature, the *liquidus* temperature. The difference of the heat transferred through the interface from the liquid to the solid phases is consumed by the phase change enthalpy and determines the growth of the interface. The additional thermal insulation provided by the solid formed determines the end of the phase change process, and a steady state condition is established.

For a wax solution formed by multiple components, a more complex situation governs the formation of the deposit. Fluid flow, heat transfer, mass transfer, complex thermodynamics and nucleation processes, rheological transformations of the incipient gel-like structure formed by the first nucleated crystals, all interact to determine the deposit formation. The complex wax deposit formation mechanism has been the focus of different models available in the literature in which, simplifying hypothesis are proposed to enable the prediction of the deposit formation at a reasonable cost for modeling field application (Matzain, 1996; Singh et al., 2000; Bidmus and Mehrotra, 2004; Huang et al., 2011). Some of these models include assumptions about the temperature of the deposit-liquid interface. However, the open literature in the field does not offer reliable experimental information on the evolution of the interface temperature. The small temperature probe available, together with the well-defined experimental conditions of the test section constructed and employed in the present work, offer a good opportunity to acquire accurate and original information on the evolution of the interface temperature. The experiments conducted with this objective will be described in this chapter.

7.1
Interface temperature probe setup

The measurements of the deposit interface temperature were performed at the location of the temperature probe in the annular section, i.e., at x/L =0.8. The determination of the position of the probe thermocouple junction as it touched the interface was obtained with the aid of a MotionPro X3Plus digital camera observing the annular section through the transparent plexiglass outer pipe. The camera was equipped with a 105-mm Nikkor lenses, mounted with two 27.5-mm extensions rings, model PK13 by Nikkor. Figure 7.1 presents a picture of the thermocouple probe with its junction touching the wax deposit. The magnification obtained with the optical setup employed can be estimated in the figure by observing that each wire forming the thermocouple had a diameter of 0.05 mm, while the junction had a diameter of approximately 0.1 mm.

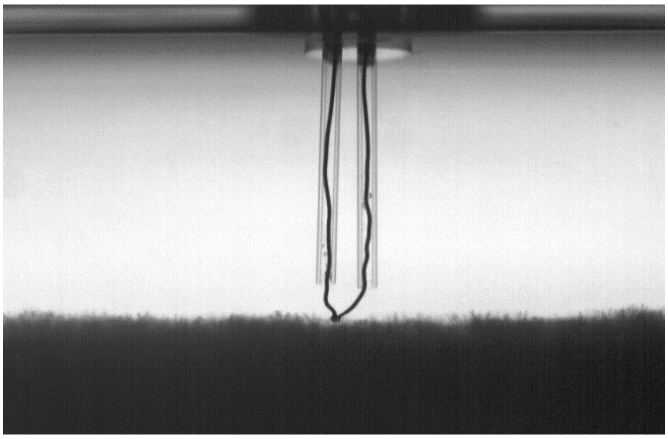

Figure 7.1: Temperature probe model 3 positioned inside the annular section over a wax deposit, as imaged by the digital camera.

Previous experiments aimed at measuring the interface temperature conducted in our laboratory by Lima (2018) with Probe 1 (see section 3.5.1) indicated that flow recirculation cells were induced by the 1-mm diameter glass tubing that supported the thermocouple. This recirculation brought warmer bulk fluid to the interface, distorting the temperature measurements. Probe 3 with smaller junction dimensions, and longer and smaller diameter glass tubing supports, solved this flow recirculation problem. However, the preliminary measurements indicated interface temperatures that were warmer than the WDT for the solution, what did not seem reasonable. A closer investigation revealed that the positioning of the probe junction at the interface was not accurate enough. The camera axis initially mounted orthogonally to the annular section, imaging the deposit from the side, did not allow an accurate determination of the position of the junction entering the deposit. This was due to the formation of wax crystals out of the focus plane of the probe junction that did not allow a clear view of the probe tip as it entered the deposit.

To improve the visualization of the probe tip entering the deposit, the camera was mounted on a swivel base that allowed its inclination in relation to the test section. An angle of approximately 23° was found optimal and allowed the observation of the probe tip inclined and from the top, as it penetrated into the deposit interface. The temperature of the interface was taken as the reading of the thermocouple at the position where the junction was completely immersed in the deposit. Figure 7.2 present two images captured by the inclined camera just before the junction entered the interface, and with the junction completely immersed in the interface.

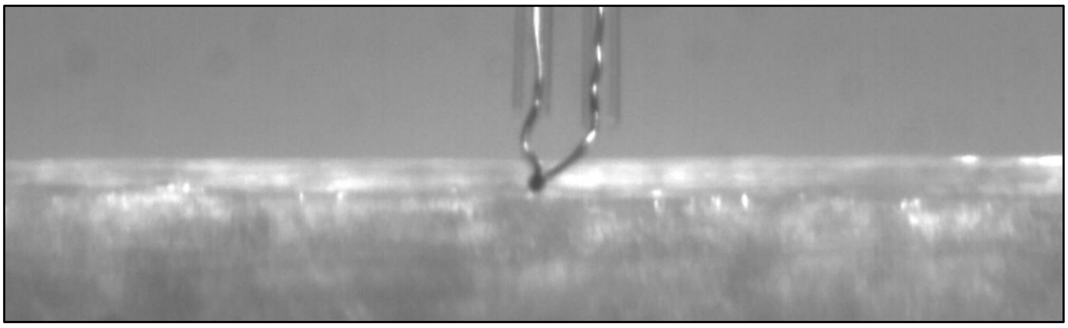

(a)

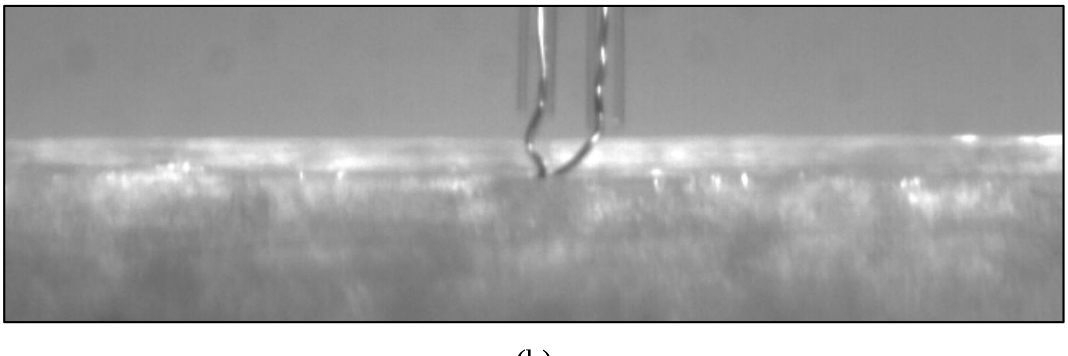

(b)

Figure 7.2: Probe positioning for measurements: (a) Right before the insertion (b) Position considered as the deposit-liquid interface temperature.

7.2
Experimental procedure for interface temperature measurements

The preparation for an experiment for measuring the interface temperature was the same as that for a temperature profile measurement described in section 6.1. The main difference between the two procedures was that for the interface temperature measurements only the temperature of one radial position was acquired, instead of the complete temperature profile across the annular space.

The temperatures of the thermocouples positioned inside the annular section measuring the wax solution entrance and exit were registered by the data acquisition system during the interface temperature measuring experiments. Also registered were the temperature of 3 of the thermocouples installed in the copper wall. These readings of the solution inlet and exit temperatures and copper wall temperatures were acquired along the experiment in order to assure that there was a good control of the conditions across the pipe throughout the interface temperature measurement experiment. The temperatures of these six thermocouples were acquired all along the experiments at a 1 Hz rate. Prior to the moment at which the interface temperature would be acquired, the acquisition rate was doubled to 2 Hz.

The interface temperature was determined for different deposition times in order to capture its time evolution. The determination of the precise moment when the temperature probe totally penetrated the interface was a delicate operation that could not be performed by observing the images of the probe tip in real time through the camera monitor. For that reason, when the desired time for measurement of the interface temperature was approaching, the camera was turned on and synchronized with the temperature data acquisition system. The camera was set to acquire images at 30 Hz. With the camera registering the images of the probe tip, the probe was manually lowered until it penetrated the deposit. The exact time when the probe tip was totally immersed was determined by inspecting each individual image frame in a post processing operation, after the experiment was completed. The time stamp in the camera fame selected was registered and the corresponding temperature was determined from the time log registered by the data acquisition system.

7.3
Deposit-liquid interface temperature results: high cooling rates

The experiments for determining the time evolution of the interface temperature were conducted for the high and low cooling rates defined in chapter 5. The results obtained for the high cooling rate experiments are presented in Table 7.1. Each value presented in the table represents the average of three replicated experiments. The total uncertainty of the deposit-liquid interface temperature was estimated to be ±0.3°C. The details of the uncertainty estimate can be found in Appendix A.

Table 7.1: Deposit-liquid interface temperature for the high cooling rate experiments.

Interface Temperature			
Time (min)	**Temperature (°C)**		
	Re = 736	**Re = 1440**	**Re = 2073**
5	35.99	36.16	36.16
30	36.32	36.48	36.59
60	36.53	36.40	36.52
90	36.55	36.44	36.55
120	36.54	36.45	36.50
150	36.47	36.36	36.46
180	36.41	36.45	36.46
210	36.33	36.41	36.53
240	36.33	36.37	36.44
270	36.37	36.40	36.46
300	36.36	36.41	36.50
330	36.33	36.34	36.44
360	36.37	36.38	36.41
390	36.38	36.41	36.47
420	36.44	36.35	36.49

The data from Table 7.1 can be better visualized in the plots presented in Figure 7.3 to Figure 7.5. In these figures the time evolution of the interface temperature is presented for each value of the Reynolds number. The horizontal dashed lines in the figures represent the WAT and WDT measured for the original solution by cross-polarized microscopy, following the procedures described in section 4.1. The horizontal dotted lines represent the average of the temperature data acquired after 60 minutes. These lines were included to facilitate the analysis of the results.

A general observation of the results of Figure 7.3 to Figure 7.5 reveals that the evolution of interface temperature displays the same trend for the three Reynolds numbers tested. The interface temperature rises from values above the WAT at approximately 5 minutes after deposition started, reaching in about 30 minutes a constant value that is preserved for up to 7 hours when the experiments were ended. The dotted horizontal lines in each figure fits the data within the uncertainty bands, indicating that the interface temperature attains a constant value after around 30 minutes of deposition time. The results clearly indicate that this constant interface temperature level achieved in neither the WAT, nor the WDT measured by microscopy for a sample of the solution taken from the test section tank.

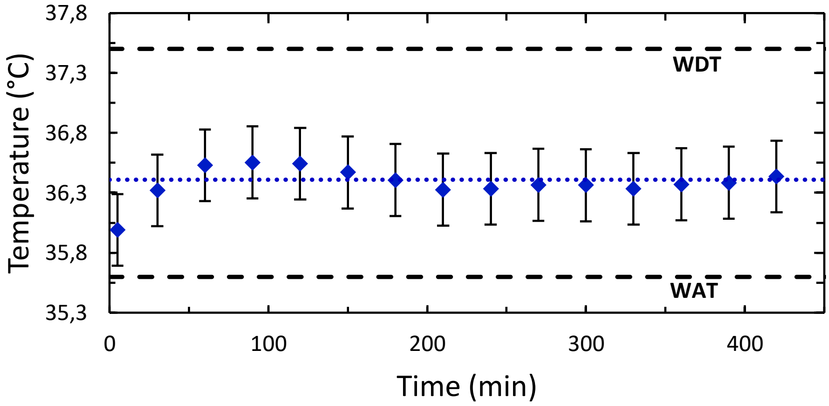

Figure 7.3: Time evolution of the deposit-liquid interface temperature for Reynolds number of 736. High cooling rate experiments.

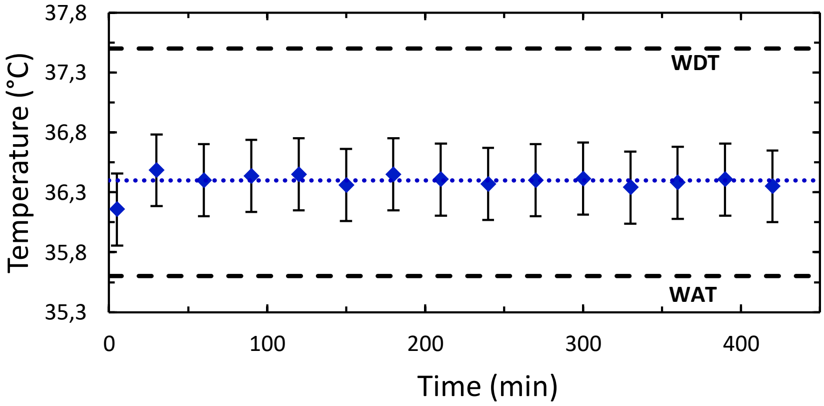

Figure: 7.4 Time evolution of the deposit-liquid interface temperature for Reynolds number of 1440. High cooling rate experiments.

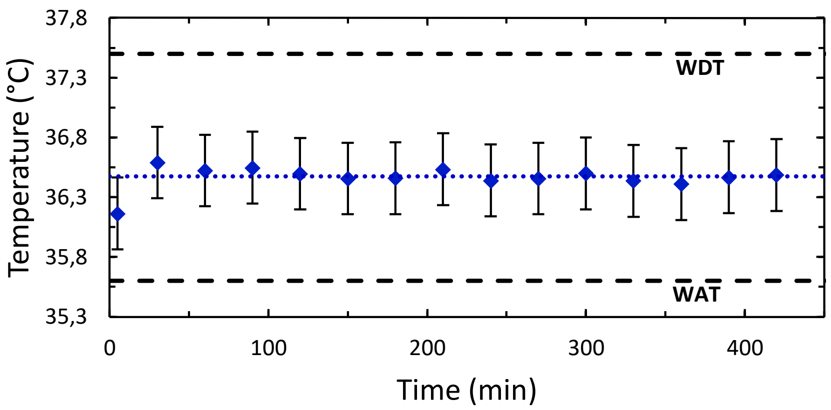

Figure 7.5: Time evolution of the deposit-liquid interface temperature for Reynolds number of 2073. High cooling rate experiments.

Figure 7.6 combines the data for the three values of the Reynolds numbers tested. The results indicate that there is not a detectable difference in the evolution of the interface temperature for the range of Reynold numbers tested.

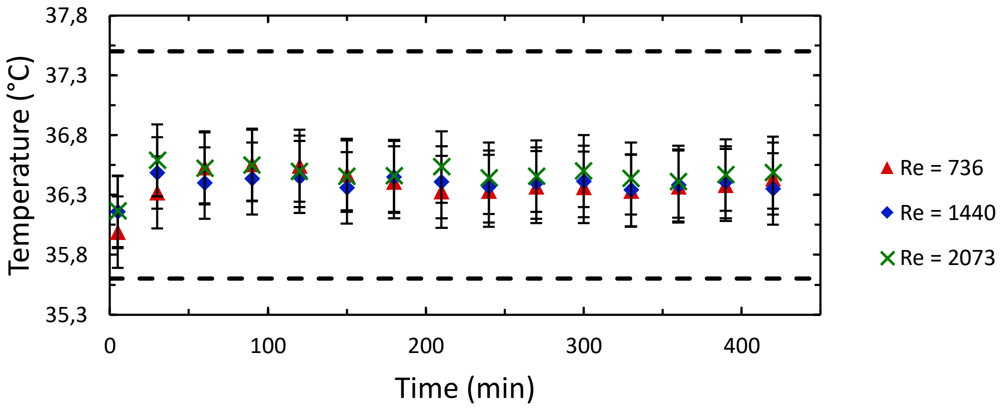

Figure 7.6: Time evolution of the deposit-liquid interface temperature for different Reynolds numbers for the high cooling rate experiments.

7.3.1

Deposit-liquid interface temperature: results for initial times

As it will be commented shortly in this chapter, the results just presented indicating that the interface temperature evolves at values above the original WAT for the solution has implications on the understanding of the deposit formation process and, as a consequence, on the deposition models proposed in the literature. For that reason, it was necessary to investigate the apparent increase of the interface temperature for times as close as possible to the initiation of the deposition processes. At these early stages, however, the deposit growth rate was fast and did not allow enough time for the use of the procedure employed before for longer deposition times, whereby the probe was carefully lowered until it penetrated the interface. In view of that, an alternative procedure was devised and implemented to measure the interface temperature.

In the alternative measuring procedure, prior to the initiation of the deposition experiment, the temperature probe was positioned at a pre-determined position in relation to the copper wall. As the experiments started, the deposition front evolved and surrounded the probe tip. The experiments were registered by the digital camera and synchronized to the temperature acquisition unit. In a post-processing operation, the image frames were individually searched to identify the time at which the interface involved the probe tip. The corresponding temperature was then registered as the temperature associated with that particular deposition time. After that, the deposit was removed, and the probe moved to a new position in relation to the wall, and a new experiment could be performed.

It was conceivable that the presence of the probe close to the copper wall since the early stages of the deposition process could influence the deposit formation by locally disturbing the flow field. In order to assess this possibility, verification experiments were run. These experiments measured the interface temperature 5 minutes after starting the deposition. For this time interval, the first measuring procedure could also be applied, as already described in the previous section. So, the alternative procedure was implemented by placing the probe tip at a position corresponding to the position at which the interface would reach after 5 minutes of deposition. The temperature obtained from the two procedures could be compared.

Table 7.2 summarizes the results obtained for the early stages of the deposition process for the three Reynolds numbers investigated. The table indicates the distances from the wall where the probe was positioned, the corresponding times for the interface to reach these positions, and the measured interface temperatures. Each data point in the table represents an average value of three replications of the experiments.

The results for the verification tests with the new temperature measurement procedure yielded good results. This can be observed by comparing the temperature data corresponding to 5 minutes (300 s) from Tables 7.1 and 7.2. The difference in the measured interface temperature procedures lie within the uncertainty band estimated for the measurements.

The interface temperature data for the early stage of deposition displayed in Table 7.2 can be better interpreted with the aid of the graphical presentation of Figure 7.8 to Figure 7.10, each corresponding to one of the three values of the Reynolds numbers tested. In these figures, each temperature data point is sided by a number representing the deposit thickness corresponding to the position at which the probe was pre-set. The data corresponding to 5 minutes, was obtained by the first procedure where the probe was traversed until it penetrated the deposit interface.

The time evolution of the interface temperature for the three values of the Reynolds numbers in Figure 7.8 to Figure 7.10 is quite similar. At 15 seconds after the initiation of the wall cooling the temperature of the interface equals the WAT measured for the original solution by cross-polarized microscopy. The interface temperature is kept at the WAT for up to 3 minutes when the deposit thickness has reached approximately 3 mm. Beyond this point the interface temperature is observed to increase, reaching the plateau between WAT and WDT already indicated in Figures 7.3 to 7.6. Overall, the combination of the results from the early stages of the deposition process with those for longer times seem compatible and present a reasonable physical behavior. The possible implications of these results on the proposed wax deposit formation mechanisms will be addressed at the end of this chapter, after the presentation of the low cooling rate results.

Figure 7.10 combines the results for the three Reynolds numbers in the same plot, what makes it possible to verify that the influence of the Reynolds number is not relevant on the deposit interface temperature evolution also at the early stages of the deposition process.

Table 7.2: Deposit liquid interface temperature results for alternative method with probe already lowered on pre-determined positions.

	Deposit Interface Temperature		
	Distance (mm)	**Time (s)**	**Temperature (°C)**
Re = 736			
	1	16	35.68
	2	40	35.59
	3	139	35.67
	4	300	35.98
Re = 1440			
	1	16	35.60
	2	47	35.39
	3	154	35.77
	3.91	300	36.02
Re = 2073			
	1	14	35.56
	2	49	35.39
	3	172	35.78
	3.62	300	36.21

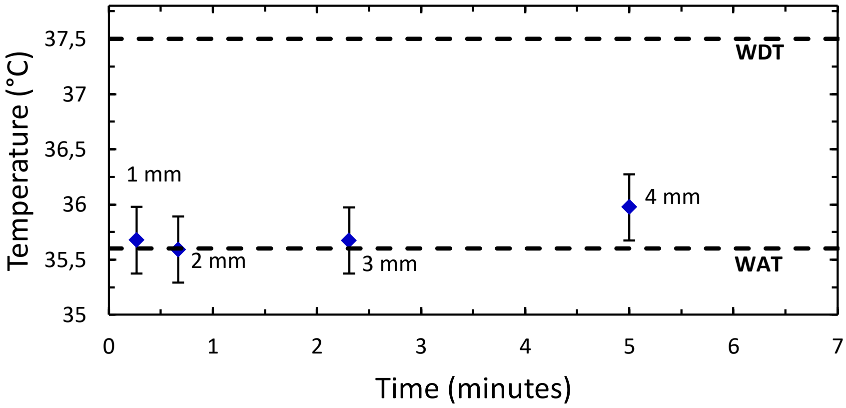

Figure 7.7: Deposit-liquid interface temperature for pre-positioned distances at a Reynolds number of 736.

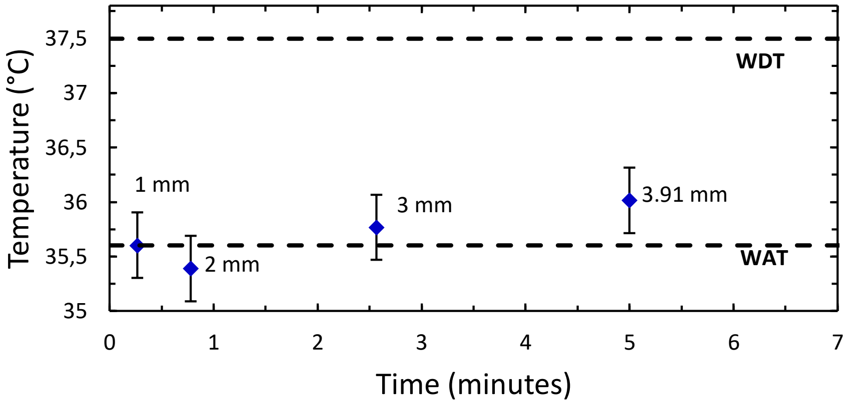

Figure 7.8: Deposit-liquid interface temperature for pre-positioned distances at a Reynolds number of 1440.

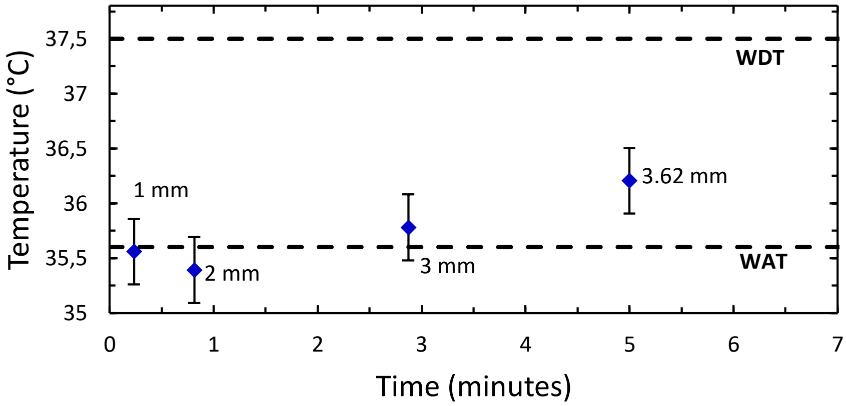

Figure 7.9: Deposit-liquid interface temperature for pre-positioned distances at a Reynolds number of 2073.

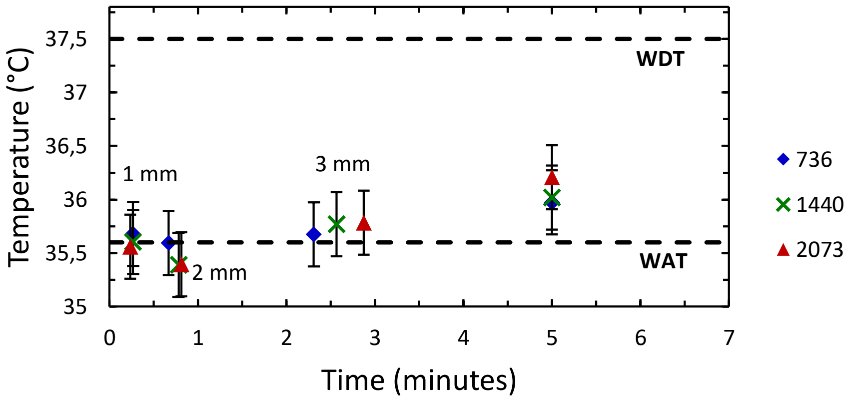

Figure 7.10: Deposit-liquid interface temperature for pre-positioned distances for Reynolds numbers of 736, 1440 and 2073.High cooling rate experiments.

7.4
Deposit-liquid interface temperature results: low cooling rates

For the low cooling rate experiments performed at 0.25°C/min, it was not possible to investigate the temperature at the early stages of the deposit formation, as it was done for the high cooling rate experiments. This was due to the fact that at this low cooling rate the growth rate of the deposit is rather low, and the presence of the temperature probe tip close to the wall caused significant disturbances on the deposit formation. For instance, crystal agglomerates carried by the flow were seen to attach to the probe tip forming a relatively large body that distorted the flow field in the vicinity of the wall. For that reason, the interface temperature results for the low cooling rate case are presented beyond 25 minutes after the beginning of the imposed cooling ramp. The deposition with this low cooling rate started at approximately 14 minutes after the start of the cooling ramp. Table 7.3 presents the results for the deposit interface temperatures from 25 minute to 4 hours and 5 minutes, when the experiments were terminated. The results are presented for the three Reynolds numbers tested. Each data point represents the average of three replications of the experiments. The total uncertainty of the temperature measurements was of the order of ±0.3 ºC.

Table 7.3: Results of the deposit-liquid interface temperature for low cooling rate.

Interface Temperature

Time (min)	Temperature (°C)		
	Re = 736	Re = 1440	Re = 2073
25	36.06	36.43	36.26
35	36.02	36.37	36.34
45	36.07	36.33	36.54
55	36.11	36.21	36.47
65	36.13	36.14	36.54
75	36.20	36.17	36.54
85	36.18	36.23	36.49
95	36.03	36.21	36.59
105	36.01	36.20	36.50
115	36.12	36.24	36.47
125	36.17	36.35	36.39
135	36.16	36.30	36.41
145	36.25	36.31	36.48
155	36.27	36.35	36.44
165	36.32	36.39	36.51
175	36.35	36.44	36.43
185	36.32	36.38	36.45
215	36.21	36.44	36.43
245	36.16	36.42	36.30

The data from Table 7.3 are presented in graphical form in Figures 7.10 to 7.12. For the three values of the Reynolds numbers tested, the interface temperature presents a behavior similar to that observed for the high cooling experiments. Indeed, the interface temperature is seen to be nearly constant from 25 minutes to the end of the experiments at a value above the WAT and below the WDT obtained by microscopy for the original solution. The superficial structure of the deposit formed at these lower cooling rates produced a less defined interface for the first 115 minutes, as compared to that of the high cooling rate experiments. For this reason, the determination of the moment the probe tip totally penetrated the interface was associated with higher uncertainty, what justifies the higher levels of data spreading in the plots, when compared with the results for the higher cooling rate experiments. It is noteworthy to mention that the deposit interface presented this clear defined interface, just as the high cooling rate, after the 0.25°C/min cooling ramp reached its final temperature of 12.6°C. Although the data presented a higher level of spread, a horizontal dotted line could be fitted using a least squares procedure. The line is seen to pass through the uncertainty bands of the data points indicating that a constant value for the interface temperature is an observation consistent with the measured data.

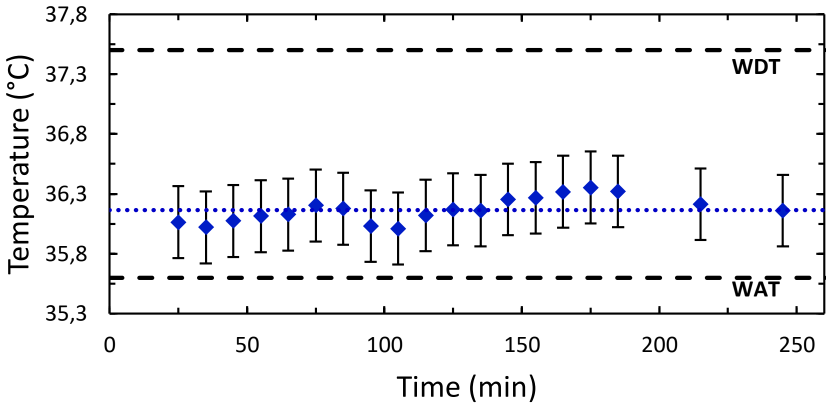

Figure 7.10: Time evolution of the deposit-liquid interface temperature for Reynolds number of 736 at a cooling rate of 0.25°C/min.

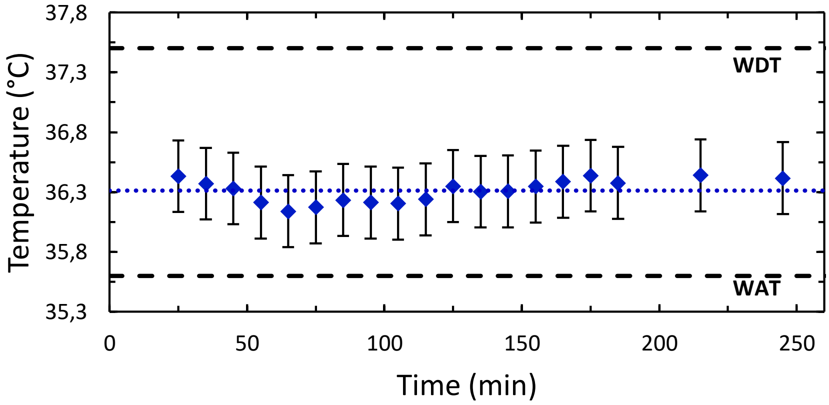

Figure 7.11: Time evolution of the deposit-liquid interface temperature for Reynolds number of 1440 at a cooling rate of 0.25°C/min.

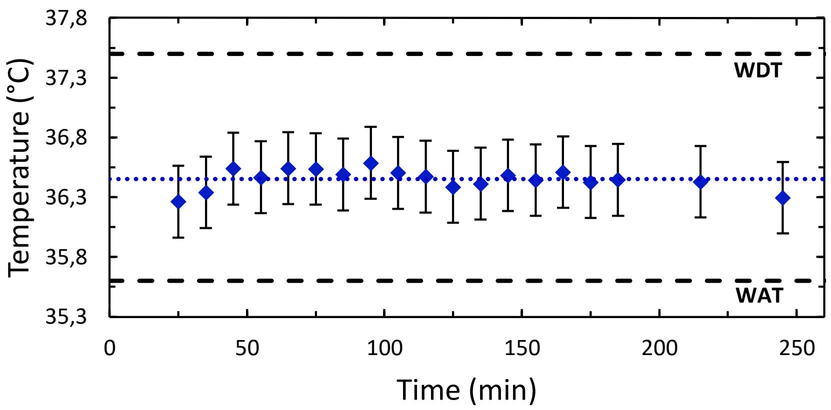

Figure 7.12: Time evolution of the deposit-liquid interface temperature for Reynolds number of 2073 at a cooling rate of 0.25°C/min.

Figure 7.13 presents a comparison of the time evolution of the interface temperature data for the three Reynolds numbers tested. Differently from the case for the high cooling rate experiments, Figure 7.6, where the dependence on Reynolds was not significant, here for the low cooling experiments an effect of Reynolds number is present, although not too pronounced. It is not easy to find a trend in the data of Figure 7.13 due the proximity of the differences between the different Reynolds number data from the uncertainty levels. The data seem to indicate that there is a trend for increasing the interface temperature with Reynolds number, which is more pronounced for the first 2 hours of experiment.

It is interesting to compare the interface temperature evolution for the high and low cooling rates. This comparison is presented in Figures 7.14 to 7.16, for the Reynolds numbers tested. For the lower Reynolds number, Figure 7.14, a lower interface temperature is observed for the lower cooling rates at the first hours of deposition. This difference, nearly vanishes as the Reynolds number is increased, as indicated in Figures 7.15 and 7.16. A plausible explanation for this behavior can be based on the competition between convection from the flowing warm fluid heating the deposit from its top surface, and the conductive cooling of the deposit through the wall. At higher Reynolds numbers, convective transport is more intense and the rate of cooling through the wall becomes less relevant.

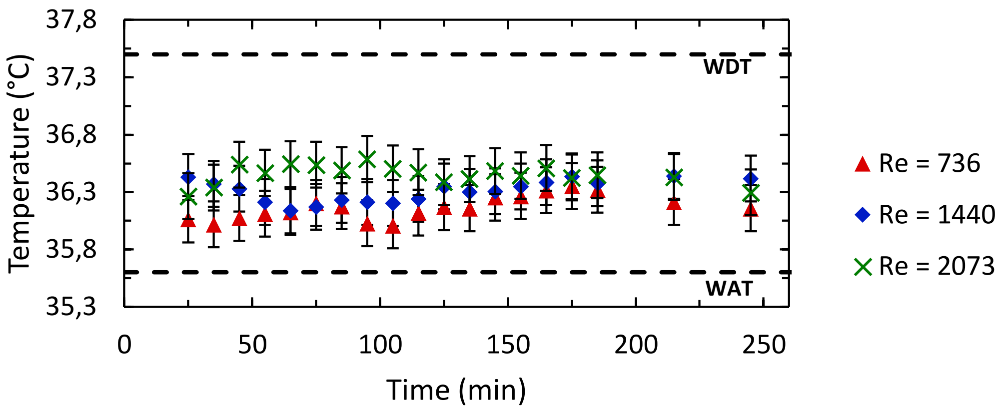

Figure 7.13: Time evolution of the deposit-liquid interface temperature for different Reynolds numbers at a cooling rate of 0.25°C/min.

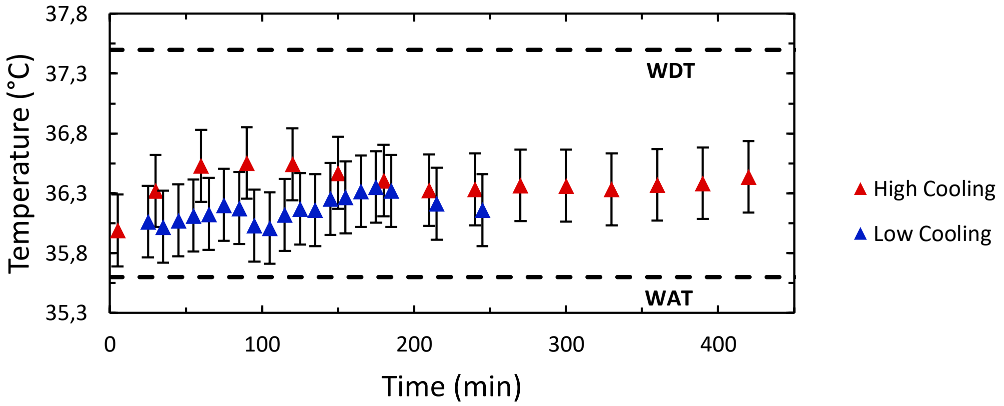

Figure 7.14: Comparison between the time evolution of the deposit-liquid interface temperature for low and high cooling rate for Reynolds number of 736.

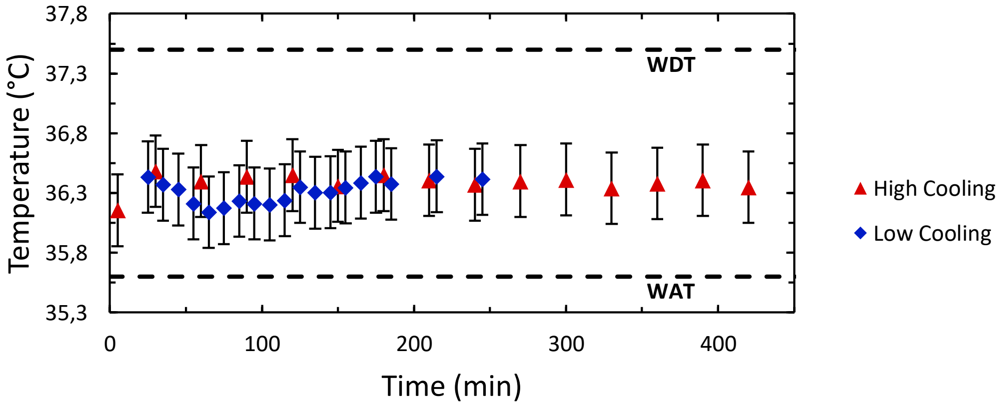

Figure 7.15: Comparison between the time evolution of the deposit-liquid interface temperature for low and high cooling rate for Reynolds number of 1440.

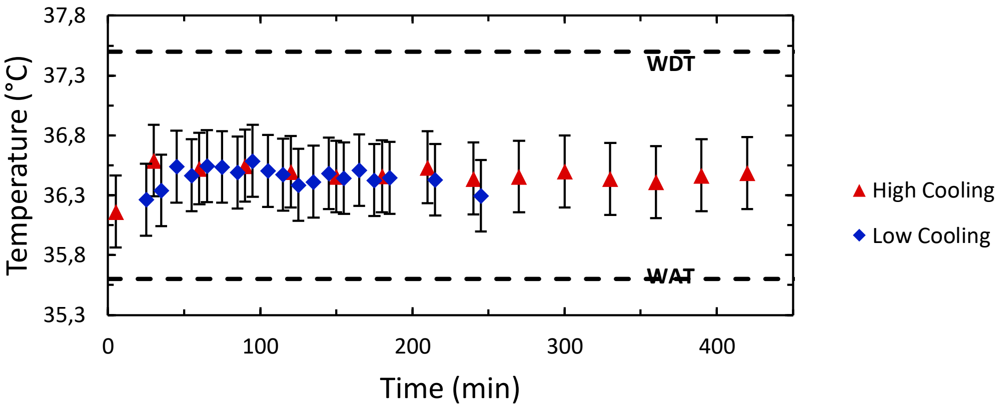

Figure 7.16: Comparison between the time evolution of the deposit-liquid interface temperature for low and high cooling rate for Reynolds number of 2073.

7.5
Comments on deposit-liquid interface temperature results

As mentioned in the introductory text of this chapter, different models were proposed in the literature to predict the transient growth of the wax deposit on a cooled wall. The experimental information obtained on the time evolution of the interface temperature can be used to asses some of the hypothesis considered by these models.

Probably the most widely employed deposition model considers molecular diffusion as the deposition mechanism (Matzain, 1996; Singh et al., 2000; Lindeloff and Krejbjerg, 2002; Huang et al., 2011). In these models the temperature imposed by the cooled wall induces a concentration gradient in the wax solution, provided the wall and, as time proceeds, the interface temperatures are below the WAT. In this situation, since the solubility of wax decrease with temperature, solid crystals will form and the concentration of liquid wax in solution will decrease in the vicinity of wall and induce the formation of the concentration gradient that drives the mass flux toward the wall, forming the deposit. Still in this model, as the interface temperature approaches the WAT, the deposition ceases. As it was demonstrated in the measurements, the interface temperature is never below the WAT, and the deposit continues to grow at a constant temperature that displays an intermediate value between the WAT and the WDT. Therefore, the deposit interface measurements obtained contradict the mechanism associated with the molecular diffusion model.

The group led by professor Mehrotra have already criticized the molecular diffusion deposition models using arguments similar to the ones proposed above (Bidmus and Mehrotra, 2004; Bhat and Mehrotra, 2004; Bidmus and Mehrotra, 2008; Ehsani and Mehrotra, 2019; Mehrotra et al., 2020). In a series of studies, these authors proposed that wax deposition was a purely phase change problem controlled solely by heat transfer. They stated the interface evolved at a constant temperature equal to the WAT. Measurements of the interface temperature performed by the same group confirmed that the interface evolved at the WAT. However, after the experience acquired with the present research and from previous studies conducted at PUC-Rio, it is clear that the measurements from Bidmus and Mehrotra (2008a; 2008b) did not offer the necessary control of the experiment and did not display the required spatial resolution to resolve the interface temperature. Indeed, the probe used was about 20 times larger than the one used in the present experiment and as it was earlier presented, this was a critical factor on obtaining reliable results.

The proposition of a deposit interface evolving at a constant temperature equal to the WAT was, however, verified by the present experiments for times shorter than 5 minutes at the high cooling rate case. As pointed out by Bidmus and Mehrotra (2008a; 2008b), this result is a strong evidence that in the first moments of our experiment the deposit formation is controlled solely by heat transfer. Without the existence of a temperature gradient the molecular diffusion mechanism could not considered. For longer deposition times, however, the interface temperature evolves to a value higher than the WAT measured for the original solution by cross polarized microscopy. Interestingly, for the low cooling rate case, the temperatures measured are in this same intermediate region between the WAT and WDT since the beginning of the deposition. Three possible reasons can be proposed to explain this increase in the interface temperature from a value corresponding to the WAT to a constant value between the WAT and the WDT, as will be discussed next.

The WAT is the crystallization temperature resulting from the necessary degree of subcooling for the nucleation of wax crystals. The magnitude of this necessary subcooling is directly proportional to the cooling rate, i.e., the higher the cooling rate, the higher the necessary subcooling for nucleation. At the start of the cooling at high cooling rates, the present experiments have measured temperatures equivalent to the original WAT measured by microscopy (see Figure 7.10). As the deposit forms, the thermal insulation produced by the deposit gradually reduced the effective cooling rate felt by the fluid just above the interface. Thus, at that position the prevailing WPT would be higher than the original WAT and the deposit could continue to grow, governed mainly by a phase change process, in other words, governed mainly by heat transfer.

A second plausible explanation could be that after nucleation of first wax crystals, the deposit already formed would serve as a nucleation site of new crystals through a secondary nucleation. This secondary nucleation is known to occur at higher temperatures than that of the primary nucleation (Agrawal and Paterson, 2015). In the case of the high cooling rate, in the first instants of deposition the temperature gradient is so high that primary nucleation occurs rapidly forming a thick deposit layer. However, in a second moment, when the temperature gradient is no longer as steep, secondary nucleation takes place leading to an increase in the deposit interface temperature. In the case of the low cooling rate, at the time of the first interface temperature measurement, the temperature gradients are not so high and there is already a deposit formed possibly with the contribution of the secondary nucleation, making the interface temperature higher than WAT since the first measurement.

Another mechanism that can induce an increase in the WAT above the deposit is the selective enrichment of the solution by diffusive mechanisms. Veiga et al. (2020) have presented numerically predicted concentration profiles of the heavier wax components where the increase in the concentration of these components in the fluid above the interface was evident. In this case a new higher local WAT could prevail and justify the temperature measurements of the present work.

A more recent proposition for deposit formation considers that the deposit grows by a combination of heat-transfer controlled phase change and diffusive fluxes, but the thickness is governed by the relative magnitude of the shear stress imposed by the flow on the interface and the yield stress of the gel-like structure of the deposit. This a promising mechanism for modeling the deposit formation, and the temperature measurements obtained in the present research need to be accompanied by flow and concentration measurements to be proper validated.

8
Wax Crystals Cloud observations

The presence of suspended wax crystals moving along with the flow in the neighborhood of the deposit interface have been observed and registered in previous visualization experiments (Bidmus and Mehrotra, 2009; Cabanillas et al., 2016; Jemmet et al., 2013; Ehsani et al., 2019b). In situations where the bulk flow temperature is below the solution WAT, the so called cold flow configuration, the presence of suspended crystal is quite common, and a plausible explanation for the presence of crystals is available. For this cold flow scenario, the bulk flow temperature is below the WAT what triggers the formation of crystals in the bulk. In case the temperature of the wall is above the fluid temperature, there is no deposit formation at the wall, and the crystals are transported by the flow. However, in the situation where the bulk flow temperature is higher than the WAT and the wall temperature, the hot flow configuration, the presence of crystals flowing along with the flow is less commonly reported. Some works (Singh et al. 2000; Huang et al., 2011), have rationalized the presence of flowing crystals by considering that close to the cooling wall, or close to the forming deposit interface, there would be a region of subcooled fluid where crystal could exist. This argument, implied that the deposit interface had a temperature below the WAT for the solution. This consideration was the key hypothesis for the molecular diffusion mechanism widely employed to model the deposit formation. As some authors have already pointed out (Ehsani et al., 2019a; Ehsani et al., 2019b; Veiga, 2017) and the present study demonstrated in chapter 7, the temperature of the interface evolves at values that are above the original WAT of the solution, contradicting the explanation based on the subcooled region above the deposit.

In the present chapter, temperature measurements were performed within the regions of flowing crystals above the deposit in order to provide original information to help understand the phenomena. The presentation of the temperature results is preceded by visualization studies that registered the flowing crystal region.

8.1
Wax crystal cloud visualization results

The deposit formation process was registered by the digital camera available in the test section. The experimental procedure utilized was the same as that for the temperature profile measurements. Visualization experiments were conducted for the high and low cooling rates.

Figure 8.1 presents four images extracted from the movies obtained of the wax formation process for the high cooling rate tests. These movies can be viewed by assessing the links available in Appendix B. Figure 8.1 (a) shows the moment in which the cooling of the of the copper wall is initiated. The dark horizontal line is the clean copper wall. In Figure 8.1(b) the solid deposit is already formed attached to the wall, and very small wax crystal can already be seen flowing near the interface. As the cooling continues and the deposit thickness grows, the size and the number concentration of the crystal increase significantly, forming a dense cloud of crystals, as shown in Figure 8(c). As the deposit growth rate decreases, the number concentration of crystals decrease steadily, until no more crystals are observed, Figure 8(d)

The same three stages of crystal formation observed for the high cooling rate experiments were also observed for the low cooling rate experiments. Figure 8.2 presents four images extracted from movies that are also available in Appendix B. Figure 8.2(a) shows the clean copper pipe, while in Figure 8.2(b) the first small crystals are observed close to the copper wall. While for the high cooling rate experiments the first small crystal appeared on the deposit surface already formed, for the low cooling rate experiments the first flowing crystal are observed before any fix deposit wax layer was formed. As the cooling proceeds, a thin deposit layer forms and the size and number concentration of wax crystal increase significantly, as shown in Figure 8.2(c). As the cooling continues, the deposit thickness grows, and the number of flowing crystals decrease and eventually vanish, Figure 8.2(d).

The images presented in Figures 8.1 and 8.2 were captured at the visualization window located at x/L =0.8, the same location as the temperature probe. Additional visualization studies, not reported here, were conducted at an axial position closer to the annular pipe inlet section, x/L =0.2. These experiments were intended to verify if deposits were already present near the annular pipe inlet section. In that case, the crystals observed at x/L=0.8 could, possible, have originated form sheared crystals from upstream deposits. The visualization conducted at the entrance, however, revealed the same patterns as those already described for the downstream, position x/L=0.8.

8.1.1
Temperature measurements within the wax crystal cloud

Temperature measurements were performed inside the wax crystal cloud formed over the deposit, as described in the previous section. These measurements were carried out using the same temperature probe and experimental procedures employed in the experiments for measuring the deposit interface temperature described in chapter 7.

Since the crystals cloud commences right at the beginning of the experiments, the temperature probe was already lowered close to the position where the crystals were observed to appear. As soon as the crystals started to appear in suspension, the tip of the probe was placed completely inside the crystals cloud by manually adjusting the barrel of the micrometer holding probe. As the deposit grew and the crystal cloud was displaced, the position of the temperature probe was adjusted so as to be kept within the cloud. The positioning of the probe in the cloud was guided by live images from the Motion pro X3 camera which was synchronized with the temperature acquisition by the data logger Agilent model 34970A. The temperature acquisition rate was set at 2 Hz.

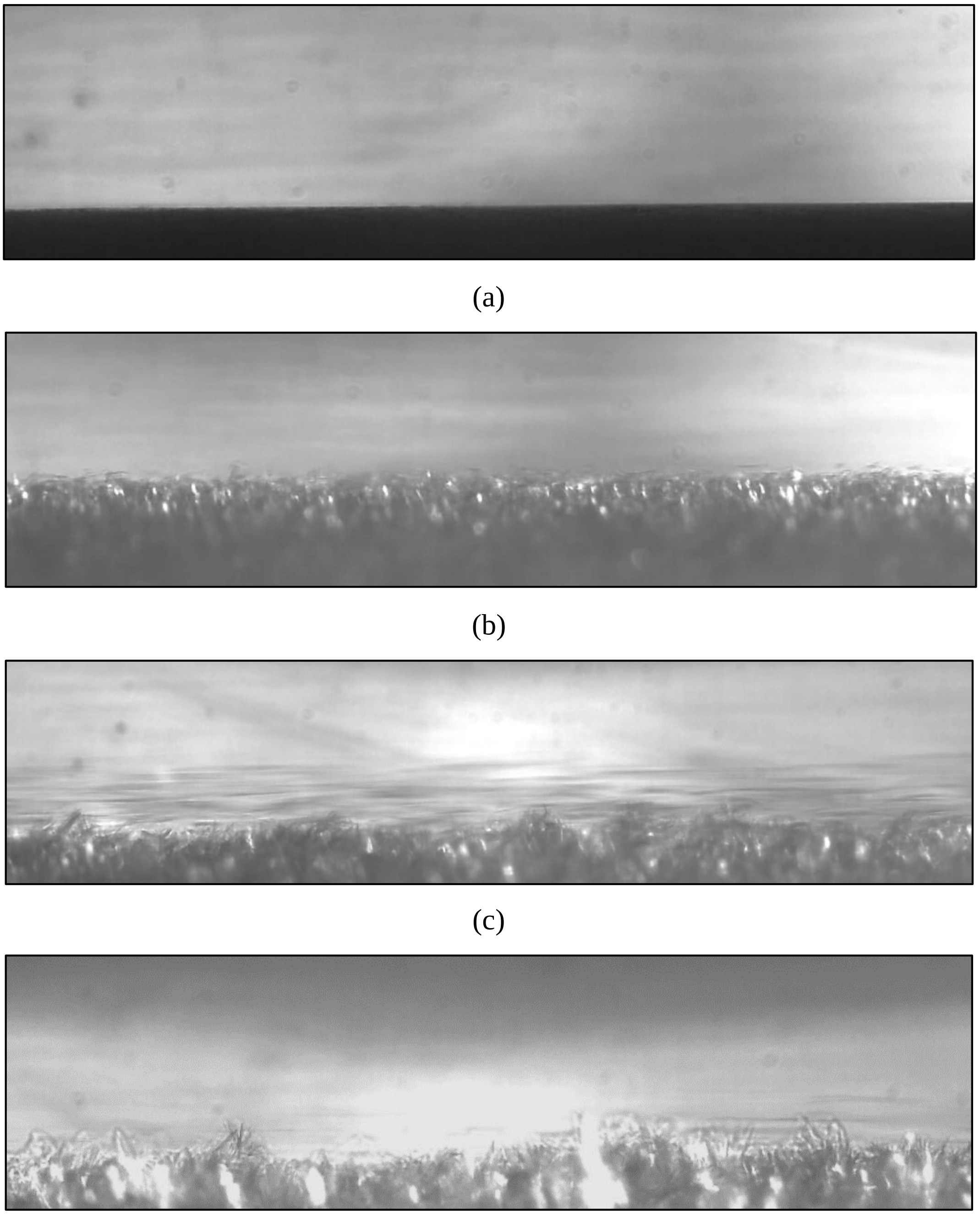

(a)

(b)

(c)

(d)

Figure 8.1: Three stages of the suspended wax crystals phenomena for the high cooling rate case: (a) bare copper pipe (b) Appearance of tiny crystals cloud (c) Increase in quantity and size of crystals (d) Reduction of the phenomena.

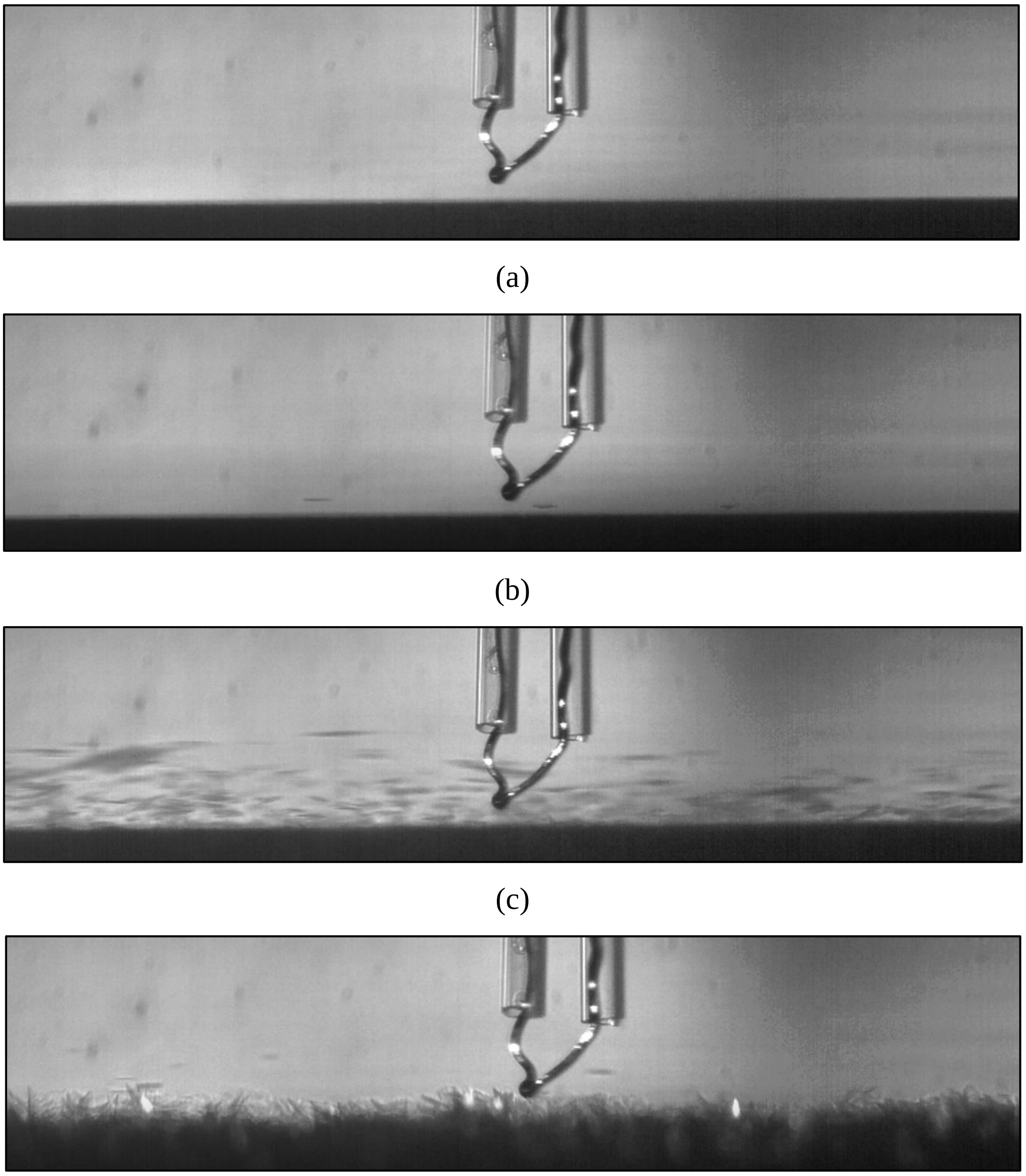

(a)

(b)

(c)

(d)

Figure 8.2: Three stages of the suspended wax crystals phenomena for the low cooling rate case: (a) bare copper pipe (b) Appearance of tiny crystals cloud (c) Increase in quantity and size of crystals (d) Reduction of the phenomena.

The temperature measurements of the suspended crystals for the high cooling rate are presented in Figure 8.3, for the three values of the Reynolds numbers tested. In the figure the temperature is presented as a function of time, counted from the initiation of the cooling. Each data point represents an average of three replications of the experiments. The total uncertainty on the measurements was estimated to be of the same order as the deposit-liquid interface temperature measurements. Also shown in the figure are the temperature data of the cooled wall measured at the same time of the crystals cloud temperature. The wax crystal cloud results are presented on the left ordinate while the copper wall temperature is referenced on the right ordinate. Furthermore, in the same figure, two horizontal dashed lines representing the WAT and WDT for the solution measured by microscopy are presented.

The observation of the time variation of the cooled wall together with the cloud temperature for all three Reynolds numbers indicates that the wall temperature has no influence on the crystals cloud temperature for the high cooling rate. Due to the earlier appearance of the wax crystals cloud for the Reynolds 2073 case, it is possible to see that Figure 8.3(c) present higher wall temperature values. As expected, the temperature level within the cloud is always above the deposit interface temperature presented in chapter 7 for the same experimental conditions. For the first time instants presented on Figure 8.3 the deposit-liquid interface temperature was the same as the initial solution WAT.

Figure 8.4 presents the crystal cloud temperature variation for the three Reynolds numbers. As it can be observed, the influence of Reynolds number is not significant.

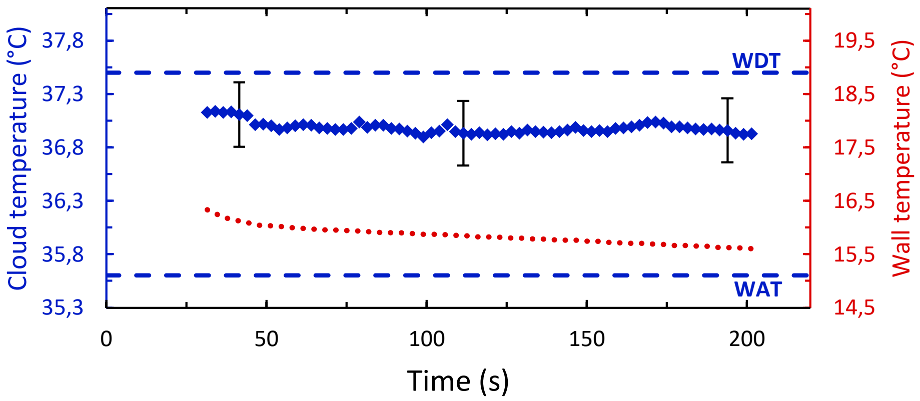

(a)

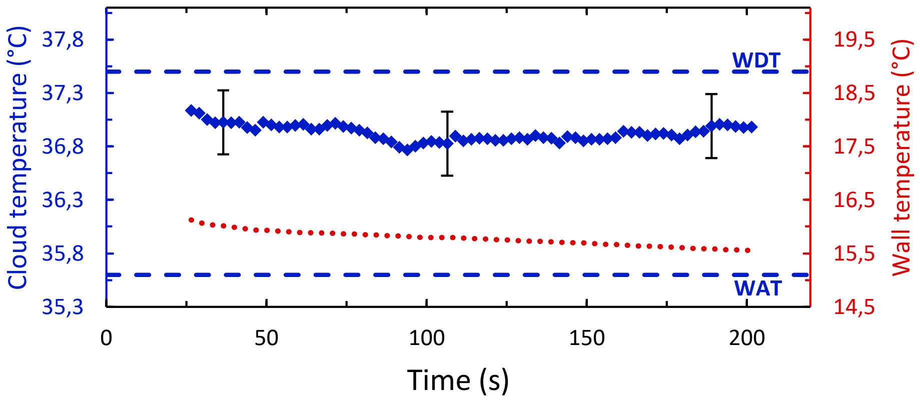

(b)

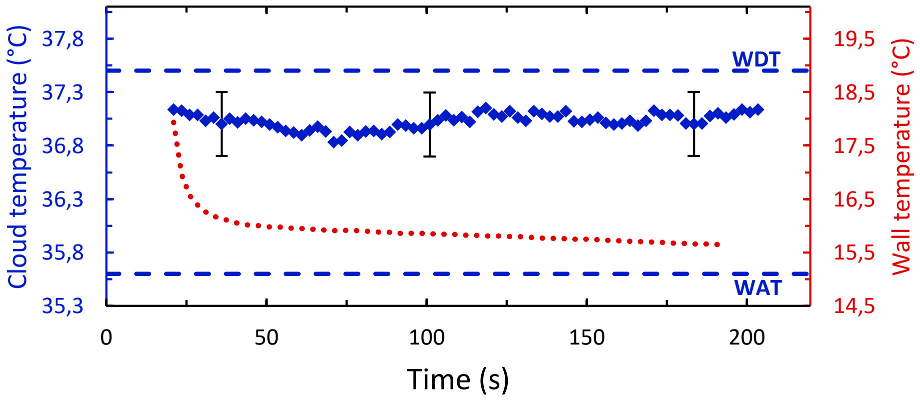

(c)

Figure 8.3: Temperature evolution of the suspended wax crystals region for the high cooling rate. Reynolds numbers of (a) 736 (b) 1440 (c) 2073.

The fact that wax crystals are formed above the original WAT for the solution can be explained by the combination of two effects, as already mentioned in chapter 7. It is known that the wax precipitation temperature (WPT) increases as the cooling rate decreases (Ronningsen et al., 1991, Jiang et al., 2001, Kasumu et al., 2013, Japper-Jaafar et al. 2016). For the high cooling rate experiments, the fluid in the vicinity of the wall experienced the highest cooling rates and, therefore, precipitate at the lowest values of the WAT. As the deposit grows, the thermal insulation provided by the deposit layer exposed the fluid flowing over the deposit to a lower cooling rate, as compared to that prevailing at the copper wall. So, it is conceivable that crystals form at a higher WAT over the deposit interface. Another effect that might contribute to the formation of crystal above the deposit is related to the enrichment of the heavier carbon components above the interface, as predicted by the simulations of Veiga et al. (2020). A local higher WAT would prevail over the deposit and justify the formation of crystals.

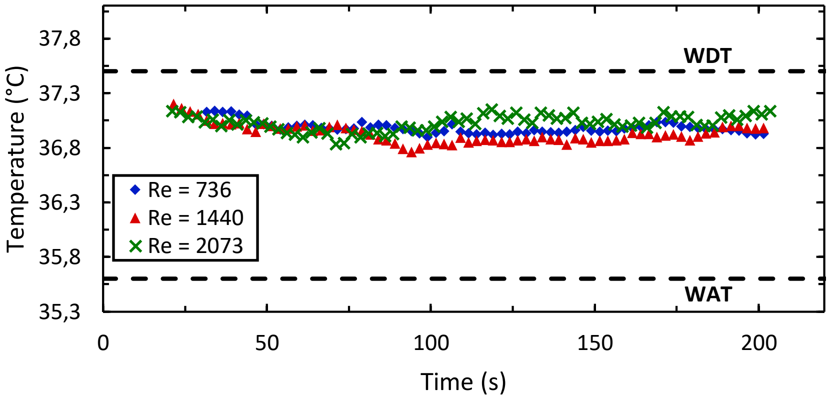

Figure 8.4: Temperature evolution of the suspended wax crystals region for the high cooling rate for different Reynolds numbers.

For the low cooling rate experiments, the first crystals could be seen flowing above the wall as soon as the copper pipe reached 35.6°C, which is the same value of the original WAT for the solution measured by microscopy, considering the uncertainty of the measurements. The temperature of the copper pipe was obtained by the thermocouples installed inside its wall as explained on section 3.4 and this same temperature value was obtained for all the three Reynolds tested (736, 1440 and 2073). Fluid flow have been reported to disturb the equilibrium that facilitate crystal formation, thus dynamic values for the WAT tend to be lower than the ones measured statically (Ijeomah et al., 2008). However, in the present experiments, it is interesting to observe that, even though the temperature above the copper pipe might be slightly higher than the actual wall temperature, the WPT for both cases present a very similar value, what could be explained due to the relatively low Reynolds number values used in the experiments. It is noteworthy to mention that, at first, no deposit could be seen forming above the copper pipe, and only the flowing crystals appeared as the cooled wall reached the WAT. Moreover, the first crystals to appear in the low cooling rate were bigger than those first ones observed in the high cooling rate experiments.

Differently from the high cooling rate experiments, a strong deposit was not instantaneously formed at the beginning of cooling, and the wax crystals that were formed above the wall were not strongly attached to the surface. Some of them were observed to be removed from the surface by the flow. It is also possible to observe the suspended crystals reducing its velocities when passing very close to the wall suggesting that a competition between the yield stress of the solution and the shear stress imposed by the flow exist.

It is important to mention that due to the probe tip being positioned close to the copper surface or deposit interface, small fragments of wax sheared from the deposit at some moments got stuck around the probe tip, causing a sudden drop in the measured temperature. In order to reduce this effect, the data presented was an average over 5 measurements performed within 2.5 seconds. Also the replications of the experiments helped attenuate this effect. Moreover, as these stuck wax crystal agglomerates normally took no more than three seconds to come off, this method was considered satisfactory for our investigation.

The temperature within the crystals cloud formed at low cooling rates is presented in Figure 8.5. The data in the figure presents a wider spread as compared to the high cooling rate case, due to the effect mentioned of periodic crystal agglomeration at the thermocouple tip. But even with larger spread, it possible to observe that the temperature of the cloud of crystals is warmer than that for the low cooling rate, and closer to the WDT. This is probably due to higher temperature level prevailing in the annular channel, at the same time instant, for the low cooling rate experiments.

Figure 8.6 demonstrates that the effect of the Reynolds number on the crystal cloud temperature is not significant.

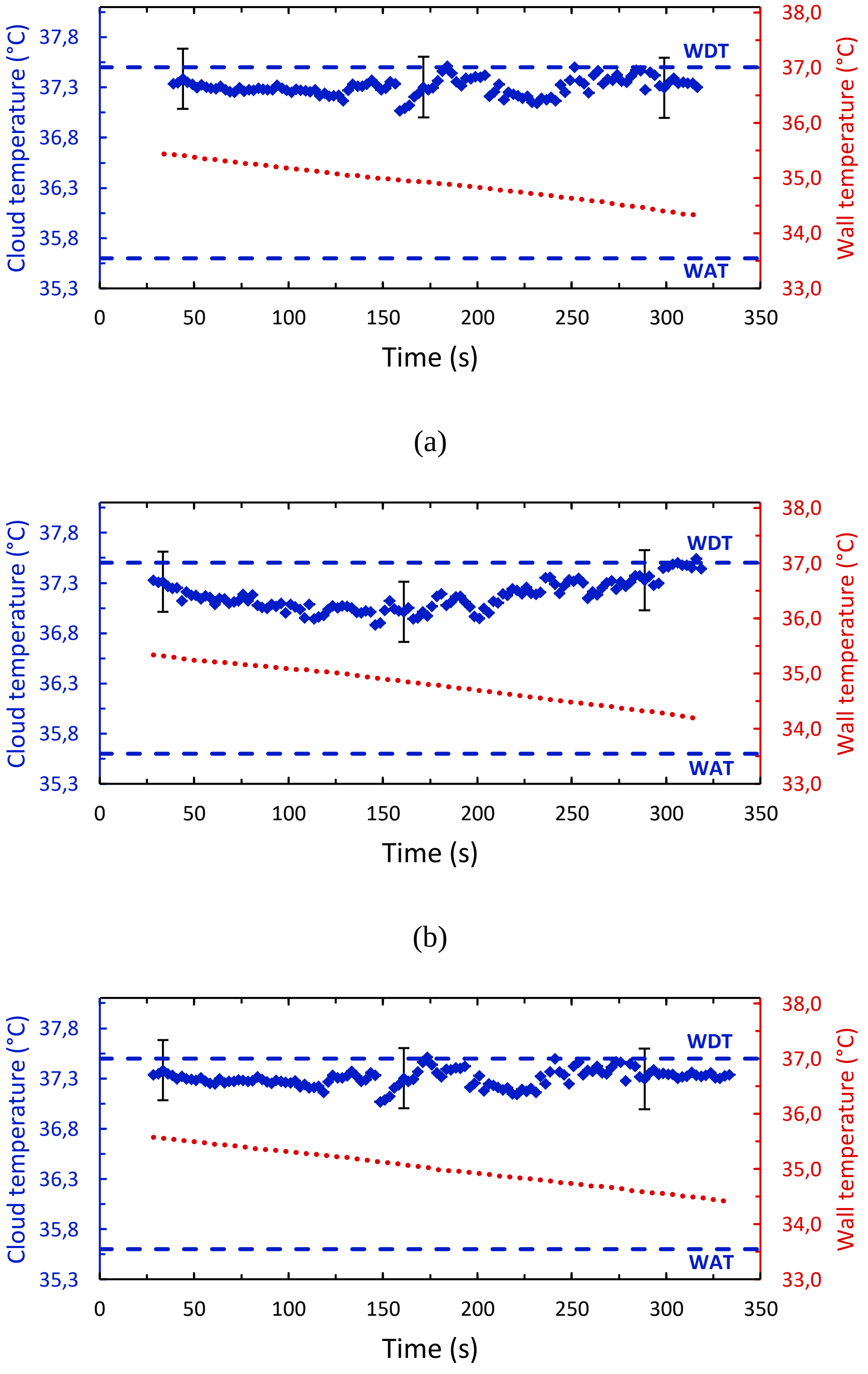

(a)

(b)

(c)

Figure 8.5: Temperature evolution of the suspended wax crystals region for the low cooling rate. Reynolds numbers of (a) 736 (b) 1440 (c) 2073.

A comparison between the three different Reynolds employed for the low cooling rate is shown in Figure 8.6. As for the high cooling rate, the Reynolds number does not seem to influence the wax crystals cloud temperature.

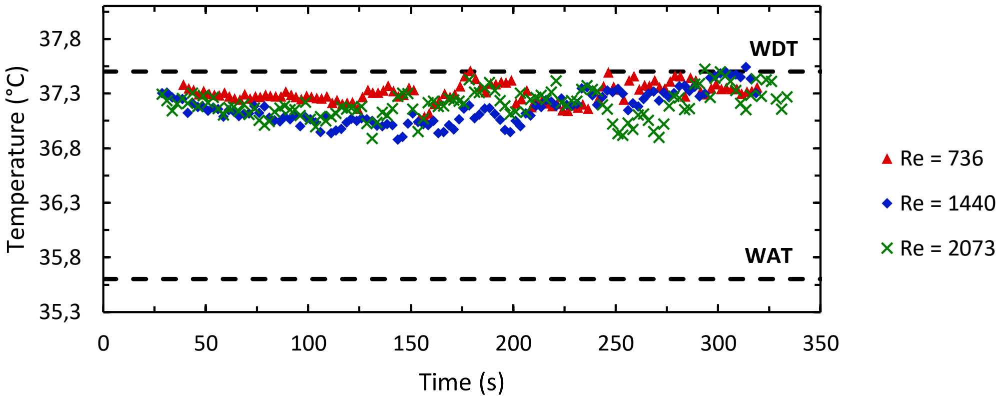

Figure 8.6: Temperature evolution of the suspended wax crystals region for the low cooling rate for different Reynolds numbers.

A comparison between the high and low cooling rates results of the wax crystal cloud temperature is presented on Figure 8.7 for each Reynolds number. Even though the crystal cloud temperature for the low cooling rate present consistently a higher value than the high cooling rate, under our uncertainty measurements these temperatures are considered the same.

It is possible to see that the duration of the wax crystals cloud is longer for the low cooling than the high cooling rate. A possible explanation is that for the high cooling rate case as the deposit rapidly forms above the cooled pipe, the effective cooling rate felt by the oil quickly decreases until not being able to form the cloud. For the low cooling rate case, the time to form a wax deposit layer, which serves as insulation, takes much longer, what could lead to this difference. The investigation of lower cooling rates than 0.25°C/min would be a valuable contribution to help understand the cooling rate influence on the formation of the crystals cloud, however these experiments could not be performed on time for the present work.

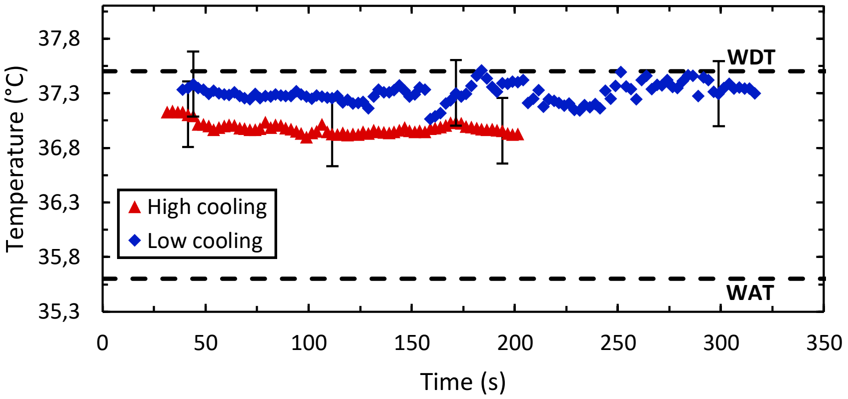

(a)

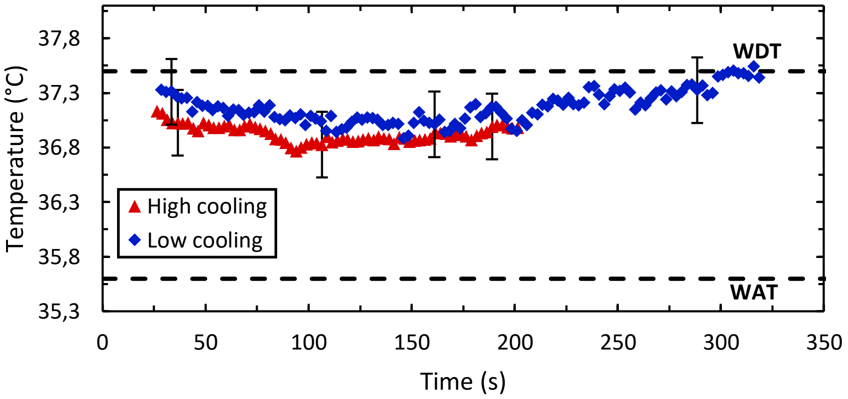

(b)

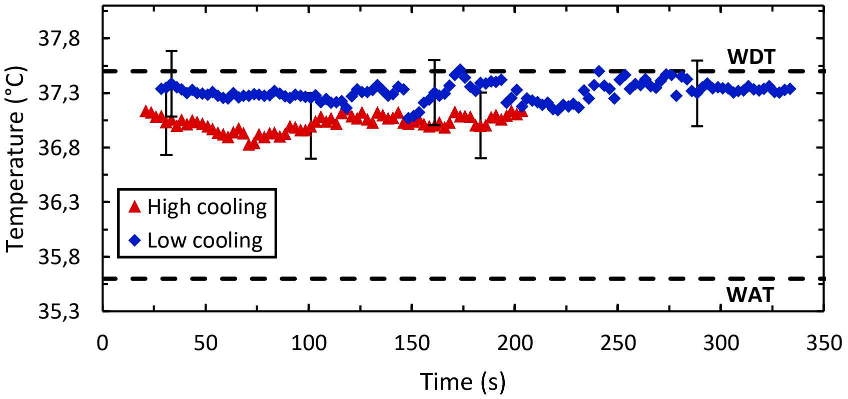

(c)

Figure 8.7: Comparison between the temperature evolution of the suspended crystals region for low and high cooling rate for Reynolds number of (a)736 (b)1440 (c)2073.

8.2
Comments on the wax crystals cloud results

The presence of suspended wax crystals in the flow has only been observed and studied in the literature for the cold flow regime and, according to some authors (Ehsani et al., 2019a), the presence of solid suspensions is inconceivable in a hot flow regime. The results presented in this chapter, however, clearly showed that the formation of a wax crystals cloud in the hot flow regime is possible.

The joint analyses of the wax crystals cloud duration with the crystals cloud temperature and the deposit-liquid interface temperature can provide some interesting insights into the physics behind the wax deposition process. Before jumping to conclusions and propositions, a detailed description of the initial deposition times is presented in conjunction with representative illustrations. First, the high cooling rate will be described and for that purpose, Figure 8.8 shown previously in chapter 7 is exhibited here again to indicate the important events described in the illustrations presented in Figure 8.9. Above each measured temperature, the number of the corresponding illustration in Figure 8.9 is indicated.

At first, Figure 8.9 (a) shows that as the cold water starts to cool down the copper wall, wax crystals form instantaneously in the vicinity of the wall. At this time, no temperature measurement of the deposit was performed thus only a steep temperature gradient is indicated in the illustration. After that, in Figure 8.9(b), the deposit is still growing rapidly, and the interface temperature corresponds to the WAT. In Figure 8.9(c), the deposit starts to slow down its growth, although it is still rapid. At this time a wax crystal cloud is formed above the deposit and the interface temperature is still equal to the WAT. In Figure 8.9(d) the deposit growth becomes slower, the deposit-liquid interface temperature starts to show an increasing trend, while the wax crystals cloud drastically decreases in thickness and number concentration. Later, in Figure 8.9(e), the wax crystals cloud has already vanished and the deposit interface temperature is higher than the WAT, close to the final deposit-liquid interface temperature value.

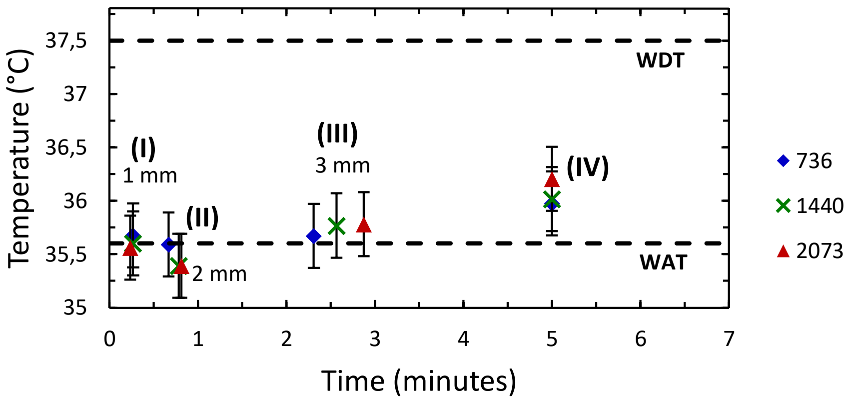

Figure 8.8: Deposit-liquid interface temperature for pre-positioned distances for Reynolds numbers of 736, 1440 and 2073. High cooling rate experiments. The roman numbers indicate the different events measured presented in Figure 8.9.

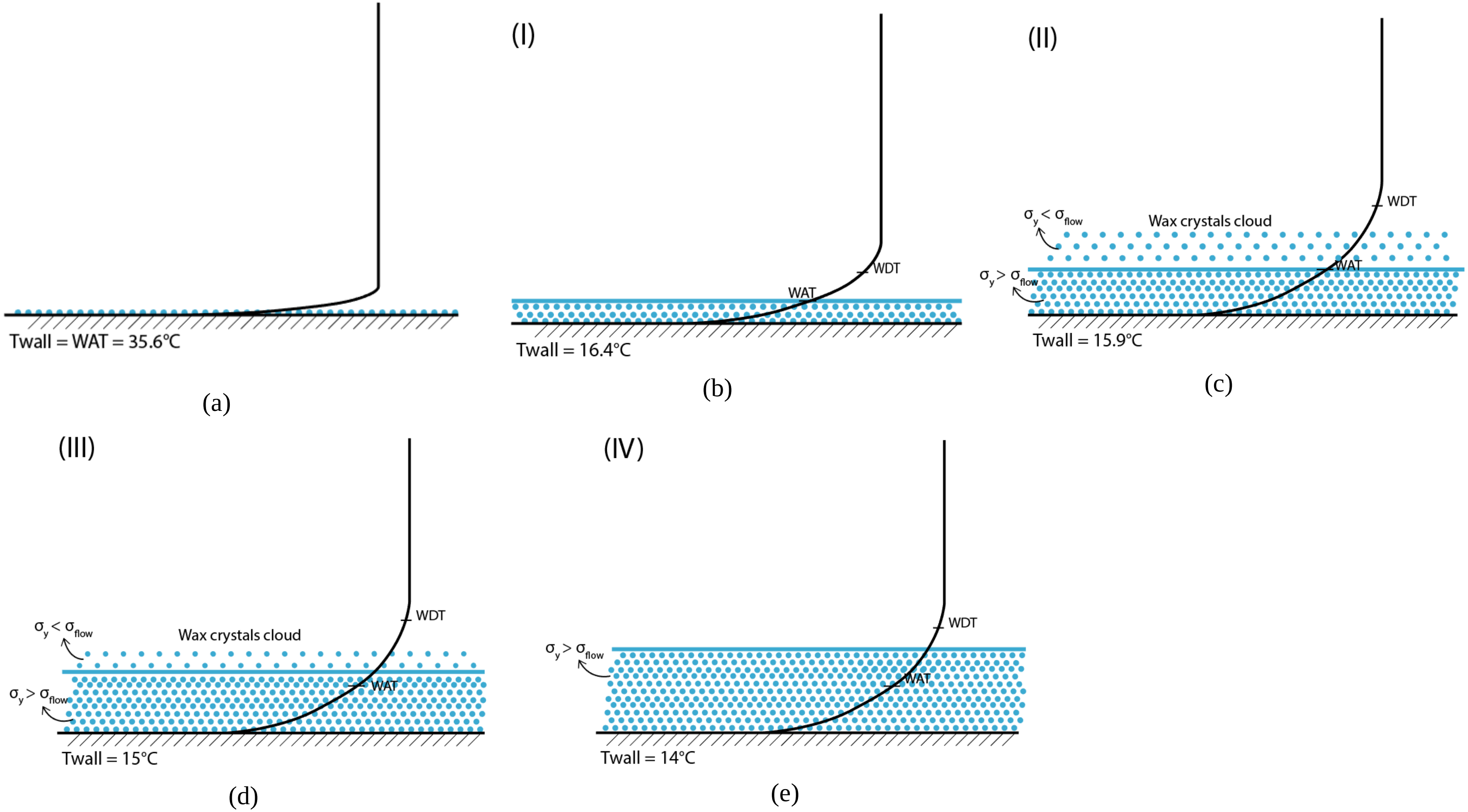

Figure 8.9: Illustration presenting the different stages of the wax deposition process for the high cooling rate case.

For the low cooling rate case, the deposition process just seemed to skip the first two stages described for the high cooling rate as shown in Figure 8.10. When the copper wall temperature reaches the WAT, a wax crystal cloud starts to form above the bare copper pipe, Figure 8.10(a). Later, Figure 8.10(b), the copper wall temperature continues to decrease, a stationary wax deposit is formed and the wax crystals cloud vanishes. The deposit continues to increase until the copper wall reaches the final temperature of 12.6°C after approximately 115 minutes.

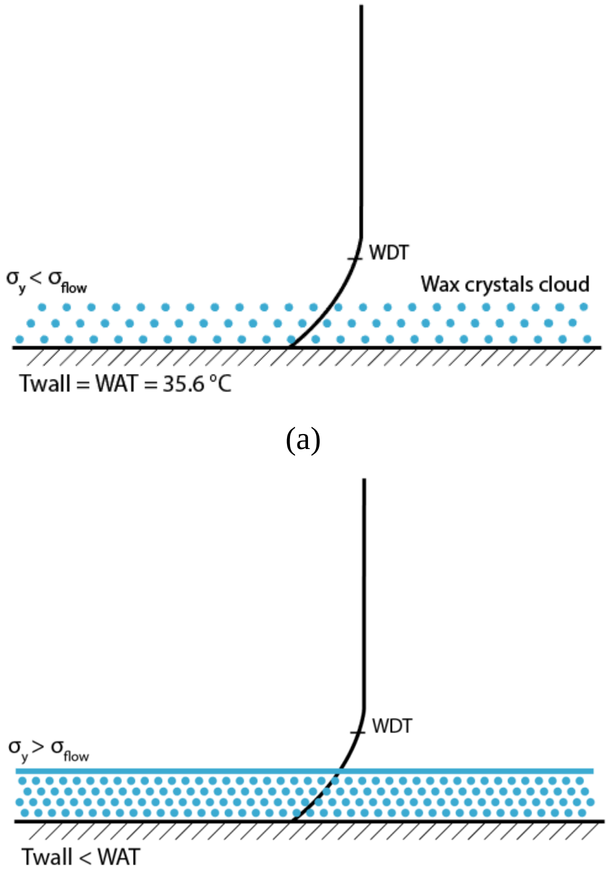

(a)

(b)

Figure 8.10: Illustration presenting the different stages of the wax deposition process for the low cooling rate case.

Now a wax deposition scenario is proposed, based on the results obtained in the previous chapters, together with the videos presented in appendix B.

For the high cooling rate, at first (Figure 8.9Figure 8.10a), when the wall temperature is cooled down, a high temperature gradient is formed and wax crystals appear in the vicinity of the wall. Moments after that, Figure 8.9(b), there is still a high temperature gradient and therefore, in the region that is below the WAT, a large amount of solid is available to form a deposit with a high yield stress that is higher than the shear stress imposed by the flow, thereby forming a immobile wax deposit. As the deposition continues, Figure 8.9(c), the strong fixed deposit still forms in the region below the WAT, but as the temperature gradient is not that steep the amount of solids available decreases, and the yield stress formed by them is not high enough to form a stationary deposit, thereby forming a wax crystals cloud. In Figure 8.9(d), the deposit interface slowly starts to increase its temperature as the solids formed at a higher WPT starts to increase its quantity and interlock. The wax crystals cloud is drastically reduced as the temperature gradient continues to decrease. Later, Figure 8.9(e), the temperature gradient is much lower and no wax crystals cloud is able to be formed, as the available solids are slowly being formed on the vicinity of the already established deposit. At this final moment, conditions are more favorable for any of the three reasons used to explain the increase in the temperature of the deposit interface in chapter 7, and therefore, from that moment on, the temperature of the interface increases until it reaches a plateau between the WAT and the WDT.

As mentioned before, the low cooling rate case seem to be contained within the high cooling rate case. A relevant data that supports this hypothesis is that the temperature of the surface below the wax crystals cloud at the moment it starts to appear is exactly the WAT for both the high and low cooling rates, where in the former the surface is the deposit interface and in the later is the bare copper wall. The analysis of the wax deposition process for the low cooling rate is therefore analogous to the latest stages of the high cooling rate previously commented. First, in Figure 8.10(a), as the copper wall reaches the WAT, the temperature gradient is not big enough to precipitate the necessary solid to form a stationary deposit, however, it is enough to form a visible wax crystals cloud. As the copper wall temperature continues to decrease, Figure 8.10(b), the available solid in the region above it increases until reaching a yield stress sufficient enough to resist the shear stress imposed by the flow, forming an immobile deposit. This deposit act as an insulation decreasing even more the temperature gradient, causing the wax crystals cloud to cease. As the wall temperature continues to decrease for 115 minutes, until reaches the constant temperature of 12.6°C, the deposit thickness continues to increase in a slow process with a constant interface temperature correspondent to an intermediate value between the WAT and the WDT.

It is important to emphasize that the results obtained in this chapter, together with the videos presented in appendix B, led us to the conclusion that the wax deposition process is undoubtedly a complex rheological problem. In the low cooling rate case videos, it is possible to clearly see the shear stress imposed by the flow competing with the changing yield stress of the new mixture formed with precipitated wax solids above the wall. In these videos, it is possible to observe large wax deposition blocks being sheared until finally forming a stationary wax deposit.

9
Conclusions

The present research was able to provide valuable original information regarding the physical mechanisms involved in the wax deposition. The motivation for this work was the existence of divergent opinions on the mechanisms that govern this process, which consequently leads to inaccurate simulation models that do not have the necessary inputs to encompass all aspects of the wax deposition process.

This study followed the research strategy of carrying out experiments with simple geometries and using a model fluid with well-known properties. In addition, the experimental test section was carefully developed to provide well-defined boundary conditions and to be able to perform measurements while wax deposition experiments were running. Thus, the data obtained at this work is a reliable basis for validating new models of wax deposition.

In this work, measurements were performed for the deposit thickness, the temperature profile of the deposit, the temperature of the deposit-liquid interface and the temperature of the region of suspended crystals. The experiments were performed in the axial position of the annular section corresponding to x / L = 0.8 for three different Reynolds numbers, namely, 736, 1440 and 2073. In order to investigate the effect of the cooling rate, two different cooling rates were employed in all the experiments except those for measuring the temperature profile of the deposit, where only experiments for the high cooling rate were performed due to time limitations.

The results obtained for the deposit temperature profile indicated that the heat transfer that occurs inside the deposit is controlled only by thermal conduction. This conclusion was obtained by the excellent match between the pure conductive temperature profiles and the results obtained. This result is valid for all the range of Reynolds numbers employed in this work.

Measurements of the temporal evolution of the temperature of the deposit-liquid interface indicate that there is an increase in the initial value corresponding to the WAT until reaching a constant intermediate value between the WAT and the WDT. The Reynolds number did not have any influence on the temperature of the deposit interface. Three scenarios have been proposed in order to explain the evolution of the interface temperature to values above WAT. In the first, as the effective cooling rate of the deposit decreases as the paraffin deposit forms and grows, the degree of subcooling necessary for the formation of paraffin crystals decreases, consequently allowing the appearance of crystals at higher temperatures as time passes. Another possibility could be that after the nucleation of the first wax crystals, the already established deposit would serve as a nucleation site of new crystals through a secondary nucleation, which is known to occur at higher temperatures. The last possibility considered was the selective enrichment of the solution by diffusive mechanisms above the deposit interface. Veiga et al. (2020) have presented numerically predicted concentration profiles of the heavier wax components where the increase in the concentration of these components in the fluid above the interface was evident. In this case a new higher local WAT could prevail and justify the temperature measurements of the present work. These results contradict the current models of wax deposition in which it is assumed that the formation of wax deposits only occurs at temperatures below or equal to the WAT. It is important to mention that the precise measurements corresponding to the interface region were only possible due to the development of a miniature temperature probe.

Moreover, the initial formation of the wax deposits for two different cooling rates were registered by a high speed camera. The presence of a transient wax crystal cloud was observed at the initial moments of deposit formation in the hot flow regime. This wax crystals cloud was observed both above the wax deposit, at high cooling rates and above the bare copper pipe at low cooling rates. These suspended wax crystals were found to present three different stages. At first, small crystals appear above the interface flowing. Afterwards, they increase in size and in quantity, forming a dense wax crystal cloud. At last, the deposit growth rate decreases and the number concentration of crystals decrease steadily, until no more wax crystals are observed. Temperature measurements of this region showed that the wax crystals cloud is warmer than the deposit-liquid interface but is still lower than the WDT. The different cooling rates did not seem to influence the wax crystal cloud temperature as well as the different Reynolds numbers employed.

The results obtained in this work open doors to several interesting investigations. The collection of fluid samples from the region of the wax crystals cloud that forms just above the deposit would be an interesting contribution, in order to identify not only the composition of this region but also to identify the WAT of this collected fluid, checking if the increase in WAT is verified. In this way, it will be possible to identify whether the increase in WAT is due simply to the change in the effective cooling rate or whether the increase is in fact due to a selective enrichment of heavier components in the region. In addition, it would also be interesting to measure the deposit temperature profiles for the low cooling rates case and verify whether under such conditions the heat transfer in the deposit is also purely conductive. Regarding the cooling rates employed, it would be interesting to carry out experiments with cooling rates lower than 0.25 ° C / min, the lowest used in this work, in order to verify its influence on the formation of the observed cloud of crystals.

10
References

AGRAWAL, S. G.; PATERSON, A. H. J. Secondary Nucleation: Mechanisms and Models. **Chemical Engineering Communications**, v. 202, n. 5, p. 698–706, 2015.

ANDRADE, D. E. V.; MARCELINO NETO, M. A.; NEGRÃO, C. O. R. The importance of supersaturation on determining the solid-liquid equilibrium temperature of waxy oils. **Fuel**, v. 206, p. 516–523, 2017.

AZEVEDO, L. F. A.; TEIXEIRA, A. M. A critical review of the modeling of wax deposition mechanisms. **Petroleum Science and Technology**, v. 21, n. 3–4, p. 393–408, 2003.

BANKI, R.; HOTEIT, H.; FIROOZABADI, A. Mathematical formulation and numerical modeling of wax deposition in pipelines from enthalpy-porosity approach and irreversible thermodynamics. **International Journal of Heat and Mass Transfer**, v. 51, n. 13–14, p. 3387–3398, 2008.

BERN, P. A.; WITHERS, V. R.; CAIRNS, R. J. R.; PETROLEUM, B. **Wax deposition in crude oil pipelines**. European offshore petroleum conference exhibition. **Anais**...1980

BHAT, N. V.; MEHROTRA, A. K. Measurement and prediction of the phase behavior of wax-solvent mixtures: Significance of the wax disappearance temperature. **Industrial and Engineering Chemistry Research**, v. 43, n. 13, p. 3451–3461, 2004.

BIDMUS, H.; MEHROTRA, A. K. Measurement of the liquid-deposit interface temperature during solids deposition from wax-solvent mixtures under static cooling cconditions. **Energy and Fuels**, v. 22, n. 6, p. 1174–1182, 2008a.

BIDMUS, H.; MEHROTRA, A. K. Measurement of the liquid-deposit interface temperature during solids deposition from wax-solvent mixtures under sheared cooling. **Energy and Fuels**, v. 22, n. 6, p. 4039–4048, 2008b.

BIDMUS, H. O.; MEHROTRA, A. K. Heat-Transfer Analogy for Wax Deposition from Paraffinic Mixtures. **Industrial and Engineering Chemistry Research**, v. 43, n. 3, p. 791–803, 2004.

BIDMUS, H. O.; MEHROTRA, A. K. Solids deposition during “cold flow” of wax-solvent mixtures in a flow-loop apparatus with heat transfer. **Energy and Fuels**, v. 23, n. 6, p. 3184–3194, 2009.

BURGER, E. D.; PERKINS, T. K.; STRIEGLER, J. H. Studies of Wax Deposition in the Trans Alaska Pipeline. **JPT, Journal of Petroleum Technology**, v. 33, n. 6, p. 1075–1086, 1981.

C.E. REISTLE, J.; O.C, B. Laboratory study of rod waxes. 1932.

CABANILLAS, J. P.; LEIROZ, A. T.; AZEVEDO, L. F. A. Wax Deposition in the Presence of Suspended Crystals. **Energy and Fuels**, v. 30, n. 1, p. 1–11, 2016.

CAZAUX, G.; BARRÉ, L.; BRUCY, F. Waxy crude cold start: Assessment through gel structural properties. **Proceedings - SPE Annual Technical Conference and Exhibition**, v. 1999- Septe, p. 729–739, 1998.

CHANG, C.; BOGER, D. V.; NGUYEN, Q. D. Influence of thermal history on the waxy structure of statically cooled waxy crude oil. **SPE Journal**, v. 5, n. 2, p. 148–157, 2000.

CORDOBA, A. J.; SCHALL, C. A. Application of a heat transfer method to determine wax deposition in a hydrocarbon binary mixture. **Fuel**, v. 80, n. 9, p. 1285–1291, 2001.

COUTINHO, J. A. P.; MIRANTE, F.; PAULY, J. A new predictive UNIQUAC for modeling of wax formation in hydrocarbon fluids. **Fluid Phase Equilibria**, v. 247, n. 1–2, p. 8–17, 2006.

CREEK, J. L.; LUND, H. J.; BRILL, J. P.; VOLK, M. Wax deposition in single phase flow. **Fluid Phase Equilibria**, v. 158–160, p. 801–811, 1999.

EDMONDS, B.; MOORWOOD, T.; SZCZEPANSKI, R.; ZHANG, X. Simulating wax deposition in pipelines for flow assurance. **Energy and Fuels**, v. 22, n. 2, p. 729–741, 2008.

EHSANI, S.; HAJ-SHAFIEI, S.; MEHROTRA, A. K. Deposition from waxy mixtures in a flow-loop apparatus under turbulent conditions: Investigating the effect of suspended wax crystals in cold flow regime. **Canadian Journal of Chemical Engineering**, v. 97, n. 10, p. 2740–2751, 2019a.

EHSANI, S.; HAJ-SHAFIEI, S.; MEHROTRA, A. K. Experiments and modeling for investigating the effect of suspended wax crystals on deposition from 'waxy' mixtures under cold flow conditions. **Fuel**, v. 243, n. January, p. 610–621, 2019b.

EHSANI, S.; MEHROTRA, A. K. Validating Heat-Transfer-Based Modeling Approach for Wax Deposition from Paraffinic Mixtures: An Analogy with Ice Deposition. **Energy and Fuels**, v. 33, n. 3, p. 1859–1868, 2019.

EHSANI, S.; MEHROTRA, A. K. Investigating the gelling behaviour of 'waxy'' paraffinic mixtures during flow shutdown'. **Canadian Journal of Chemical Engineering**, 2020.

ERICKSON, D. D.; NIESEN, V. G.; BROWN, T. S. Thermodynamic measurement and prediction of paraffin precipitation in crude oil. **Proceedings - SPE Annual Technical Conference and Exhibition**, v. Pi, p. 933–948, 1993.

FONG, N.; MEHROTRA, A. K. Deposition under turbulent flow of wax-solvent mixtures in a bench-scale flow-loop apparatus with heat transfer. **Energy and Fuels**, v. 21, n. 3, p. 1263–1276, 2007.

GLUYAS, J. G.; UNDERHILL, J. R. The Staffa Field, Block 3/8b, UK North Sea. **Geological Society Memoir**, v. 20, n. 1, p. 327–333, 2003.

HAJ-SHAFIEI, S.; WORKMAN, B.; TRIFKOVIC, M.; MEHROTRA, A. K. In-Situ Monitoring of Paraffin Wax Crystal Formation and Growth. **Crystal Growth and Design**, v. 19, n. 5, p. 2830–2837, 2019.

HAJ-SHAFIEI, S.; MEHROTRA, A. K. Achieving cold flow conditions for ‘waxy’ mixtures with minimum solid deposition. **Fuel**, v. 235, n. July 2018, p. 1092–1099, 2019.

HAMOUDA, A. A.; RAVNØY, J. M. Prediction of wax deposition in pipelines and field experience on the influence of wax on drag-reducer performance. **Proceedings of the Annual Offshore Technology Conference**, v. 1992- May, p. 669–679, 1992.

HOTEIT, H.; BANKI, R.; FIROOZABADI, A. Wax deposition and aging in flowlines from irreversible thermodynamics. **Energy and Fuels**, v. 22, n. 4, p. 2693–2706, 2008.

HU, Z.; MENG, D.; LIU, Y.; DAI, Z.; JIANG, N.; ZHUANG, Z. Study of wax deposition law by cold finger device. **Petroleum Science and Technology**, v. 37, n. 15, p. 1846–1853, 2019.

HUANG, Z.; SU LEE, H.; SENRA, M.; FOGLER, S. A Fundamental Model of Wax Deposition inSubsea Oil Pipelines. **AIChE Journal**, v. 59, n. 4, p. 215–228, 2011.

HUANG, Z.; ZHENG, S.; FOGLER, H. S. **Wax Deposition: Experimental Characterizations, Theoretical Modeling, and Field Practices**. [s.l: s.n.].

HUNT, E. B. Laboratory study of paraffin deposition. **Journal of Petroleum Technology**, 1962.

IJEOMAH, C. E.; DANDEKAR, A. Y.; CHUKWU, G. A.; KHATANIAR, S.; PATIL, S. L.; BALDWIN, A. L. Measurement of wax appearance temperature under simulated pipeline (dynamic) conditions. **Energy and Fuels**, v. 22, n. 4, p. 2437–2442, 2008.

JANAMATTI, A.; LU, Y.; RAVICHANDRAN, S.; SARICA, C.; DARABOINA, N. Influence of operating temperatures on long-duration wax deposition in flow lines. **Journal of Petroleum Science and Engineering**, v. 183, p. 106373, 2019.

JAPPER-JAAFAR, A.; BHASKORO, P. T.; MIOR, Z. S. A new perspective on the measurements of wax appearance temperature: Comparison between DSC, thermomicroscopy and rheometry and the cooling rate effects. **Journal of Petroleum Science and Engineering**, v. 147, n. September, p. 672–681, 2016.

JEMMETT, M. R.; MAGDA, J. J.; DEO, M. D. Heterogeneous organic gels: Rheology and restart. **Energy and Fuels**, v. 27, n. 4, p. 1762–1771, 2013.

JESSEN, F. W.; HOWELL, J. N. Effect of Flow Rate on Paraffin Accumulation in Plastic, Steel, and Coated Pipe. **Transactions of the AIME**, v. 213, n. 01, p. 80–84, 1958.

JIANG, Z.; HUTCHINSON, J. M.; IMRIE, C. T. Measurement of the wax appearance temperatures of crude oils by temperature modulated differential scanning calorimetry. **Fuel**, v. 80, n. 3, p. 367–371, 2001.

KASUMU, A. S.; ARUMUGAM, S.; MEHROTRA, A. K. Effect of cooling rate on the wax precipitation temperature of "waxy" mixtures. **Fuel**, v. 103, p. 1144–1147, 2013.

LEIROZ, A. T.; AZEVEDO, L. F. A. Studies on the mechanisms of wax deposition in pipelines. **Proceedings of the Annual Offshore Technology Conference**, v. 2005- May, p. 102–112, 2005.

LIMA, J. C. B. **Estudos sobre a formação de depósitos de parafina em dutos**. [s.l.] Pontifícia Universidade Católica do Rio de janeiro, 2018.

LINDELOFF, N.; KREJBJERG, K. A compositional model simulating wax deposition in pipeline systems. **Energy and Fuels**, v. 16, n. 4, p. 887–891, 2002.

LIRA-GALEANA, C.; FIROOZABADI, A.; PRAUSNITZ, J. M. Thermodynamics of Wax Precipitation in Petroleum Mixtures. **AIChE Journal**, v. 42, n. 1, p. 239–248, 1996.

MAHIR, L. H. A.; VILAS BÔAS FÁVERO, C.; KETJUNTIWA, T.; FOGLER, H. S.; LARSON, R. G. Mechanism of Wax Deposition on Cold Surfaces: Gelation and Deposit Aging. **Energy and Fuels**, v. 33, n. 5, p. 3776–3786, 2019.

MATZAIN, A. **Single-Phase Liquid Paraffin Deposition Modeling**. [s.l.] The University of Tulsa, 1996.

MEHROTRA, A. K.; EHSANI, S.; HAJ-SHAFIEI, S.; KASUMU, A. S. A review of heat-transfer mechanism for solid deposition from "waxy" or paraffinic mixtures. **Canadian Journal of Chemical Engineering**, 2020.

MEHROTRA, A. K.; BHAT, N. V. Modeling the effect of shear stress on deposition from "Waxy" mixtures under laminar flow with heat transfer. **Energy and Fuels**, v. 21, n. 3, p. 1277–1286, 2007.

MERINO-GARCIA, D.; CORRERA, S. Cold flow: A review of a technology to avoid wax deposition. **Petroleum Science and Technology**, v. 26, n. 4, p. 446–459, 2008.

PARTHASARATHI, P.; MEHROTRA, A. K. Solids deposition from multicomponent wax-solvent mixtures in a benchscale flow-loop apparatus with heat transfer. **Energy and Fuels**, v. 19, n. 4, p. 1387–1398, 2005.

PASO, K.; KALLEVIK, H.; SJÖBLOM, J. Measurement of wax appearance temperature using near-infrared (NIR) scattering. **Energy and Fuels**, v. 23, n. 10, p. 4988–4994, 2009.

PEDERSEN, K. S.; THOMASSEN, P.; FREDENSLUND, A. Thermodynamics of Petroleum Mixtures Containing Heavy Hydrocarbons . 1 . Phase Envelope Calculations by Use of the Soave-Redlich-Kwong Equation of State. p. 163–170, 1984.

RIBEIRO, F. S.; SOUZA MENDES, P. R.; BRAGA, S. L. Obstruction of pipelines due to paraffin deposition during the flow of crude oils. **International Journal of Heat and Mass Transfer**, v. 40, n. 18, p. 4319–4328, 1997.

RONNINGSEN, H. P.; BJORNDAL, B.; HANSEN, A. B.; PEDERSEN, W. B. Wax Precipitation from North Sea Crude Oils. 1. Crystallization and Dissolution Temperatures, and Newtonian and Non-Newtonian Flow Properties. **Energy and Fuels**, v. 5, n. 6, p. 895–908, 1991.

RUWOLDT, J.; KURNIAWAN, M.; OSCHMANN, H. J. Non-linear dependency of wax appearance temperature on cooling rate. **Journal of Petroleum Science and Engineering**, v. 165, n. February, p. 114–126, 2018.

SINGH, P.; VENKATESAN, R.; FOGLER, H. S.; NAGARAJAN, N. Formation and aging of incipient thin film wax-oil gels. **AIChE Journal**, v. 46, n. 5, p. 1059–1074, 2000.

SINGH, P.; VENKATESAN, R.; FOGLER, H. S. Formation and Aging of waxes 2000, Singh and Fogler. **AIChE Journal**, v. 46, n. 5, p. 1059–1074, 2000.

SINGH, P.; YOUYEN, A.; FOGLER, H. S. Existence of a critical carbon number in the aging of a wax-oil gel. **AIChE Journal**, v. 47, n. 9, p. 2111–2124, 2001.

SOEDARMO, A. A.; DARABOINA, N.; SARICA, C. Validation of wax deposition models with recent laboratory scale flow loop experimental data. **Journal of Petroleum Science and Engineering**, v. 149, p. 351–366, 2017.

TIWARY, R.; MEHROTRA, A. K. Deposition from wax-solvent mixtures under turbulent flow: Effects of shear rate and time on deposit properties. **Energy and Fuels**, v. 23, n. 3, p. 1299–1310, 2009.

TODI, S.; PETROLEUM, S.; DEO, M.; UTAH, U. **Experimental and Modeling Studies of Wax Deposition in Crude - Oil - Carrying Pipelines**. Offshore Technology Conference. **Anais**...2006

VEIGA, H. M. B. **Study of wax deposits in pipelines**. [s.l.] Pontifícia Universidade Católica do Rio de Janeiro, 2017.

VEIGA, H. M. B.; BOHER E SOUZA, L.; FLEMING, F. P.; IBANEZ, I.; LINHARES, R. C.; NIECKELE, A. O.; AZEVEDO, L. F. A. Experimental and Numerical Study of Wax Deposition in a Laboratory-Scale Pipe Section under Well-Controlled Conditions. **Energy & Fuels**, v. 34, n. 10, p. 12182–12203, 2020.

VEIGA, H. M. B.; FLEMING, F. P.; AZEVEDO, L. F. A. Wax Deposit Thermal Conductivity Measurements under Flowing Conditions. **Energy and Fuels**, v. 31, n. 11, p. 11532–11547, 2017.

VENKATESAN, R.; NAGARAJAN, N. R.; PASO, K.; YI, Y. B.; SASTRY, A. M.; FOGLER, H. S. The strength of paraffin gels formed under static and flow conditions. **Chemical Engineering Science**, v. 60, n. 13, p. 3587–3598, 2005.

WON, K. W. Thermodynamics for solid solution-liquid-vapor equilibria: wax phase formation from heavy hydrocarbon mixtures. **Fluid Phase Equilibria**, v. 30, n. C, p. 265–279, 1986.

YANG, J.; LU, Y.; DARABOINA, N.; SARICA, C. Wax deposition mechanisms: Is the current description sufficient? **Fuel**, v. 275, n. December 2019, 2020.

ZHAO, Y.; KUMAR, L.; PASO, K.; SAFIEVA, J.; SARIMAN, M. Z. B.; SJÖBLOM, J. Gelation behavior of model wax-oil and crude oil systems and yield stress model development. **Energy and Fuels**, v. 26, n. 10, p. 6323–6331, 2012.

ZHENG, S.; SAIDOUN, M.; PALERMO, T.; MATEEN, K.; FOGLER, H. S. Wax Deposition Modeling with Considerations of Non-Newtonian Characteristics: Application on Field-Scale Pipeline. **Energy and Fuels**, v. 31, n. 5, p. 5011–5023, 2017.

11
Appendix A

In order to perform reliable analysis on the data acquired, it is essential to provide the uncertainty of the measurements conducted. In this section the calculations of the uncertainty for the experiments carried out in this dissertation will be detailed as well as the calibration of the thermocouples employed.

11.1
Temperature probe calibration

For the temperature measurements the first step was to conduct the calibration of the temperature probe and for that purpose a certified calibrated thermometer was used. The measurements were performed at the Fluids Engineering Laboratory of PUC-Rio.

Two different thermometer models were used for the calibration of two different temperature ranges. The information regarding each of the certified thermometers as well as the temperature data obtained for each of them altogether with the corresponding temperature probe values are presented in tables.

For each thermometer 4 temperatures values were chosen for performing the calibration. For every temperature 10 measurements were taken with 20 seconds interval between them and its averaged values are found in Table 11.1 and Table 11.2. The temperature probe and the thermometer were kept at rest for 10 minutes in the water bath at the desired temperature set before taking any measurements.

Table 11.1: Temperature calibration data of the thermometer employed for the range of 38.6°C to 41.4°C.

Mercury thermometer		**Manufacturer:**	Incoterm
Model:	120C	**Temperature range:**	38.6 °C a 41.4 °C
Serial Number:	4562/14	**Division:**	0.05 °C
Certificate number:	T0128/2019	**Error (°C):**	+0.02
Temperature Measurements (°C)			
Standard:	**Probe:**	**Probe Error:**	
39	38.43	0.58	
39.5	38.89	0.61	
40	39.35	0.65	
40.5	39.83	0.67	
	Average:	0.63	

Table 11.2: Temperature calibration data of the thermometer employed for the range of 28.6°C to 31.4°C.

Liquid in glass thermometer		**Manufacturer:**	AMA
Model:	1 18C	**Temperature range:**	28.6 °C a 31.4 °C
Serial Number:	9021856	**Division:**	0.05 °C
Certificate number:	T0148/2018	**Error (°C):**	+0.02
Temperature Measurements (°C)			
Standard	**Probe**	**Probe Error (°C):**	
29	28.45	0.55	
29.5	28.94	0.56	
30	29.44	0.56	
30.5	29.95	0.56	
	Average:	0.56	

With the results obtained above for both calibrated thermometers, a calibration curve was prepared (Figure 11.1). As indicated in Figure 11.1 all of our temperature measurements performed with the probe need an increase of 0.3 °C. Therefore, all temperature results presented on previous chapters of this work have already this correction embedded in their value.

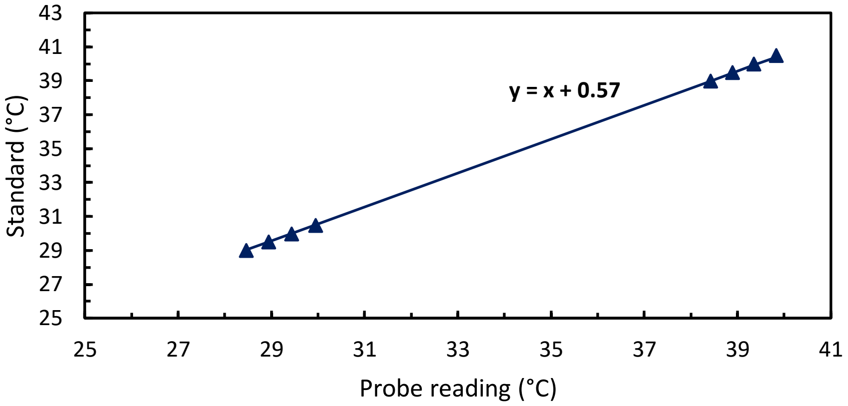

Figure 11.1: Temperature calibration curve.

11.2
Uncertainty calculations

Deposit liquid interface temperature

For the calculation of the uncertainty associated to the deposit liquid interface temperature measurements two types of uncertainties were estimated, one related to the resolution of the equipment used (type B) and the other related to the repeatability of the measurements (type A).

The probe was connected to an Agilent 34970A and the resolution of the equipment was 0.01 °C. Admitting that the error has the same probability for the interval of ±0.01°C, a rectangular distribution was considered and the standard uncertainty calculated:

$$u_{standard} = \frac{0.01}{\sqrt{3}} = 0.01\ °C \tag{11.1}$$

The average of the standard deviation of the interface temperature measurements for all times and Reynolds was calculated to be 0.11 °C. The standard uncertainty can be calculated as,

$$u_{Ti} = \frac{\sigma}{\sqrt{(N-1)}} = \frac{0.11}{\sqrt{2}} = 0.08\ °C \tag{11.2}$$

And then the two types of uncertainties were combined to find a final value, however as the uncertainties from the repeatability are much bigger than the one from the equipment resolution, the first one is dominant.

$$u_{comb} = \sqrt{(Type\ A)^2 + (Type\ B)^2} \tag{11.3}$$

$$u_{comb} = \sqrt{(0.08)^2 + (0.01)^2} = 0.08\ °C \tag{11.4}$$

Considering that the results probability distribution will be approximately the t-student, to find the coverage factor we need first to find the effective degrees of freedom associated to the standard uncertainty calculated. For this reason, the Welch Satterthwaite equation (Eq.11.5) was employed:

$$DF_{effective} = \frac{u_{comb}^4}{\sum_{i=1}^{N_{components}} \frac{\left(\frac{\partial f}{\partial X_i} u_{X_i}\right)^4}{DF_i}} \tag{11.5}$$

However, as the type B uncertainties are considered to have an infinity degree of freedom, they do not need to be calculated on the denominator, leading in our case to,

$$DF_{effective} = \frac{0.08^4}{\frac{(0.08)^4}{2}} = 2 \tag{11.6}$$

Thereby, expanding this uncertainty for a 95% reliability, using the t-student table we find that the coverage factor for our case is k=4.3. Therefore, our expanded uncertainty is,

$$u_{exp} = u_{comb}.k = 0.3\ °C \tag{11.7}$$

Wax Deposit thickness

The same procedure was employed for the calculation of the uncertainties associated to the deposit thickness measurements. The resolution of the micrometer was 0.01 mm and using a rectangular distribution the standard uncertainty was calculated to be 0.01 mm.

The average of the standard deviation of the deposit thickness measurements for all Reynolds and times employed was calculated to be 0.06 mm. The standard uncertainty calculations can be seen in equation 11.8.

$$u_{thickness} = \frac{\sigma}{\sqrt{(N-1)}} = \frac{0.06}{\sqrt{2}} = 0.04\ mm \qquad (11.8)$$

The uncertainties were combined by equation 11.3 and the value found was 0.04 mm, while the degrees of freedom were calculated to be 2. Once again, using the t-student table for a 95% confidence the coverage factor is 4.31 and therefore, the expanded uncertainty for the deposit thickness measurements is 0.17 mm.

12
Appendix B

The images obtained in this dissertation provide valuable information on the wax deposition process and can be very useful to its understanding. In this section, a brief description of the videos that are attached to this dissertation will be made and a few events during the videos considered important will be indicated. Every experiment is presented with its filmed frame rate, window size and exposure. The time where interesting events occur will be indicated as “minute: second”.

The recording of these videos presented challenges where the higher the frame rate, the faster the camera’s internal memory was filled. Therefore, when making high quality videos capturing the shape of the crystals, the frame rate chosen had to be high and the video duration was short. On the other hand, when capturing the entire deposition process time and its features the quality had to be lowered.

It is important to mention that the frame rate indicated on the video correspond to the frame rate used to make the video, but in the slow motion videos the actual frame rate displayed is different, and will be mentioned on the video description.

If you have problems accessing the videos, please go to the website http://lef.mec.puc-rio.br/.

Wax crystal cloud experiments

The videos shown here presents how the wax crystals cloud temperature measurements were performed. The videos are presented on its original frame rate, 30 fps, thus the speed of the crystals seen is their real speed during the experiments. As the goal of this video was mainly to capture the entire duration of the wax crystal cloud the frame rate used could not be very high otherwise the camera memory would rapidly fill.

- **Nuvem_low_cooling_736**

This video presents a low cooling rate with Reynolds 736. The Reynolds number is 736. Some interesting events to be highlighted are:

00:06 - As this is a low cooling rate experiment, it is possible to see that the first crystals appear above the bare copper pipe

00:25 - It is possible to see a small crystal right below the probe sliding on the vicinity of the copper pipe in a velocity much slower than the crystals that flow above, indicating some kind of force preventing the crystal to detach from the wall.

00:38 – There is a significant increase in the crystals flowing above the pipe and the temperature probe is already positioned measuring the region temperature.

0:58 – There is a considerable amount of crystals flowing, however until this time, no crystal can be seen fixing on the copper pipe wall. The pipe still clear.

01:45 – In the upstream of the video frame, it is possible to see a large crystal sliding on the copper wall with certain difficulty to detach from the wall, seeming to exist a force holding it. Also, at this time the crystals in the wax crystal cloud are larger.

01:38 – 02:22 – In a spot between the middle of the left frame and the temperature probe a crystallization process start to occur, it is possible to note that the crystal forms not due to the wax crystal cloud. Later, the shear forces of the flow remove a crystal from the upstream and bring together this aggregate.

02:30 – 03:30 – The same formation seems to occur again in the same spot and, again, is sheared from the pipe wall.

02:53 – It is interesting to observe that differently from the initial crystal cloud, the cloud has a contained pattern above the pipe wall, in an organized way, but it is also possible to see big chunks of crystal flowing. At this moment it is believed that sheared crystals is a great contribution to the wax crystals cloud.

04:11 – A big wax deposit formed is slowly removed by shear and only a thin layer of deposit remains.

04:20 – 05:12 – This thin layer formed start to grow as a solid and well attached deposit.

05:40 – The wax crystal cloud cease and crystals flowing above the deposit are barely seen.

- **Nuvem_low_cooling_1440**

This video presents a low cooling rate experiment with Reynolds 1440. Some interesting events to be highlighted are:

00:15 – First crystal is seen flowing above the copper pipe.

00:40 – Significant amount of crystals flowing

04:20 – 04:50 – Big deposit growth.

04:55 – Large deposit is removed by shear and only a thin layer of deposit remains.

05:22 – Wax crystals flowing decreases significantly and cease.

05:30 – 06:40 – Solid deposit grows.

- **Nuvem_low_cooling_2073**

This video presents a low cooling rate experiment with Reynolds 2073. Some interesting events to be highlighted are:

00:11 – First crystal flowing.

04:53 – Large crystal removed by shear.

05:23 – In left side of the frame it is possible to see the deposit being "peeled" but not removed.

05:43 – Large deposit starts to be slowly removed.

05:48 – 05:57 – A thin deposit layer is quickly formed and removed by shear.

05:59 – A thin deposit layer that still remained is slowly peeled. The deposit start sliding in the copper pipe until stops.

Slow motion videos

As the main objective of the slow motion videos was to capture high quality images of the crystals flowing, the lowest Reynolds was preferred as this one would possibly provide smaller velocities of the flowing crystals.

- **Nuvem_low_736_inicio**

This video presents the initial formation of the wax crystal cloud in slow motion, from the first crystal appearance until the formation of a denser crystal cloud. The Reynolds for this case is 736. The video was captured with 300 fps and converted to 30 fps, giving the slow motion effect. As the original frame rate capture was high, it is possible to see the crystals with higher definition. The first crystal appears after 33 seconds.

- **High_cooling_736**

This video presents the initial formation of the wax crystal cloud in the high cooling rate. The video was captured with a rate of 50 fps and was transformed to 15 fps.

00:13 – It is already possible to observe very small suspended crystals flowing above the wax deposit.

01:00 – At this moment the suspended crystals are a little bit bigger and it is easier to see them flowing above the deposit.

01:46 – The suspended crystals now are even larger and they increase in number.

03:10 – Due to the high growth of the deposit in the high cooling rate case, the light must be adjusted to properly focus on the wax crystal cloud, thus it is possible to see its adjustment.

03:13 – A dense wax crystal cloud can be seen formed above the deposit. A significant increase in size and quantity can be observed.

09:00 – The wax crystal cloud thickness is already reduced and starts to decrease.

- **Slower_high_cooling_736**

This video was made to better observe the increase in size and quantity of the suspended wax crystals in the high cooling rate case. The Reynolds number is 736. This video was captured originally with a rate of 400 fps and was transformed to 15 fps. The video commences with an already formed deposit and the small crystals flowing above the deposit can already be seen. This long video slowly shows the wax crystal cloud evolution process until forming a dense cloud.

- **Slow_low_cooling_2073**

This video is simply to show an interesting event that occurred in one of our videos, in which a big deposit part is sheared and before being detached from the wall it causes a recirculation of crystals in front of it. This occurred for the low cooling rate experiments with a Reynolds of 2073.

13
Appendix C

As one of the purposes of this work was to provide reliable experimental data, this chapter was prepared to provide all the necessary information and data to validate new numerical models.

13.1
Geometry

The annular test section was composed of a copper pipe inside an acrylic pipe. The copper pipe had 19 mm external diameter and 12.7 mm internal diameter. The surrounding acrylic pipe had 40 mm external diameter and 34 mm internal diameter. The copper pipe, in which the deposition occurs above, had 1.05 m.

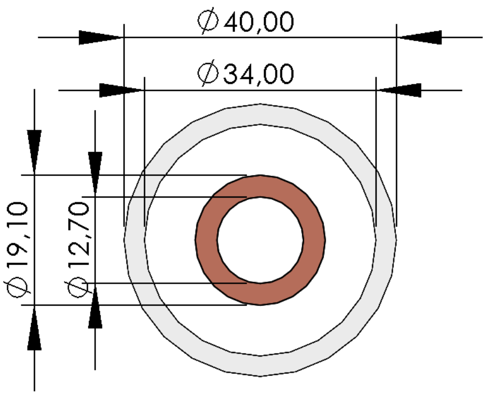

Figure 13.1: Annular assembly dimensions.

13.2
Boundary and initial conditions

One of the great advantages of this work is the well-controlled boundary conditions throughout the experiments, including the time that the measurements were taken. As the experiment control was already detailed on chapter 3, in this section the focus will be on the boundary conditions that our set-up was able to achieve.

The schematic view of the boundary conditions employed is presented on Figure 13.2. The annular assembly was placed inside water at 38.6°C. The wax solution was directed to the annular region formed between the copper pipe and the external acrylic pipe. The wax solution inlet was controlled to be always at 38.6°C and the progressive cavity pump employed allowed for a constant uniform flow rate. The flow rates employed were 0.21 m^3/h, 0.42 m^3/h and 0.61 m^3/h, which correspond to the Reynolds numbers of 736, 1440 and 2073 respectively. The copper pipe cooling can be performed by accessing the excel files attached to this work. This files contain the wall temperature values acquired throughout the experiments for both cooling rates employed until reaching the constant temperature of 12.6°C.

The initial conditions of the experiment were, wax solution flowing in the annular region at 38.6°C, copper wall at 38.6°C and external ambient surrounding the annular assembly at 38.6°C.

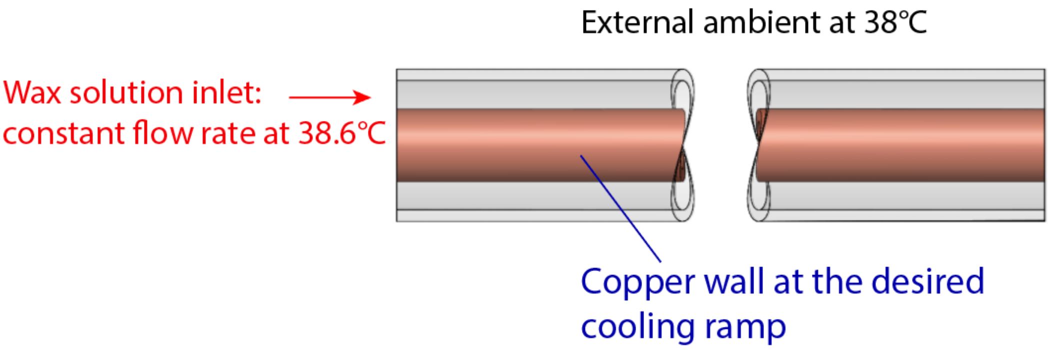

Figure 13.2: Schematic view of the experiment boundary conditions.

13.3
Wax solution composition

The wax solution used was a multicomponent mixture and the knowledge of its composition is important to model the wax precipitation and the deposit formation. The composition of the mixture employed is presented on Table 13.1.

Table 13.1: Composition of the wax solution employed in the experiments.

Carbon number	Molar composition (z_i)	Carbon number	Molar composition (z_i)
C_{12}	9.03×10^{-1}	C_{31}	7.20×10^{-3}
C_{22}	6.61×10^{-5}	C_{32}	4.63×10^{-3}
C_{23}	4.59×10^{-4}	C_{33}	2.91×10^{-3}
C_{24}	2.49×10^{-3}	C_{34}	1.81×10^{-3}
C_{25}	7.00×10^{-3}	C_{35}	1.13×10^{-3}
C_{26}	1.21×10^{-2}	C_{36}	7.20×10^{-4}
C_{27}	1.56×10^{-2}	C_{37}	4.71×10^{-4}
C_{28}	1.60×10^{-2}	C_{38}	3.16×10^{-4}
C_{29}	1.38×10^{-2}	C_{39}	2.07×10^{-4}
C_{30}	1.05×10^{-2}		